UNIVERSITÀ
DEGLI STUDI
DI PADOVA

Administrative unit: **University of Padova**

Department: **Land, Environment, Agriculture and Forestry (TESAF)**

PhD Program: **Land, Environment, Resources and Health (LERH)**

Batch: XXXV

THESIS TITLE

Structure-function relationships of the hydraulic architecture of trees under climate change

Thesis financially supported by: CARIPARO

PhD Program Coordinator: Prof. Marco Borga

Supervisor: Giai Petit

Co-Supervisor: Michela Schiavon

PhD candidate: Dario Zambonini

Sede Amministrativa: **Università degli Studi di Padova**

Dipartimento Territorio e Sistemi Agro-Forestali (TESAF)

CORSO DI DOTTORATO DI RICERCA: **Land, Environment, Resources, Health (LERH)**

Ciclo: XXXV

TITOLO TESI

Rapporti tra struttura e funzione dell'architettura idraulica degli alberi e il cambiamento climatico

Tesi redatta con il contributo finanziario di: CARIPARO

Coordinatore: Prof. Marco Borga

Supervisore: Prof. Giai Petit

Co-Supervisore: Prof. Michela Schiavon

Dottorando: Dario Zambonini

INDEX

ABSTRACT

Climate change is pushing the need for a rapid assessment of plant vulnerability to drought stress. Low water availability conditions create a cascade of effects on plant growth and survival and an important focus in plant physiological research is carried out on the analysis of trade-offs between stress tolerance and growth. An example of this trade-off at the organ and tissue level is the conflict between xylem safety and efficiency, which suggests that plants with the greatest resistance to embolism formation should concurrently exhibit low hydraulic conductance and growth. Sparse results have been found in trade-off studies, identifying it only among some species assemblages (Gleason *et al*. 2016). Moreover, recent studies suggest that the "trade-off" should change by the axial variation of xylem traits (e.g., conduit diameter) due to the anatomy of stem xylem conduits, which are narrow at the apex of the tree, thus conferring different resistances to embolisms in different sections of the plant (Lechthaler *et al*. 2019).

The aim of the doctoral project is to improve the knowledge on the link between the anatomy of hydraulic architecture of trees and their functioning in water transport. It was tested if the hydraulic safety *vs.* efficiency trade-off applies to the axial variation of xylem traits along the longitudinal stem/branch axis. Furthermore, it was tested if environmental stresses could induce some plastic responses either at anatomical level or in the carbon resources allocation. The xylem anatomical traits were also used in the cause-response evaluation for biotic and abiotic stress. In order to fulfill the above-mentioned aims, different traits of the safety *vs.* efficiency spectrum were analyzed throughout field and laboratory experiments, followed by data analysis and statistical testing. This research is divided into three main chapters, starting from the assessment of a clear link between xylem vulnerability to embolism and the anatomical traits related to it. In the second chapter it will be discussed the plastic and non-plastic responses of trees under drought and low water availability conditions. The last chapter will be focused on how xylem characteristics can be good predictors in the evaluation of stress and the response to it.

RIASSUNTO

Il cambiamento climatico in atto a livello globale sta creando il bisogno di poter stimare in modo rapido la vulnerabilità delle piante allo stress idrico. La poca disponibilità di acqua crea diversi impedimenti alla crescita e alla sopravvivenza della vegetazione, e la ricerca nell'ambito della fisiologia vegetale si concentra sull'analisi dei "trade-off" tra tolleranza allo stress e crescita. Un esempio di questo compromesso, a livello di organo e tessuto, è il conflitto tra sicurezza ed efficienza dello xilema, il quale suggerisce che le piante con una maggiore resistenza all'embolia siano anche quella con una crescita ridotta dovuta ad un trasporto idraulico più basso. Negli studi di "trade-off" vengono solitamente trovati risultati divergenti e poco indicativi, riportati solo in alcune specie (Gleason *et al*. 2016). Inoltre, studi recenti propongono che questi compromessi idraulici possono cambiare lungo alcuni tratti assiali dello xilema (diametro dei condotti). L'anatomia del sistema di trasporto presenta dei patterns rigidi, con cellule più piccole all'apice che diventano più grandi muovendosi verso la base, conferendo così una diversa resistenze all'embolia in sezioni distinte delle piante (Lechthaler *et al*. 2019).

L'obiettivo di questo progetto di dottorato è quello di migliorare la conoscenza sulla relazione tra l'anatomia dell'architettura idraulica degli alberi e il suo funzionamento nel trasporto dell'acqua. È stato analizzato il costo di risorse di carbonio nel "trade-off" tra sicurezza ed efficienza, tenendo in conto della variazione assiale dei tratti anatomici dello xilema lungo gli assi longitudinali di rami e fusto. In seguito, è stata cercata una risposta plastica agli stress ambientali, sia a livello anatomico, sia nell'allocazione delle risorse di carbonio. I tratti anatomici dello xilema sono anche stati usati per capire cause e conseguenze agli stress biotici e abiotici. Per raggiungere questi obiettivi diversi tratti funzionali di sicurezza ed efficienza sono stati analizzati attraverso esperimenti in campo ed in laboratorio, seguiti da analisi dei dati e test statistici di validazione. La tesi è divisa in tre capitoli principali, iniziando da un'analisi nel primo capitolo in cui verrà trattata la connessione tra la vulnerabilità all'embolia dello xilema e i tratti anatomici che la caratterizzano. Nel secondo verrà discusso ampiamente delle risposte plastiche e non-plastiche degli alberi alla siccità e alla carenza idrica. Infine, l'ultimo capitolo si concentrerà sull'importanza delle caratteristiche dello xilema e come queste possano fornire informazioni essenziali nella valutazione dello stress e di come possano avvenire eventuali risposte ad esso.

STRUCTURE OF THE THESIS WITH AIMS AND OBJECTIVES

The main aim of the doctoral project was to improve the knowledge on the link between the anatomy of hydraulic architecture of trees and their functioning in water transport in the context of climate change. Six projects included in the final thesis have been completed during the 3 years of the PhD program. These projects have been divided into 3 chapters in the final dissertation and are briefly explained in this section to provide better context and background. A general introduction opens the thesis with an overview on water transport in plants, the risks and the costs associated, and how the rigid axial design of the xylem is important in anatomical and physiological studies (Figure A for reference).

Chapter 1: XYLEM AXIAL DESIGN AND VULNERABILITY TO EMBOLISM describes an experimental study titled "Pit anatomy and tracheid diameter vary in tandem from stem apex to base and determine a strong decrease in xylem embolism resistance basally". The work is ready for submission and will be presented as a research article with the PhD candidate as first name. The project focused on the assessment of the match between xylem vulnerability to embolism formation and the anatomical properties within a single tree, from the apical-most part of the crown to the trunk base. Two mature trees of *Picea abies* and *Abies alba* were cut, and more than 20 wood samples collected at different distances from the stem apex. We measured consecutive losses of conductivity at different water potential and obtained vulnerability curves (VCs) and P50s (water potential inducing 50% loss of hydraulic conductance). On the same samples, we analysed all the cells contributing to water transport through anatomical measurements. Finally, vulnerability curves were reconstructed with anatomical data, to verify if conduit diameter (Dh) could explain the P50 at a given distance from the apex.

Chapter 2: XYLEM, PHLOEM AND CARBON RESOURCES ALLOCATION UNDER DROUGHT comprises three experimental projects related to drought conditions and the assessment of potential acclimation of the transport tissues and carbon resources.

- *Ch2.1* presents "No xylem phenotypic plasticity in mature *Picea abies* and *Fagus sylvatica* tress after 5 years of throughfall precipitation exclusion" published in Global Change Biology as a research article. We investigated xylem and phloem traits from mature *Fagus sylvatica* and *Picea abies* trees after 5 years of complete exclusion of throughfall precipitation during the growing season. The experimental site from which the samples were collected was a throughfall exclusion experiment in Bavaria, called KROOF. Xylem and phloem anatomy, leaf and branch biomass were analyzed along

top branches of ~1.5 m length in 5 throughfall precipitation excluded (TE) and 5 control (CO) trees of both beech and spruce. Xylem traits were analyzed on wood cores extracted from the stem at breast height.

- *Ch2.2* presents the results of another throughfall exclusion experiment, and the study is entitled "How intensity and duration of drought influence resources allocation and xylem-phloem anatomy in a long term throughfall exclusion experiment". This work is presented as research article ready for publication with the PhD candidate as first name. The provenance of the samples is the experimental site "Sevilleta Long Term Ecological Research" (SEV-LTER) in New Mexico, USA. We measured xylem and phloem traits from mature Piñon Pine trees under different experimental drought conditions in duration and intensity. Xylem and phloem anatomy, branch and leaf biomass were assessed along branches of ~2m length in 5 trees for 4 treatments: legacy (-%45 rain, 12 years), new50 (-50%rain, 1 year), new90 (-90%rain, 1 year) and control.
- *Ch2.3* presents the results of "Phenotypic adjustments of Scouts pine to different soil and water availability conditions", which will be presented in the form of a research article with the PhD candidate as first name. Phenotypic plasticity of xylem or the photosynthetic apparatus might play a key role for pioneer isohydric species like *Pinus sylvestris* to adapt to new/ harsh environments. In this experimental study we assessed xylem anatomical hydraulic traits and biomass resources in mature Scots pines coming from 2 different soil conditions but within the same environment in the Italian Dolomites. One study area is a mature mixed forest with high water availability and the other one is a pure pine forest growing on a landslide (1814) with low water availability due to the soil conditions.

Chapter 3: IMPORTANCE OF XYLEM CHARACTERISTICS IN BIOTIC AND ABIOTIC STRESS contains two works, one regarding a bacterial pathogen and the other chemical contaminants. For both these studies it was highlighted how the xylem design plays a key role in the evaluation of the stress and the response to it.

- *Ch3.1* presents "Susceptibility to *Xylella fastidiosa* and functional xylem anatomy in *Olea europaea*: revisiting a tale of plant-pathogen interaction" published in Annals of Botany Plants as a journal article. We tested the hypothesis that the higher susceptibility to the *X. fastidiosa*'s infection in Cellina di Nardò compared with Leccino is associated to the higher vulnerability to air embolism of its larger vessels. Such hypothesis is motivated by the recognized ability of *X. fastidiosa* in degrading pit membranes and

also because air embolism would possibly provide microenvironmental conditions more favorable to its more efficient aerobic metabolism.

- *Ch3.2* presents the results of a preliminary work titled "Plant's assimilation of Perfluoroalkyl compounds (PFAS) increases hydraulic vulnerability to embolism and bioaccumulation of the contaminants in tissues". This experiment is at preliminary phase and here will be reported the major results and findings with a brief discussion. PFAS (Perfluoroalkyl compounds) are known to alter plant physiology by modifying metabolism and biochemical and physiological function. In the experimental study we tested the rate of bioaccumulation in different tissues and the hydraulic vulnerability to embolism (Vulnerability curves) in willow trees and cuttings (*Salix spp*.)

A final chapter with general discussion and conclusion, summarizes the findings of the doctoral project.

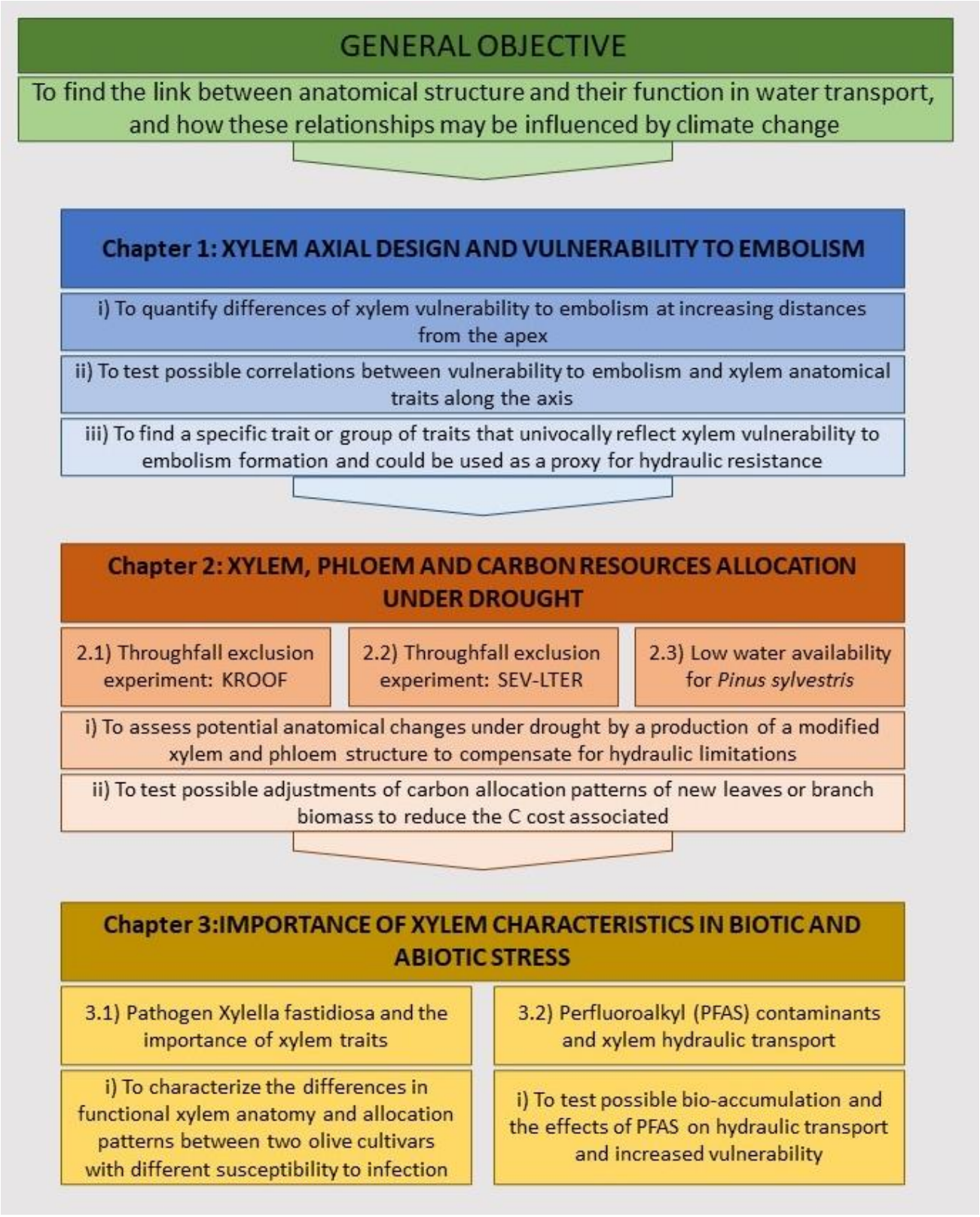

Figure A. Structure of the thesis with aims and objectives for every chapter.

GENERAL INTRODUCTION

Increased greenhouse effect is strongly influencing the average surface temperature of our planet. Over the last 50 years, temperature has risen by 1.1°C on average and future projections for the end of the century propose a temperature rise between 1.5°C and 5°C in the worst-case scenario (SRES, Special Report on Emission Scenarios AR6, IPCC 2022)). Temperature and greenhouse gases concentration are not the only changing components of our planet. In fact, sea level is rising, precipitation patterns and rivers runoff are changing, drought events are getting stronger, more frequent and lasting longer, and wind patterns and temperature have been modified (IPCC 2014, 2018). Since 2000, 11 of the 12 warmest years occurred in Europe, with an increased amount of extreme weather events and long-lasting droughts (Copernicus Climate Change Service 2020). Forest ecosystems are threatened by a changing climate with increasing intensity and frequency of drought events (Allen *et al*. 2010). Global climate changes are transforming also how acute and chronic droughts influence daily and seasonal temperatures, soil water content and atmospheric vapor pressure deficit, with a cascade of complex effects on trees' physiology and their response to the environment (Brodribb *et al*. 2020, McDowell *et al*. 2020). Drought plays a critical role in canopy desiccation and forest dieback in many biomes and ecosystems (Allen *et al*. 2010, 2015, Anderegg *et al*. 2019), but are often perceived as short and sudden events, which are the main cause of tree death. Nonetheless, mild drought conditions lasting consecutive years may strongly influence tree death, with clear announcing signals and symptoms, such as a reduction in distal and diameter growth and canopy desiccation (Carnicer *et al*. 2011, Cailleret *et al*. 2017). It is important to assess how much drought stress can be experienced by standing vegetation before productivity declines and mortality rises. Plant traits, both anatomical and physiological, are critical for the evaluation of vulnerability and responses to drought across species and ecosystems (Maherali *et al*. 2004, Engelbrecht *et al*. 2007).

The carbon dioxide needed to fuel photosynthesis comes with the trade-off of losing water from the leaves. Since producing sugars via photosynthesis is essential from plant life and functioning, the water required for this process becomes a crucial factor. Plants extract water from the soil and transfer it to the periphery of the canopy, up to the leaves. This water movement relies on a mechanism known as the 'cohesion– tension' (CT) theory (Dixon and Joly 1895). Through vessels and tracheids, which are lignified dead cells, trees generate a continuous water column between the soil and the leaves, which is kept under negative water potential. When water evaporates from the leaves, tension develops at the site of evaporation and pulls the entire water columns due to the cohesive strength between the water molecules and to their adhesion to the cell walls of xylem conduits. The role of the

hydraulic system in relation to plant function has long been recognized as one of the most essential components of life on the Earth (Melvin T. Tyree 2002, Boyer and Silk 2004, Brodribb 2009). However, transporting water under tension in a metastable state represent a threat for plants, as cavitation and embolism events can fill xylem conduits with gas phases, thus interrupting water transport. This phenomenon occurs when the tension of the sap inside a single conduit reaches a trigger point where the dissolved air expands and fill the vessel or tracheid. The tension increases when the water potential of the soil (Ψ, MPa) becomes more negative due to a reduced water content. When reaching critical Ψ levels, air is pulled from air-filled conduits into water filled conduits ("air-seeding" hypothesis), and if many of them become embolized, the transport of water becomes strongly limited until new conduits are produced or embolized ones are refilled (Hacke, Stiller, *et al*. 2001). In this scenario, the size and morphological characteristics of inter-conduit pits have a great role in avoiding embolism spread both for angiosperms and gymnosperms (Melvin T. Tyree 2002, Lens et al. 2013, Torres-Ruiz et al. 2016). The main consequence of embolized conduits is an overall reduction of hydraulic conductance, which may lead to stomatal closure, leaves dieback and lastly plant death (Tyree and Sperry 1989, Brodribb and Cochard 2009). After stomatal closure, plants start depleting carbon reserves and depending on the relative decrease of C assimilation, the carbon balance will be more or less affected. Prolonged stomatal closure will afterwards cause the depletion of C reserves (McDowell *et al*. 2008, 2011, Sala *et al*. 2010). The continuous depletion of stored carbon may lead to carbon starvation, which is strictly bonded with hydraulic failure (inability to deliver water to stomata for transpiration). These two phenomena, carbon starvation and hydraulic failure, do not occur independently and are strictly linked in causing trees' death (McDowell *et al*. 2011, Dickman *et al*. 2015).

It is possible to describe the water flow inside plants with the physical properties of its components. The overall flow is proportional to the total xylem conductance K, multiplied by the difference of water potential Ψ(ΔΨ, MPa) between soil and leaves. The hydraulic conductivity K(kg * s^{-1} MPa^{-1}) in Darcy's law ($F = \Delta\Psi \times K$) (Tyree and Ewers 1991a) is dependent on the contribution of every xylem conduit and the resistances between them. Hagen–Poiseuille's law has also been used to analyze the transport of water through xylem conduits (Tyree and Ewers 1991a, Melvin T. Tyree 2002). This law states that hydraulic conductivity K is proportional to the fourth power of the radius of the conduit (d), the fluid density (ρ) and viscosity (η) and the total number of conduits (Σ^n) ($K = \pi\rho/128\eta)\Sigma^n(d^4)$). Thus, small changes in xylem conduit diameter may result in great increases in the overall conductivity and efficiency of the system.

Ideally, plants should benefit from a transport system that is both efficient (high water transport capacity) and safe from embolism, but only a few studies have reported a clear trade-off between these traits so far (Gleason *et al*. 2016). One common result is relative to xylem conduits, which are narrower and more resistant to possible embolism formation in dry environments compared to wet environments where it is possible to find species harboring larger cells that increase conductivity but lower the overall safety (Pfautsch *et al*. 2016, Larter *et al*. 2017). These studies refer to the hypothesis of the so-called "safety vs efficiency trade-off", according to which there is an inverse relationship between hydraulic safety (conduit size) and hydraulic efficiency (K, Conductivity), leading to more resistance under dry conditions and faster growth with moist conditions (Sperry *et al*. 2008). On the contrary, some studies using different sampling approaches reported an increased efficiency and larger conduits in plant grown under drier conditions (Petit *et al*. 2016, Guérin *et al*. 2018a, Kiorapostolou and Petit 2018, Lechthaler *et al*. 2019). The two conductive tissues, xylem and phloem, are the physical link between the belowground and aboveground parts of the plants. Every year a new ring is made with an investment of carbon resources, but their plasticity under drought is still debated and with mixed results (Martínez-Sancho *et al*. 2017, Petit, Zambonini, *et al*. 2022). It is commonly expected that their phenotypic plasticity, along with the plasticity of photosynthetic biomass and carbon allocation, are the key for survival in short term acclimation to drought, which overall also determines acclimation potential of a species in a set environment.

Xylem and phloem, within every mature tree, follow a rigid axial design from the tip of the branches in the crown to the trunk base. This pattern is known as conduit widening and is considered to be the main driver of anatomical variation inside a plant (Anfodillo *et al*. 2012, 2013, Olson *et al*. 2014, Petit and Crivellaro 2014). The axial variation is found to follow a power scaling relationship ($Y = a \times X^b$) for both xylem (Anfodillo *et al*. 2013, Lechthaler *et al*. 2019) and phloem (Kiorapostolou and Petit 2018, Kiorapostolou *et al*. 2020, Petit, Zambonini, *et al*. 2022), with the b exponent usually between 0.1 and 0.3. In this equation, X and Y represent the functional and structural traits, while a and b are the allometric constant and the scaling exponent respectively. It was proposed in theory of optimality principles (West *et al*. 1999) that these trait relationships should converge towards a common scaling exponent, which exhibits the fundamental balance between structure and function in view of a stable and positive carbon balance (Anfodillo *et al*. 2016a). Eventual differences in the allometric constant "a" might be explained by different species strategies or by modification in the absolute proportion of traits (e.g. needle biomass over branch biomass) within the same species in distinct environments (Weiner 2004). This axial widening of the conductive tissues is found in branches (Petit *et al*. 2016) and the stem (Anfodillo *et al*. 2013) with a rapid increase in size in the first few meters, and slowly decrease downwards to the base (Mencuccini *et al*. 2007, Petit *et al*.

2010). Hydraulic architecture and conduit widening could explain physical limits and optimization of the water transport in vascular plants: higher tensions (lower Ψ) are usually found in leaves and apical shoots characterized by smaller conduits, while larger conduits occur at the trunk base where the tensions are lower (Tyree and Sperry 1989).

Despite the importance of conduit widening for the understanding of anatomical patterns and differences, there are many studies in the literature that are fixing the sampling by age or diameter during the sampling procedure. These studies usually confirm the hypothesis of a clear anatomical trait adaptation for trees living in different environments. Normalizing anatomical data by path length/distance from the apex show a completely different scenario, with limited or no plasticity for xylem conduits at the stem base in different precipitation gradients (Fajardo *et al*. 2020), in increasing vapor pressure deficit gradients (Olson *et al*. 2020) or in branches under drought conditions (Petit, Zambonini, *et al*. 2022). The production of a more resistant xylem would mean an increased cost due to elevated C investment for producing a higher number of smaller cells, otherwise having larger and fewer conductive elements would be translated into a smaller investment of carbon for the same total xylem conductance but with higher risk of embolization and consequently a higher PLC in case of stress. For these reasons, the rigid axial configuration was proposed to be the best possible solution for the 3 factors trade-off (safety, efficiency and C utilization) in which gain-cost is maximized to have enough xylem hydraulic conductance for a given C investment with safety high enough to prevent embolism (Mencuccini *et al*. 2007). Therefore, the aim of this doctoral project is to find a clear link between structure and function of the hydraulic architecture of trees and to unravel how climate change may push phenotypic plasticity responses. All the experimental works will always consider the axial design and patterns of xylem, phloem, and carbon allocation.

Chapter 1

XYLEM AXIAL DESIGN AND VULNERABILITY TO EMBOLISM

"Pit anatomy and tracheid diameter vary in tandem from stem apex to base and determine a strong decrease in xylem embolism resistance basally"

Abstract

Climate change is pushing the need for rapid assessment of plant vulnerability to drought stress. Vulnerability to embolism is resulting from a combination of anatomical and physiological characteristics of a given species. In this experiment, we assessed the match between xylem vulnerability to embolism formation and its anatomical properties within trees, from the apical-most part of the crown to the trunk base. One mature tree of *Picea abies* and one *Abies alba* were cut, and more than 20 wood samples collected at different distances from the stem apex. We measured consecutive losses of conductivity at different water potential and obtained vulnerability curves (VCs) and P50s (water potential inducing 50% loss of hydraulic conductance). On the same samples, we analysed through anatomical measurements all the cells contributing to water transport. Finally, vulnerability curves were reconstructed with anatomical data, by fitting anatomically derived P50s with their water potential of cavitation, to verify if conduit diameter (Dh) could explain the P50 at a given distance from the apex. Results show a clear pattern of P50, Dh, and pit size along the main axis of the tree. P50 inversely correlates with conduit diameter and pit margo area in both species. The reconstruction of VCs with anatomical data showed that tracheid's size (from the largest to the smallest) and their class frequency distribution are good proxies of hydraulic vulnerability. We conclude that there is a clear and strong structure-function relationship, with P50 being a highly variable trait across the tree, due to different anatomical patterns.

1.1) Introduction

Our planet is facing an extraordinary rapid shift in climate, with increased temperatures and modified patterns of precipitation, which are both leading to changes in species distribution and survival across different environments (IPCC 2014, 2018). The assessment of trees vulnerability to climate change stressors have become fundamental and a broadly discussed topic in scientific communities. Vulnerability to low water availability conditions, though, is a complex species-specific attribute which results from a combination of physiological and anatomical traits, further influenced by environmental parameters. For plant scientists, vulnerability to drought is commonly expressed with the risk of embolism formation in the xylem, which affect hydraulic conductivity leading to plant desiccation (McDowell et al. 2008, Brodribb and Cochard 2009, Choat *et al*. 2012).

Water transport in plants is essential to hydrate the leaves to allow the maintenance of stomatal conductance and photosynthesis (Dixon and Joly 1895). Evolution pushed towards an efficient way of water transport to sustain high rates of carbon fixation (Pittermann 2010). The xylem is the tissue responsible of the water movement from the roots to the highest leaf of the canopy. It consists of dead cells at maturity with lignified cell walls (vessels in angiosperms, tracheids in gymnosperms) and tubular-pipe structure, interconnected by pit membranes, i.e. microscopic pores which allow water movement between conduits (Hacke and Sperry 2001) When water is lost in transpiration processes at leaf level, the water potential (Ψ, -MPa) difference between leaves and soil increases and increase water movement upwards in xylem conduits from the roots. The precarious state of water columns can reach a critical tension which triggers cavitation in the tissue, i.e. a sudden change of the water state from liquid to gas (Sperry 2000). Air bubbles may spread inside the xylem conduits preventing water movement and later leading to a remarkable reduction of the total hydraulic conductance (Cochard, 2006; Hacke & Sperry, 2001). The loss of water transport capacity is usually measured as percentage loss of hydraulic conductivity (PLC) in relation to the water potential Ψ at which the loss is happening. Continued losses of conductivity can drastically influence the water transport and even lead to hydraulic failure and in some cases, death (Brodribb and Cochard 2009). One of the most commonly used traits obtained from vulnerability curves (VCs, plots of PLC and xylem Ψ) is the P50 and reflects the xylem water potential causing 50% loss of the hydraulic conductance. P50 was widely investigated and used to compare the resistance to drought-induced embolism formation among species and individuals (Gleason *et al*. 2016). Plants should benefit from a transport system that is both efficient (high water transport capacity) and safe from embolism (more negative P50 values), but only a few studies reported a clear trade-off between these traits. Investigating the relationship

between structural and functional traits (anatomical characteristics and vulnerability to embolism formation, respectively) is fundamental in order to highlight a possible trade-off.

In particular, species with narrow conduits and less vulnerable to embolism formation were found in dry climates, compared to wet/humid habitats where larger cells, potentially more vulnerable, were found (Pfautsch *et al*. 2016, Schuldt *et al*. 2016, Larter *et al*. 2017). This "trait adaptation" was hypothesised by studies that generally standardised the sampling protocol for age of the wood sampled or using branch diameter. Yet, this fixed, punctual sampling neglects the variation of hydraulic structures along the main axis of the xylem from tip to base which display a clear conduit widening (Anfodillo *et al*. 2006, 2013, Olson *et al*. 2014, Petit and Crivellaro 2014, Lazzarin *et al*. 2016, Pfautsch *et al*. 2018). In fact, conduits widening inside the xylem tissue was found both in stems and branches (Anfodillo *et al*. 2013, Petit *et al*. 2016). In particular, it shows a prompt and quick increase in the first 2 meters from the tip, then gradually decreases in magnitude until reaching a plateau (Mencuccini *et al*. 2007, Petit *et al*. 2010). Widening of hydraulic components was observed also in interconduit pits, differing in size and magnitude from species to species (Lazzarin et al. 2016, Rosell et al. 2017, Held et al. 2021). Hydraulic architecture and conduit widening might explain physical limits and optimization of the water transport in vascular plants: higher tensions (lower Ψ) are usually found in leaves and apical shoots characterized by smaller conduits, while larger conduits are found at the trunk base where the tensions are lower (Tyree and Sperry 1989). At whole-tree level, there is not a continuous widening of the conduits but appears to be segmented in the different morphological levels (roots, trunk, leaves) and found within each (Atala and Lusk 2008, Nygren and Pallardy 2008, Lintunen and Kalliokoski 2010). If conduits size and pits properties display great variation along the axis, we can therefore hypothesize that sampling at different distances from the apex could influence the VCs and P50 values, which should vary accordingly.

Hundreds of reports on xylem vulnerability to embolism formation of different species can be found in the literature, but most of them focused on one vulnerability trait (e.g. P50) which was analyzed only in one organ (leaf, apical shoot, root, Choat *et al.*, 2012; Gleason *et al.*, 2016; Savi *et al.*, 2019). Few studies performed simultaneously VCs on different organs of the same individual (Savi *et al*. 2016, Losso *et al*. 2019, Rosner *et al*. 2019) and even fewer accomplished to find a match between anatomical traits and function for specific organs (Domec and Gartner 2001, McElrone *et al*. 2004, Sperry *et al*. 2006, Blackman *et al*. 2010, Pittermann *et al*. 2010, Lens *et al*. 2011). Cai & Tyree (2010) have suggested the link between P50 and conduits diameter classes, Wheeler et al. (2005) pointed out the importance of analysing the largest pores per conduit, and several authors correlated P50 with wood density and/or maximum vessel length (Markesteijn *et al*. 2011). In this study we aim

to fill the knowledge gap between structure and function by measuring the resistance to embolism formation and anatomical traits in more than 20 sampling points from the most apical shoot to the trunk base along the main tree axis. We used a framework similar to those proposed by Domec & Gartner (2001), and advanced it by trying to reconstruct vulnerability curves by using anatomical data. Specifically, the objectives were to:

i) quantify differences of xylem vulnerability to embolism at increasing distances from the apex
ii) verify possible correlations between vulnerability and xylem anatomical traits along the main axis.
iii) find a specific anatomical trait, or a bunch of traits and their relation that univocally reflect the xylem vulnerability to embolism formation and hence could be used as fast and reliable proxy for the estimation of hydraulic resistance to embolism formation under drought.

1.2) Materials and methods

Experimental design and sample preparation

In May 2022, two conifer species were selected for the experiment. One silver fir (*Abies alba* Mill.) was fallen in Asiago (Italy) and one Norway spruce (*Picea Abies* Karst.) in Enicklberg forest, (Niederösterreich, Austria). Both trees were mature and about 25 m high. From the fallen trees, ~20 cm thick circular discs were harvested at known distances from the apex (DFA, Table 1.1). Bark and phloem were removed, the samples inserted in labeled black plastic bags with wet paper and transported to the laboratories. The discs were reduced to about 3 x 5 cm wide longitudinal segments of the most outer wood portion. The most apical samples with round shapes (branches, < 1 cm in diameter) were not further processed. All the segments were vacuum sealed and stored in freezer at -20°C. 24 hours prior to the measurements, the segments were defrosted in distilled water, carefully split along the grain in smaller pieces and re-cut. The final samples for the measurements were about 0.8 x 0.8 x 14 cm long sticks (with usually 3 of the outermost conductive rings), which were smoothed with microtome blades while keeping them constantly wet. The samples were re-saturated overnight under low-vacuum at room temperature while immersed in filtered distilled water (Hietz *et al*. 2008) containing silver ions (Micropure, Katadyn Products, Wallisellen, Switzerland) to avoid microbial growth and contamination. This method was used to re-hydrate the tissues and refill conduits of the sapwood (Rosner *et al*. 2018, 2019).

Vulnerability Curves – VCs wit air-injection technique

Low-vacuum was released and samples were re-cut again under water at both ends with sharp razor blades. Sapwood conductive area and sample length were measured at full hydration. Samples were then connected to the water reservoir and initial hydraulic conductivity was measured gravimetrically under a hydraulic pressure head of 8 kPa (0.8 m water column) by collecting the sap at the distal end using pre-weighted vials (five vials, 30 seconds interval). The first value obtained was addressed as maximum flow at full hydration or P = 0 (K_{max}). After disconnecting the segments from the tubing, they were quickly dried with paper and weighed (SW, saturated weight) with a precision balance (resolution 0.0001 g). Then, overpressure of 0.5 or 1 MPa (for basal or apical samples, respectively) was applied with a double-ended pressure collar (PMS Instruments, Corvallis, OR, USA) for 1 minute (Rosner *et al*. 2019). After drying, the fresh weight (FW) was recorded, and the samples allowed to equilibrate in water for 15/20 minutes. Afterwards, samples were re-connected to water reservoir and conductivity (K) was measured again as described above. The percent loss of conductivity (PLC, %) was calculated as $100 \times [1- (K / K_{max})]$. The pressurization in the chamber was gradually increased with steps of 0.5 or 1 MPa. The air-injection was always followed by FW and K measurements, until the percentage loss of conductivity (flow) was above 90%. Values of the applied positive pressure (=Ψ) and percentage loss of conductivity (PLC) were used as input in the fitplc package for R (Duursma and Choat 2017) to obtained vulnerability curves (VCs). P12, P50, and P88 (i.e. the Ψ inducing 12, 50 or 88% loss of conductivity) were interpolated.

Xylem anatomy

The samples used for the elaboration of VCs, were anatomically analyzed. A 2 cm long central segment was cut from each sample and rehydrated. A rotary microtome LEICA RM2245 (Leica Biosystems, Nusslock, Germany) was used to obtain 10-12 µm thin slices. Multiple transverse and radial sections were cut and stained with a solution of AstraBlue and safranin (0.5% and 1% in distilled, deionized water respectively). After staining, glass slides were permanently fixed with Eukitt mounting medium (BiOptica, Milan, Italy) and scanned at 100x resolution with Axioscan7 (Carl Zeiss Microscopy GmbH, Germany). Transverse sections were analyzed with ROXAS software (von Arx and Carrer 2014) and the totality of the cells of the samples were measured (30-100 thousand cells per sample). Lumen area (LA, μm^2) was obtained for every cell, hydraulically weighted mean conduit diameter (Dh, µm) and hydraulic conductivity of the section (Kh, $m^4 s^{-1} MPa^{-1}$), given by the sum of the conductivities of the individual cells calculated with Hagen-Poiseuille formula (Tyree & Ewers, 1991). Pit average area was obtained on the radial sections with ImageJ (National Institutes of Health, Bethesda, MD, USA) by drawing the pit aperture outline on 30-50 pits per sample.

Statistical analysis and reconstruction of VC from anatomy

Statistical analysis was carried out to test regression of the traits along the distance from the apex (DFA). We also tested differences between the two species for the allometric scaling of anatomical and physiological traits. Models were fitted with restricted maximum likelihood (REML) by using lme4 package in R (Bates *et al*. 2015). Each trait was tested for the fixed effect of DFA, species and their interaction, using Akaike Information Criterion (AIR) to choose for the best fitting model (Zuur *et al*. 2009).

The second part of the experiment consisted in the reconstruction of vulnerability curves made with single tracheid lumen area data. We compared the hydraulic conductivity obtained from the physiological measurements (Kp from VC) with the hydraulic conductivity given by ROXAS as the sum of every tracheid using Hagen-Poiseuille (Ka). A strong relation between Ka and Kp was found and we decided to use Hagen-Poiseuille to calculate the individual tracheid conductivity from every section. The cumulated sum of individual conductivities was used to assign to every cell its percentage loss of conductivity in case of embolization. ROXAS also provides data on the average diameter (D) that is contributing to a certain percentage of the total hydraulic conductivity (e.g. the diameter contributing to 5%, 12%, 50%, 88% of Kh). Using the relationship between D (diameter) and P (water potential at which is lost a certain amount of conductivity, obtained from fitplc), we tested and found that P5-D5 better explains the fitting and the first inflection point of the vulnerability curves. The final step consisted in ordering the cells from the largest to the smallest in every sample, calculating the conductivity (K) for each one. Then, we performed a cumulated sum of the single cell conductivities and assigned a percentage loss of conductivity (PLC) based on their contribution to the total. To every PLC was afterwards assigned a water potential Ψ inducing embolism formation, based on the P5-D5 relationship. Due to the higher computational power needed to handle ~2million cells we used MATLAB software (MATLAB R2019b, The MathWorks Inc, Natick, Massachusetts) for plotting and re-fitting vulnerability curves based on anatomical data.

1.3) Results

Vulnerability curves

VCs performed at different distances from the apex (DFA) showed a clear pattern of vulnerability along the xylem. In general, the samples (with ~3 conductive xylem rings) were more resistant closer to the treetop and their vulnerability increased sharply in the first two meters of DFA, reaching the maximum around 10 meters from the apex. In the most apical part of the crown, P50 values of about -4 MPa and -5.5 MPa were measured for *Picea abies* and *Abies alba*, respectively (Table1.1). Both species increased vulnerability to embolism moving downwards to the trunk base and reached a P50 value of -2.2 MPa for fir and -1.5MPa for spruce. To better highlight the pattern of decrease in P50, we selected 4 sampling points at similar DFA for both species (Figure 1.1A, B). The scaling of P50s along the main axis of the xylem decreased similarly for both species (Figure 1.2) but within different ranges. The scaling of the power relationship between P50 and DFA was significantly different for y-intercept, but not for the b exponent in the equation $Y = a * X^b$ (Figure 1.2, Table 1.2).

TABLE 1.1 Variation in P50 (-MPa) with the distance from the branch apex (DFA) in *Picea abies* (red) and in *Abies alba* (green). P50s are obtained from the vulnerability curves with fitplc package in R.

DFA (cm)	P50 (-MPa)	Species	DFA (cm)	P50 (-MPa)	Species
30	4.06	*Picea abies*	32	5.24	*Abies alba*
34	4.11	*Picea abies*	46	5.52	*Abies alba*
45	4.03	*Picea abies*	85	4.26	*Abies alba*
50	4.02	*Picea abies*	110	4.29	*Abies alba*
60	3.63	*Picea abies*	150	2.72	*Abies alba*
67	3.38	*Picea abies*	255	3.22	*Abies alba*
78	3.57	*Picea abies*	290	3.14	*Abies alba*
102	3.36	*Picea abies*	340	3.13	*Abies alba*
115	3.45	*Picea abies*	480	3.32	*Abies alba*
175	3.01	*Picea abies*	620	2.8	*Abies alba*
187	3.01	*Picea abies*	760	3.09	*Abies alba*
205	3	*Picea abies*	970	3.2	*Abies alba*
235	2.92	*Picea abies*	1490	2.22	*Abies alba*
250	2.97	*Picea abies*	2270	2.53	*Abies alba*
403	2.55	*Picea abies*	2530	2.37	*Abies alba*
707	1.85	*Picea abies*	2790	2.68	*Abies alba*
1011	1.57	*Picea abies*			
1315	2.19	*Picea abies*			
1467	1.86	*Picea abies*			
1619	1.64	*Picea abies*			
1771	2.27	*Picea abies*			
1903	1.48	*Picea abies*			
2379	1.66	*Picea abies*			

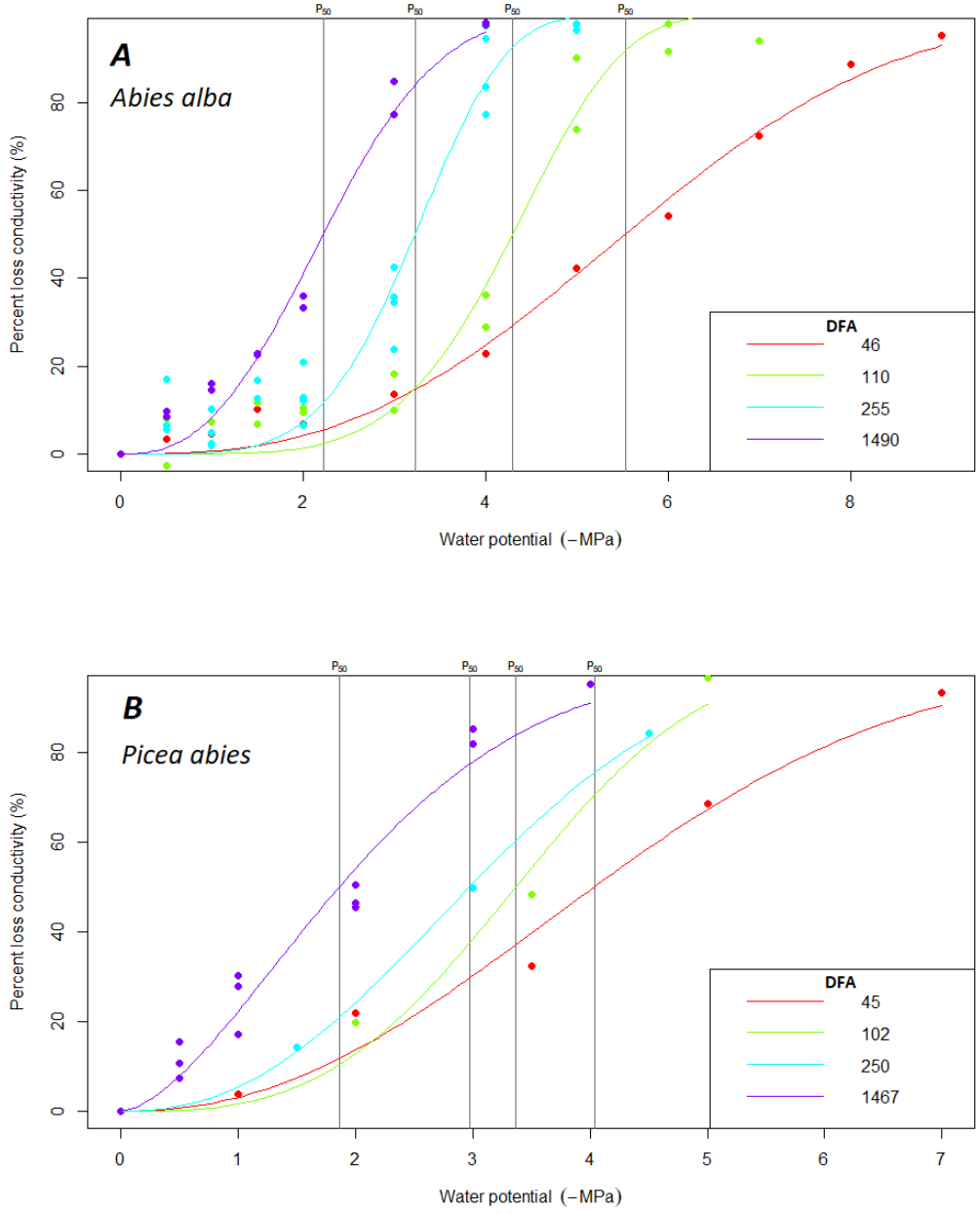

Figure 1.1 A, B Vulnerability curves obtained with air injection technique on woody segments sampled at different distances from the apex of *Abies alba* (A) and *Picea abies* (B) trees. Four points with similar distance from the apex (DFA) were selected: 45/46cm, 102/110cm, 250/255cm, 1467/1490cm. If the circular section allowed multiple segments extraction, more replicates were taken. Regression lines were fitted with fitplc package in R.

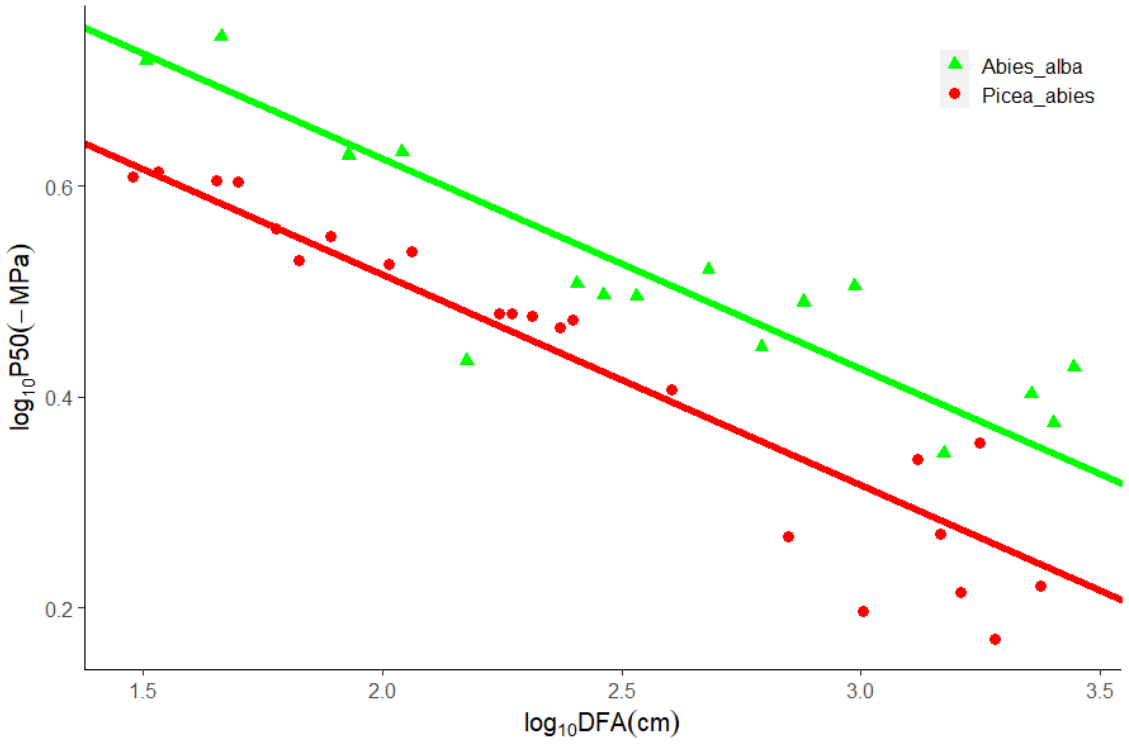

Figure 1.2 Variation in P50 (-MPa) with the distance from the branch apex (DFA) in Abies alba (green triangles) and in Picea abies (red dots). Fitting lines (solid green line for Abies and solid red line for Picea) are according to models in Table1.2. P50s were interpolated with fitplc package in R.

Xylem anatomy

Anatomical results showed a stable and clear axial pattern from the apical-most part of the crown to the trunk base for both mean hydraulically weighted conduit diameter (Dh, Figure 1.3) and pit margo area (PIT_{area}, Figure 1.4). The statistical models showed that the exponent of scaling is the same for both species (same b exponent in the equation $Y = a * X^b$), while different y-intercept and larger cells were found in *Abies alba* (Table 1.2). The pit area followed a pattern similar to that of Dh, with an increase in size from tree tip toward the base (Figure 1.4), but without differences between species. The exponent was the same for both species, but they differed in the proportion between conduit diameter and pit size (Figure 1.5). Unlike for hydraulic diameter, larger pit area was found in *Picea abies* compared to *Abies alba* at the same hydraulic diameter size (Figure 1.5, Table 1.3).

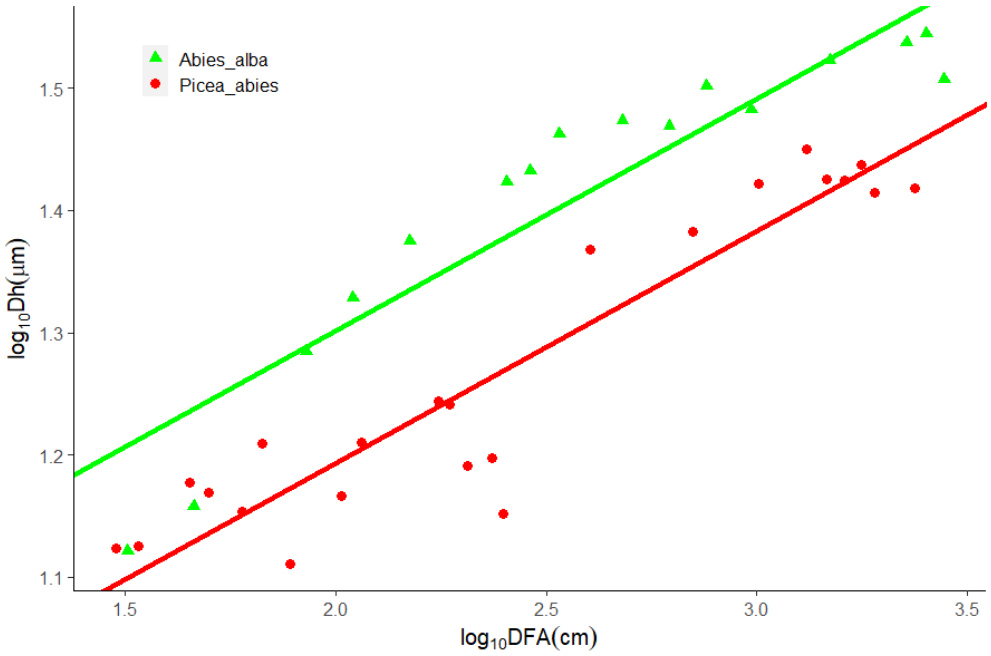

Figure 1.3 Variation in conduit mean hydraulic diameter (Dh, µm) with the distance from the branch apex (DFA) in Abies alba (green triangles) and in Picea abies (red dots). Fitting lines (solid green line for Abies and solid red line for Picea) are according to models in Table1.2. P50s were interpolated with fitplc package in R.

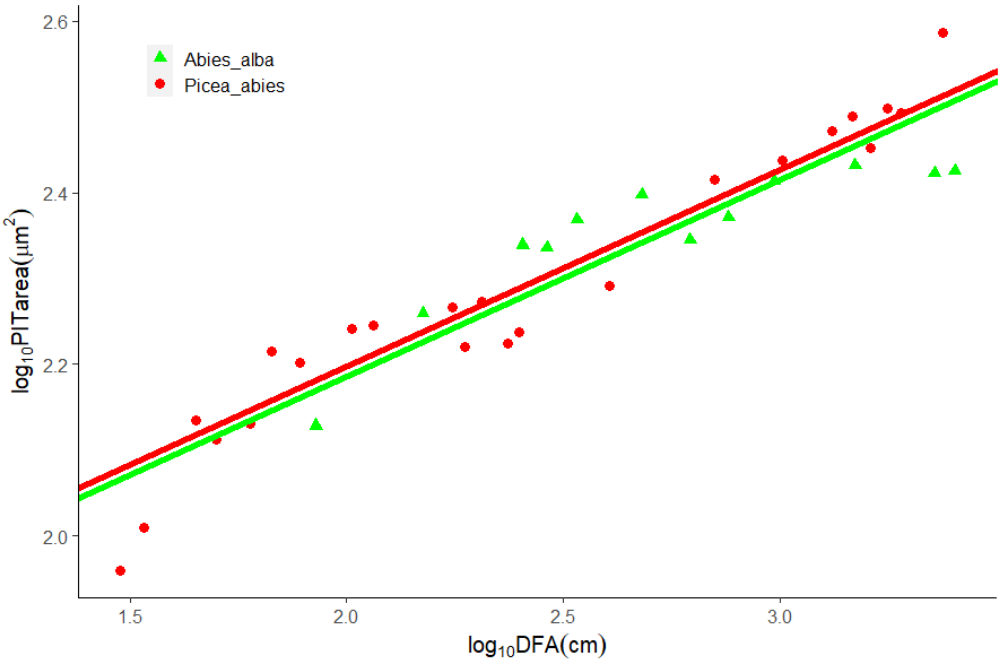

Figure 1.4 Variation in pit margo area (PIT_{area} , μm^2) with the distance from the branch apex (DFA) in Abies alba (green triangles) and in Picea abies (red dots). Fitting lines (solid green line for Abies and solid red line for Picea) are according to models in Table1 .2.

TABLE 1.2 Results of the optimal linear mixed-effect models predicting the effects of $log_{10}DFA$ and *Species* on (A) $log_{10}P50$, (B) $log_{10}Dh$ and (C) $log_{10}PIT_{area}$. Sample ID was used as random factor in all models. Asterisks indicate different estimates with significance at ** = $p < .05$, or at * = $p < .1$.

	(A) log10(P50)		(B) log10(Dh)		(C) log10(PIT_{area})	
Predictors	*Estimates*	*p*	*Estimates*	*p*	*Estimates*	*p*
(Intercept)	1.03	**<0.001**	0.92	**<0.001**	1.73	**<0.001**
DFA [log10]	-0.20	**<0.001**	0.19	**<0.001**	0.23	**<0.001**
Species [Picea abies]	-0.11	**<0.001****	-0.11	**<0.001****	0.01	0.484
Random Effects						
σ^2	0.00		0.00		0.00	
τ_{00}	0.00 $_{ID}$		0.00 $_{ID}$		0.00 $_{ID}$	
ICC	0.96				0.78	
N	37 $_{ID}$		37 $_{ID}$		34 $_{ID}$	
Observations	39		39		35	
Marginal R^2 / Conditional R^2	0.848 / 0.995		0.899 / NA		0.894 / 0.977	

Link between hydraulics and anatomy

Data from vulnerability curves and anatomy were combined to find and test possible structure-function relationships and to check for significance. Values of P50, Dh and pit area were assessed at different distances from the apex (DFA). P50 was strongly correlated with mean hydraulically weighted conduit diameter (Dh) and pit size. In particular, P50 increased at the increase in conduit size (Figure 1.6). This increase in vulnerability scaled with hydraulic diameter with an exponent of -1 for both species. However, the magnitude of increase in vulnerability was different in the two species, due to a likely combination of both conduit and pit size. Accordingly, in the more vulnerable *Picea abies* (less negative P50 at the apex) larger pits were found (Figure 1.5).

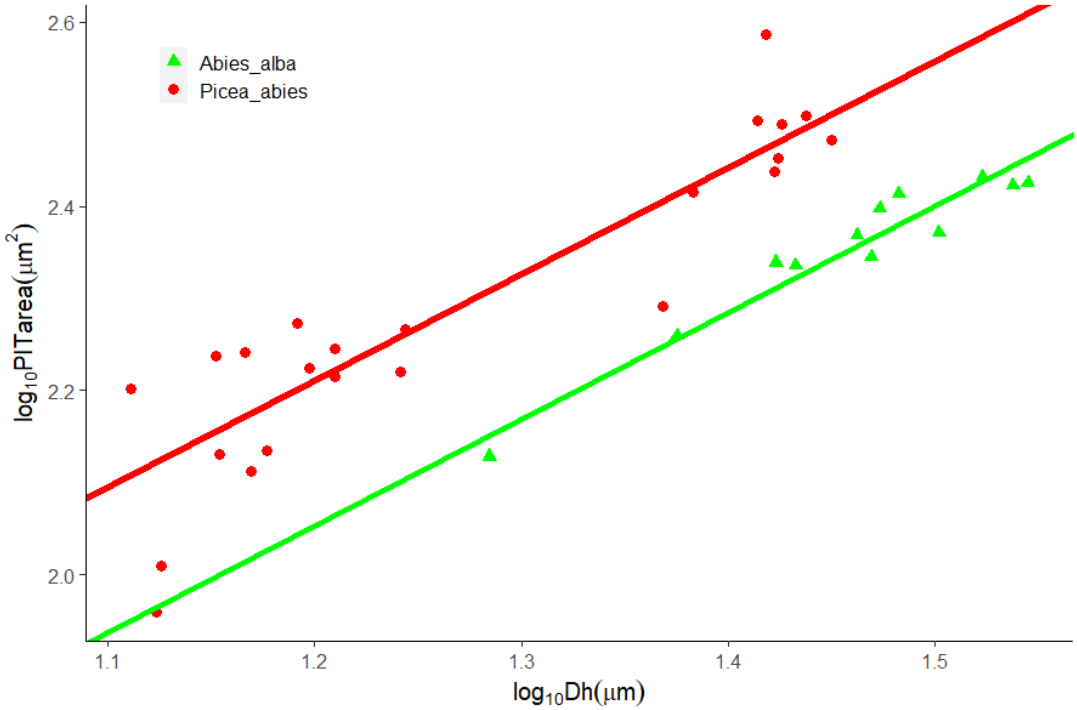

Figure 1.5 Variation in pit margo area (PIT_{area} , μm^2) with the conduit mean hydraulic diameter (Dh, µm) in Abies alba (green triangles) and in Picea abies (red dots). Fitting lines (solid green line for Abies and solid red line for Picea) are according to models in Table1.3.

TABLE 1.3 Results of the optimal linear mixed-effect models predicting the effects of $\log_{10}Dh$ and *Species* on (A) $\log_{10} PIT_{area}$, (B) $\log_{10}P50$. Sample ID was used as random factor in all models. Asterisks indicate different estimates with significance at ** = $p < .05$, or at * = $p < .1$.

	(A) log10(PIT_{area})		**(B) log10(P50)**	
Predictors	*Estimates*	*p*	*Estimates*	*p*
(Intercept)	0.66	**<0.001**	1.88	**<0.001**
Dh [log10]	1.16	**<0.001**	-0.97	**<0.001**
Species [Picea abies]	0.16	**<0.001****	-0.22	**<0.001****
Random Effects				
σ^2	0.00		0.00	
τ_{00}	0.00 $_{ID}$		0.00 $_{ID}$	
ICC	0.79			
N	34 $_{ID}$		37 $_{ID}$	
Observations	35		39	
Marginal R^2 / Conditional R^2	0.842 / 0.967		0.828 / NA	

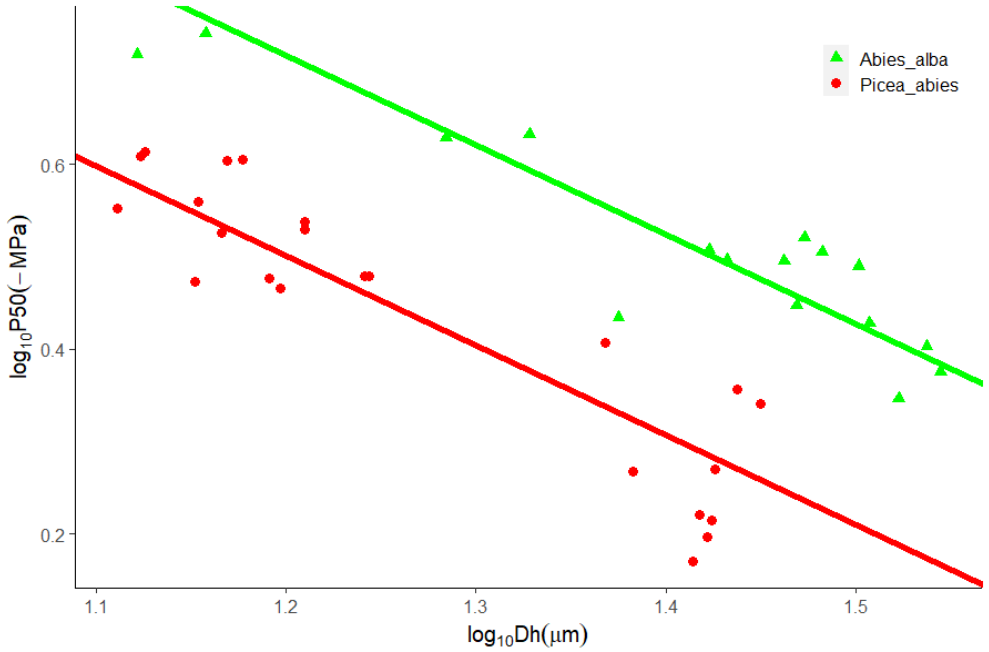

Figure 1.6 Variation in loss of 50% of conductivity (P50, -MPa) with the conduit mean hydraulic diameter (Dh, µm) in Abies alba (green triangles) and in Picea abies (red dots). Fitting lines (solid green line for Abies and solid red line for Picea) are according to models in Table1.3.

Link between anatomy and the reconstructed hydraulics

The increase in xylem conduit diameter from tip to base drastically increase the hydraulic conductivity. To reconstruct vulnerability curves based on anatomical data, i) the theoretical hydraulic conductivity (Ka) was calculated using data of cell size and distribution, as well as ii) the theoretical water potential of embolism formation in every cell. Specifically, since the conductance scales with the fourth power of the radius, the average diameter of xylem conduits was used to calculate the theoretical hydraulic conductivity (Ka) following Hagen-Poiseuille equation. The relationship between the hydraulic conductivity from hydraulic measurements (Kp) and Ka is shown in Figure 1.7. The water potential inducing embolism formation for every cell was estimated from the relation between the average diameter (D) contributing to a percentage of the total hydraulic conductivity (Ka, from anatomy) and the water potential at which the same conductivity was lost in the VC (P). Figure 1.8 report the correlation between P5 and D5, with an exponent b = -1.45 (Figure 1.8).

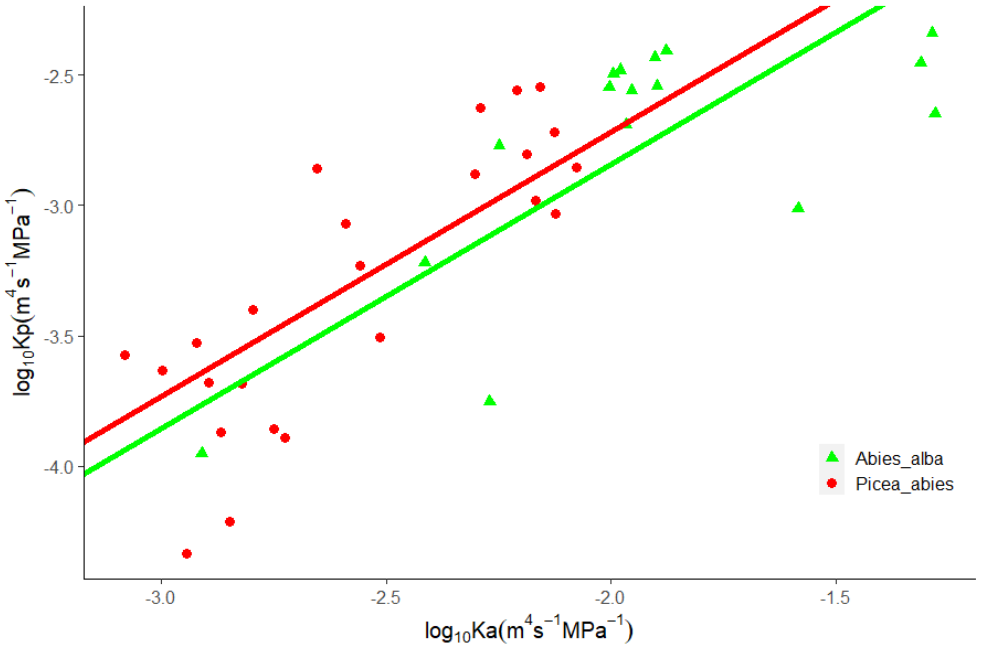

Figure 1.7 Variation in hydraulic conductivity obtained with flow measurements (Kp, VCs analyses) and anatomical measurements and Hagen-Poiseuille law (Ka). Green triangles and red dots show data of *Abies alba* and *Picea abies*, respectively. Fitting lines (solid green line for Abies and solid red line for Picea) are according to models in Table1 .4.

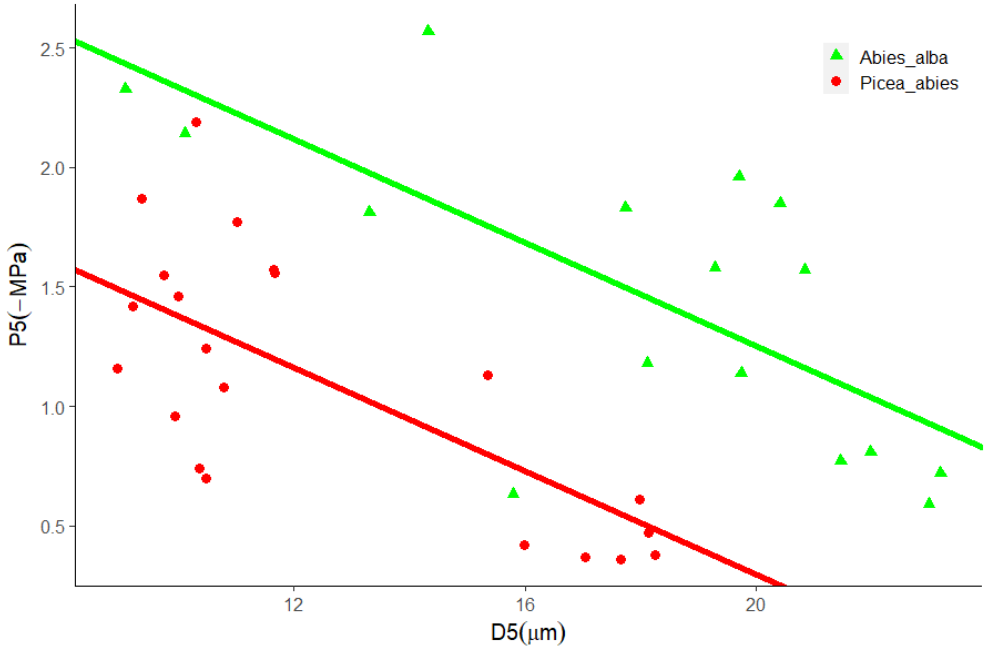

Figure 1.8 Correlation between water potential at which 5% of the hydraulic conductivity is lost (P5, hydrau lic measurements) and the diameter contributing to 5% of the total theoretical hydraulic conductivity (D5, anatomical analyses). Green circles and red triangles show data of *Abies alba* and *Picea abies*, respectively. Fitting lines (solid green line for Abies and solid red line for Picea) are according to models in Table 1.5. P5s were interpolated using fitplc package in R and D5 measured with ROXAS.

TABLE 1.4 Results of the optimal linear mixed-effect models predicting the effects of $\log_{10}$*Ka* and *Species* on $\log_{10}$ *Kp*. Sample ID was used as random factor in all models. Asterisks indicate different estimates with significance at ** = $p < .05$, or at * = $p < .1$.

	log10(Kp)	
Predictors	*Estimates*	*p*
(Intercept)	-0.81	**0.009**
Ka [log10]	1.01	**<0.001**
Species [Picea abies]	0.12	0.390
Random Effects		
σ^2	0.05	
$\tau_{00\ ID}$	0.06	
ICC	0.57	
$N_{\ ID}$	39	
Observations	40	
Marginal R^2 / Conditional R^2	0.649 / 0.851	

TABLE 1.5 Results of the optimal linear mixed-effect models predicting the effects of $\log_{10}$*D5* and *Species* on $\log_{10}$ *P5*. Sample ID was used as random factor in all models. Asterisks indicate different estimates with significance at ** = $p < .05$, or at * = $p < .1$.

	P5	
Predictors	*Estimates*	*p*
(Intercept)	3.42	**<0.001**
D5	-0.11	**<0.001**
Species [Picea abies]	-0.96	**<0.001****
Random Effects		
σ^2	0.18	
$\tau_{00\ ID}$	0.00	
$N_{\ ID}$	36	
Observations	37	
Marginal R^2 / Conditional R^2	0.530 / NA	

Figure 1.9 shows the reconstruction of vulnerability curves based on anatomical data. All cells found in the cross section were ordered from the largest to the smallest, and the hydraulic conductivity (Kh) was calculated for each cell as described above. For each cell, Kh was then transformed to PLC, based on the single cell contribution of conductivity compared to the total. With the water potential Ψ obtained from the relation in Figure 1.8, to every cell was also assigned its water potential of cavitation. Anatomical VCs fit well the hydraulic measurements and this match is found at different distances from the apex (Figure 1.9). The P50 were interpolated from the VCs reconstructed with anatomical data (P50a). Figure 1.10 reports the correlation between the P50 values interpolated from hydraulic VCs and those reconstructed with anatomical data, showing a high predictive quality (Figure 1.10).

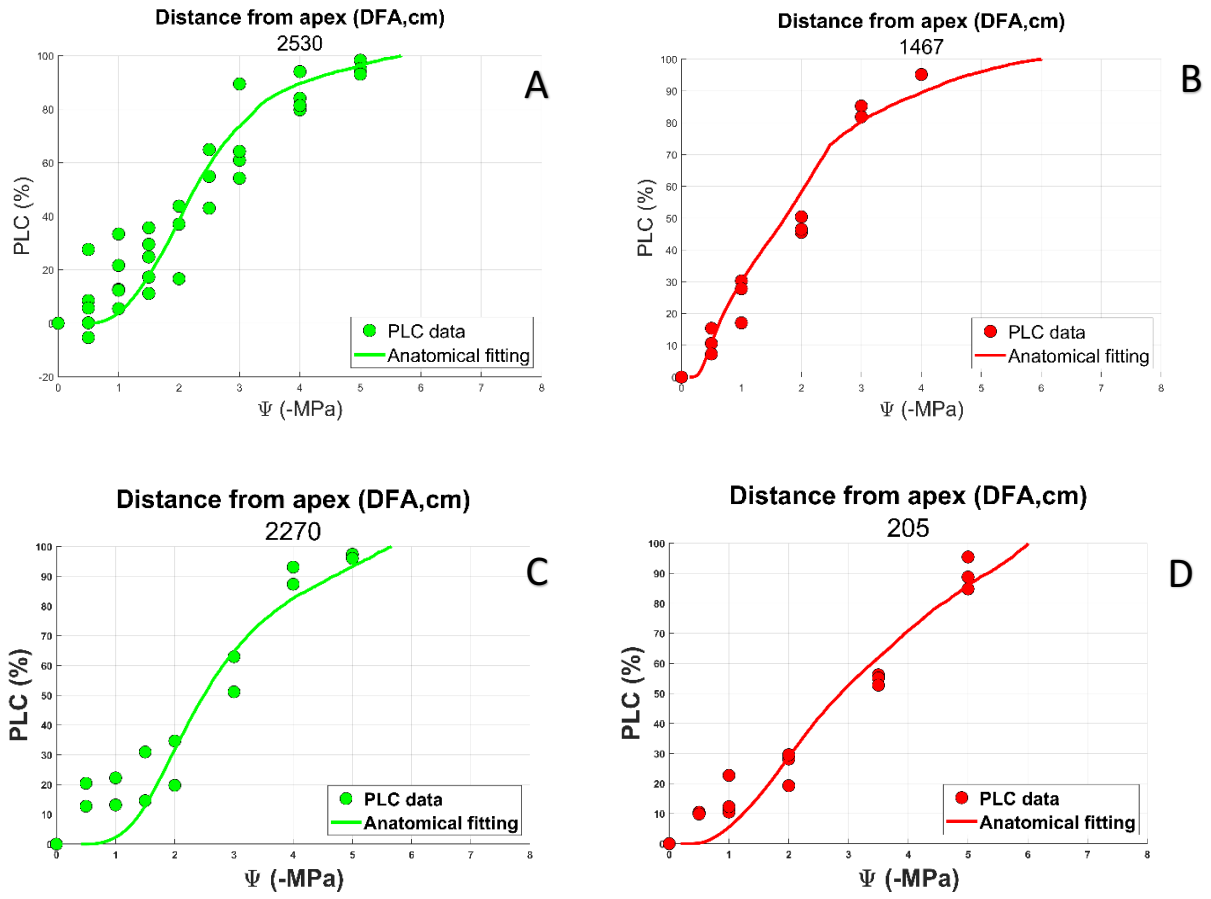

Figure 1.9 VCs reconstructed by using anatomical data (green and red for Abies and Picea, respectively) at different distances from the apex in *Abies alba* (green) and *Picea abies* (red). A = 2530cm of DFA, B = 1467cm of DFA, C = 2270cm of DFA, D = 205cm of DFA Green and red-filled circles are the actual measurements of the vulnerability curves obtained with the air injection technique.

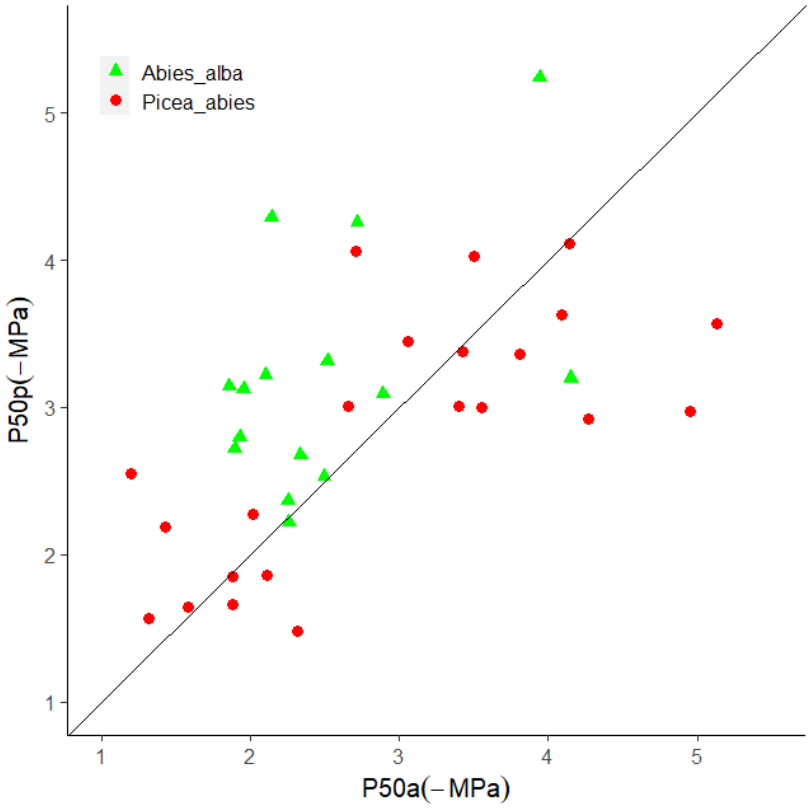

Figure 1.10 Relationship between the P50p (-MPa) interpolated from hydraulic vulnerability curves and the P50a (-MPa) obtained from the VCs reconstructed by using anatomical data in *Abies alba* (green triangles) and *Picea abies* (red dots). 1:1 line is plotted for comparison.

1.4) Discussion

Vulnerability curves followed by anatomical analyses were performed to understand the variation of vulnerability to embolism formation along the main axis of the tree and its relationship with xylem structure. We tested possible differences in xylem vulnerability at different DFA and verified whether the differences in vulnerability are associated with xylem anatomical traits along the main axis. Finally, we found a match between physiological and anatomical traits and attempted the reconstruction of VCs using only conduits lumen diameter and distribution from anatomy.

Vulnerability along the main axis

The assessment of vulnerability curves along the main axis of the xylem revealed a clear pattern of increased vulnerability moving downwards from the tree apex (main axis and top branches) to the trunk base. Our study species showed high resistance to embolism formation in the apical-most samples (-4 and -5.5 MPa for *P. abies* and *A. alba*, respectively). Despite a difference of about 1.5MPa at the treetop, the P50 values at the trunk base decrease substantially at the same rate in the two

species and reached -1.5MPa and -2.2 MPa for *P. abies* and *A. alba*, respectively. As expected, the higher safety to drought-induced embolism formation was observed at the top of the trees, where the lowest water potentials along the hydrostatic gradient are generally measured. The difference of P50 between top and bottom of the tree is remarkably wide (2.5 and 3.2 MPa for *P. abies* and *A. alba*, respectively) and mature trees should benefit by a high gradient of water potentials along the axis which favors water movement from the roots to the leaves. Controversially, it is arguable that having a P50 of -2MPa at the trunk base could represent a risk for embolism formation. However, this higher vulnerability should be balanced by reduced tensions in xylem columns which are usually measured far from the apex when the evapotranspiration demand peaked (Hellkvist *et al*. 1974). The samples collected near the trunk base, even if they showed an increased vulnerability to embolism (less negative P50), they are close to roots and soil water, thus reducing the risk of cavitation (McElrone et al. 2004). In the canopy at leaf level, where the higher resistances and fewer conductive cells are found, higher tensions are experienced and evapotranspiration demand might trigger embolism formation and spread. Our data clearly display this pattern for both species (Figure 1a,b, Table1), with slightly different steepness between inflection points in the vulnerability curves.

A similar study made on 4 different heights along the main axis of a mature Douglas fir (5^{th} , 15^{th} , 35^{th} and 105^{th} internode), showed a similar pattern of P50s (Domec and Gartner 2001). The overall variation of vulnerability was high in the topmost part from the first two sample points (5^{th}-15^{th} internode) and slowly decreased towards the base. According to the statistical models (Table 1A), the VCs of our two study species were significantly different for the y-intercept of P50 values (corresponding in the power scaling Equation 1 $Y = a * X^b$ to the $\log_{10}$ transformation of a) but not for slope: they had different absolute vulnerability to embolism formation, but the same axial pattern of P50 variation. Distance from the apex should be always standardized during sampling of branches for VCs analyses, since it significantly influences the resistance to embolism formation, especially in the apical 2 m of the tree canopy.

Xylem structure and water transport

The mean hydraulic diameter of tracheids increased in size with increasing distance from the tree apex independently of the species and with the same scaling exponent b = 0.2 (Eq 1). This result is in accordance to several other anatomical studies which showed a strong conservativism of xylem axial widening design (Anfodillo *et al.*, 2006; Olson *et al.*, 2014; Prendin *et al.*, 2018) under different environmental conditions (Anfodillo *et al*. 2013, Kiorapostolou *et al*. 2020). According to Hagen-

Poiseuille law, the conductance of a given conduit scales with the fourth power of the diameter (Tyree & Ewers, 1991), hence even a small increase in the conduits average size could greatly influence the hydraulic conductivity of the overall system. Plants should benefit from an efficient water transport pathway with wide conduits, but at the expense of the resistance to embolism formation (Sperry *et al*. 2006, Larter *et al*. 2017). The rigid axial scaling found in many studies and in different environments likely represent the best compromise between safety, efficiency and carbon investment, maximizing xylem hydraulic conductance at the price of a balanced vulnerability along the axis (Mencuccini *et al*. 2007).

Another clear anatomical pattern found in our species is the increase in pit size from the apex to the trunk base, which is in line with other anatomical studies addressing pit size increment with DFA (Lazzarin *et al*. 2016, *Sequiadendron Giganteum* Lindl.). Pit area scales independently of species with an exponent b=0.23, and no statistically significant differences in slope or intercept between spruce and fir were highlighted. Pits and conduits anatomical properties are clearly intercorrelated and both contribute to the overall vulnerability of the water transport system. Wheeler *et al.* (2005) suggested that pit size inversely correlate with resistance to embolism formation. In particular, membrane thickness, porosity and chamber depth are strongly correlated with drought vulnerability and an increased margo resistance regulate overall conductivity (Pittermann *et al*. 2010). We tested also how the pit size scales with hydraulic diameter and we found differences in intercept but not slope. *Picea abies* had larger pits for given Dh compared to *Abies alba*, therefore explaining why spruce is more vulnerable in absolute values of P50 than fir. If the "absolute" vulnerability is explained by pit properties, the variation of vulnerability along the axis may be justified by the inverse correlation of P50 and Dh, which showed a difference in intercept but not in slope.

Anatomy used to re-fit VCs

In our, as well as in other studies, the theoretical conductivity of the xylem is calculated as a sum of conductivity of all cells found in the anatomical section (see Materials and Methods). However, the use of Hagen-Poiseuille equation over-estimates the conductivity of the system because it reduces the complexity of the xylem network to simple capillary tubes and does not take into account the inter-conduit resistance given by pit membranes (Tyree and Zimmermann, 2002; Loepfe *et al.*, 2007). The xylem network is highly complex and embolism spread is titghly related to the number, location and size of vessels and pits (Wason et al. 2021). Even if over-estimated (with a different y-intercept), our Ka showed the same slope of increment along the axis at different distances from the apex. We

explored the relationships between different water potentials inducing a specific loss of conductivity obtained from VCs (P12, P20, P50, P88 etc.) and the corresponding theoretical hydraulic diameter obtained from ROXAS analyses (D12, D20, D50, D88 etc.). The relation P5-D5 had the highest r^2 in both species (Fig. 8), indicating that the D5 well explains the first inflection point of the VCs. These results suggest that the anatomical parameter D5, which can be quite easily obtained with a semi-automatic software like ROXAS, can be used as a reliable proxy for the minimum tension leading to early embolism formation in xylem. Moreover, the reconstruction of VCs based on anatomical data (cells ordered from the largest to the smallest) gave us decent, yet useful information about the importance of anatomically rigid patterns in the evaluation of xylem vulnerability to embolism (Figure 1.9).

1.5) Conclusions

In conclusion, a strong inverse correlation between conduits and pit size with P50 was found, suggesting that the variation of embolism vulnerability with DFA is changing due to anatomical patterns along the main axis. Caution should be always taken during sampling of material for VCs analyses, since our data showed clearly that hydraulic architecture and apex-to-base conduit widening may significantly affect the VCs shape, as well as the derived parameters (e.g. P50). Anatomical data were used to successfully reconstruct some vulnerability curves, but the described method has some limitations due to the high contribution of species-specific traits. To validate the curves made with anatomical data, we also retrieved the predicted P50 values and matched them with the ones from the vulnerability curves, showing a good correlation and a fit on the 1:1 line. Even though conifer might be easier to use in the anatomical reconstruction of vulnerability curves, this study pushes further the concept of vulnerability being a complex "trait" which can vary within the same plant or tissue. The approach presented here should be tested on additional species, both gymnosperms and angiosperms, with the aims to improve its predicting power and to reach a wider application of anatomical traits for quantitative analyses of vulnerability to embolism formation. The results described above give strength to the hypothesis that conduits embolization is not a random phenomenon, but is tightly related to cell lumen area, conduits distribution and pit membrane size, all of which show great differences between the tree apex and the trunk base.

Chapter 2

XYLEM, PHLOEM AND CARBON RESOURCES ALLOCATION UNDER DROUGHT

Chapter 2.1

"No xylem phenotypic plasticity in mature Picea abies and Fagus sylvatica tress after 5 years of throughfall precipitation exclusion"

Giai Petit [1] , Dario Zamboni [1] , Benjamin D. Hesse [2] , Karl-Heinz Häberle [3]

1 University of Padova, Dept. Land, Environment, Agriculture and Forestry (LEAF), Legnaro (PD), Italy

2 Technical University of Munich, School of Life Sciences, Land Surface-Atmosphere Interactions, Freising, Germany

3 Technical University of Munich, School of Life Sciences, Chair of Restoration Ecology, Freising, Germany

Global Change Biology 2022, *28*, 4668–4683. https://doi.org/10.1111/gcb.16232

Abstract

Forest trees are experiencing increasing frequency and intensity of drought events with climate change. We investigated xylem and phloem traits from mature *Fagus sylvatica* and *Picea abies* trees after 5 years of complete exclusion of throughfall precipitation during the growing season. Xylem and phloem anatomy, leaf and branch biomass were analyzed along top branches of ~1.5 m length in 5 throughfall precipitation excluded (TE) and 5 control (CO) trees of both beech and spruce. Xylem traits were analyzed on wood cores extracted from the stem at breast height. In the top branches of both species, the lumen diameter (or area) of xylem and phloem conduits did not differ between TE and CO trees. At breast height, TE trees of both species produced narrower xylem rings and conduits. While allocation to branch (*BM*) and needle biomass (*LM*) did not change between TE and CO in *P. abies*, TE *F. sylvatica* trees allocated proportionally more biomass to leaves (*LM*) than *BM* compared with CO. Despite artificial drought increased the mortality in the TE plots, our results revealed no changes in both xylem and phloem anatomies, undermining the hypothesis that successful acclimation to drought would primarily involve increased resistance against air embolism.

2.1.1) Introduction

In the last decades, the increasing frequency of extreme events, such as droughts and heatwaves, is occurring worldwide, and often has been recognized as triggers of phenomena of tree vigor decline and tree mortality in natural ecosystems (Allen *et al*. 2010, 2015, Schuldt *et al*. 2020). At present, the actual cascade of events affecting the tree physiological status preceding death under theeffects of episodic droughts and chronic increase in temperature and atmospheric vapor pressure deficit has still to be thoroughly identified (McDowell *et al*. 2020). Most commonly, exceptional events of drought-related tree mortality are perceived as sudden events. However, in most cases, they are preceded by long-term signals, such as the long-term reduction in diameter growth (Cailleret *et al*. 2017) and/or crown condition decline with desiccation symptoms (Carnicer *et al*. 2011). Trees are long living organisms that translocate aqueous solutions over very long distances through transport tissues of xylem and phloem, which are seasonally produced *ex novo*. Water flows along a gradient of negative water potential developing along soil– plant–atmosphere-continuum (SPAC). Under high tension due to drought, air bubbles can seed through pit membranes and expandto fully embolize xylem conduits. This interrupts water transport and consequently decreases the total xylem hydraulic conductance (Cochard 2006). The percentage loss of xylem conductance (*PLC*) for decreasing xylem water potential (Ψ_{xyl}) (i.e., the so-called vulnerability curves) depends on the different combination of anatomical traits of vascular elements (e.g., conduit length and diameter; pit size and density, etc.) (Hacke and Sperry 2001). Therefore, the xylem vulnerability to drought-induced embolism formation is species-specific (Choat *et al*. 2012), but it has been also reported to vary across environmental settings (Barnard *et al*. 2011, Skelton *et al*. 2021).

In trees, drought conditions can negatively affect the maintenance of a positive C balance at the tissue or individual level by exerting limitations to the water transport sustaining leaf transpiration and photosynthesis. A theoretical framework has been proposed to explain the possible physiological failures causing tree death under drought (McDowell *et al*. 2008). More isohydric species maintain a safe margin between the Ψ_{xyl} at stomata closure and the critical Ψ_{xyl} at which air embolism would develop into xylem conduits (Meinzer *et al*. 2009, Choat *et al*. 2012). When isohydric species experience prolonged limitations to stomatal conductance, it is supposed that they can exhaust their internal carbon reserves, negatively affecting the overall C balance and possibly leading to death by carbon starvation (McDowell *et al*. 2008). On the other extreme, anisohydric species maintain stomatal conductance beyond the critical level for embolism formation, and Ψ_{xyl} can lower so much that the majority of its xylem conduits gets embolized. Consequently, the leaf water supply would be compromised by the hydraulic failure of the xylem transport system, with consequent crown

desiccation and plant death (McDowell *et al*. 2008). The vulnerability to drought-induced embolism formation often has been reported to be significantly related to the xylem conduit diameter (Pittermann *et al*. 2006, Hacke *et al*. 2006). However, this relationship is likely not causal but possibly arises from covariation with other functional traits, like pit size, number and density (Becker *et al*. 2003, Lazzarin *et al*. 2016). In the context of drought-related tree mortality, the leafwater supply in trees exposed to lethal doses of drought has been commonly reported to be compromised by widespread air embolism in xylem conduits (Adams *et al*. 2017). Drought acclimation (i.e., the maintenance of a long-term positive C balance) would imply that either the limitations to xylem and phloem transport are somehow compensated to maintain their hydraulic efficiency, or the C costs, get somehow reduced, especially those associated to the production of new biomass and the maintenance metabolism of the whole living tissues. Therefore, the assessments of species-specific drought thresholds are currently recognized of key importance in order to better predict the effects of climate change on forest ecosystems (Brodribb *et al*. 2020).

Beyond the restriction in the water transport as a driver of drought-induced tree vigor decline and mortality, also the limitations to phloem transport have been hypothesized to play a relevant role (Sevanto *et al*. 2014). The transport of sugars along the phloem is tightly coupled to the xylem water transport (Hölttä *et al*. 2006, De Schepper *et al*. 2013). Consequently, a drought-induced reduction in xylem water potential should be accompanied by a contextual re- duction in phloem water potential, which can be defined either passively by tissue dehydration or actively by tissue osmoregulation (i.e., by increasing the amount of osmolytes [primarily sugars and ions] in the phloem sap solution). In either case, phloem conductance would decrease due to the increase in sap viscosity (i.e., according to the Hagen Poiseuille law: Savage *et al*. 2017), possibly limiting the translocation of sugars from source to sink tissues (Sevanto *et al*. 2018). The C allocation to growth has been commonly known to be limited under drought conditions. Besides, a few recent studies reported higher leaf biomass in healthy trees from drier compared with moister conditions, suggesting that this modified biomass allocation can compensate for the negative effects of drought on gas exchanges and ultimately on the plant C balance (Anfodillo *et al*. 2016, Petit *et al*. 2016).

In this context, having a clearer panorama on the degree of phenotypic variability in those functional traits playing a key role in the survival of trees facing drought events is of primary importance. The concept of xylem and (to a minor extent) phloem phenotypic plasticity being key determinants of the acclimation potential of the different tree species is pervasive in plant ecology. Since the conductive system of both xylem and phloem is periodically renewed with the allocation of C into new xylem and phloem biomass, it is a common expectation that the newly formed xylem and phloem vascular elements differ in key anatomical features, such as lumen size, and thus provide better

acclimation potentials to changing environmental conditions.

Recently, contradictory results have been found from anatomical studies applying different sampling approaches. Punctual anatomical analyses (fixed age or fixed diameter for sampling) typically revealed significant phenotypic trait variability in trees growing under different environmental conditions. Such studies mostly reported a more embolism resistant xylem with narrower conduits in trees from drier environments, as opposed to trees from moister environments showing larger and more conductive vascular elements with less resistance to embolism (Pfautsch *et al*. 2016, Schuldt *et al*. 2016, Larter *et al*. 2017). These types of evidence appeared to support the hypothesis of an existing trade-off between embolism resistance and hydraulic conductivity (usually called safety vs. efficiency trade off), with resistance being prioritized under drier conditions and hydraulic efficiency supporting fast growth rate being prioritized under moister conditions (Sperry *et al*. 2008). Furthermore, anatomical analyses on tree cores typically showed that xylem cell production and conduit size are limited under drier environmental conditions (Castagneri *et al*. 2015, 2020). Most often analyses of functional xylem anatomy are punctual, that is they report data from samples extracted either at the stem base or from branches of fixed age (e.g., 2–3 years) or diameter (e.g., 1–2 cm). This type of analysis is neglecting the axial distance from the apex, which has been shown to be the primary driver of xylem anatomical variations (e.g., conduit diameter: Anfodillo *et al*. 2013; Olson *et al*. 2014; vessel clustering Lazzarin *et al*. 2016; Pfautsch *et al*. 2018; Lechthaler *et al*. 2019; pit ultrastructure Christof *et al*. 2020).

On the contrary, analyses removing or accounting for path length effects supported the hypothesis of a marginal degree of phenotypic plasticity, if any. In recent years, it has been documented that the assessment of phenotypic plasticity in anatomical traits is a delicate operation, because rather rigid axial designs characterize both xylem (Anfodillo *et al*. 2013, Lechthaler *et al*. 2019) and phloem (Kiorapostolou and Petit 2018, Kiorapostolou *et al*. 2020) anatomies. Power scaling relationships $Y = a \times X^b$ with exponent $b \sim 0.1$ to 0.3 have been commonly reported to well describe the axial variation in xylem and phloem conduits with the increasing distance from the apex at both the stem (Anfodillo *et al*. 2013) and branch level (Petit *et al*. 2016). Accordingly, the increase in conduit diameter is sharp within a few meters from the apex, but below it typically approaches a more constant size towards the stem base (Mencuccini *et al*. 2007, Petit *et al*. 2010). Without implying variations in the allometric constant a, conduit diameter would be larger either at the stem base of taller trees (Olson *et al*. 2014) and at given cambial age in fast growing trees (Carrer *et al*. 2015), simply because of the occurrence of the axial conduit diameter variation (b). Ecological studies applying such an allometric approach to anatomical analyses reported a completely different scenario, than punctual

analysis/studies. When accounting for the effect of tree height, the xylem conduit diameter at the stem base was reported either not to vary across precipitation gradients (Fajardo *et al*. 2020) or even to increase with increasing VPD (Olson *et al*. 2020). Consistently, more detailed analyses reporting conduit diameter variations along the longitudinal axis of stem or branches showed invariant axial scaling exponents *b* (i.e., the rate of variation with increasing distance from the apex), but either invariant or higher allometric constant *a* (i.e., larger diameters all along the longitudinal stem/branch axis) under drier conditions (Petit *et al*. 2016, Guérin *et al*. 2018, Kiorapostolou and Petit 2018, Lechthaler *et al*. 2019).

The context of this study is a throughfall exclusion experiment in the Kranzberg forest in south-east Germany. Due to the throughfall exclusion system, a mature stand of intermixed *Picea abies* Karst. and *Fagus sylvatica* L. has been drought stressed for five consecutive growing seasons (2014-2018 Grams *et al*. 2021). This resulted in a strong decrease in physiological functionality for both species (Tomasella *et al*. 2018, Grams *et al*. 2021). Mortality events increased under drought by 7.5% and 1.5% in the coexisting spruce and beech trees, respectively (Pretzsch et al. 2020). The specific aim of this study was to apply the allometric approach to assess potential anatomical changes under drought in both species:

- By producing modified xylem and phloem structures to compensate for the hydraulic limitations in the long-distance transport of water and sugars.
- By adjusting the allocation patterns of the new foliage and branch biomass to reduce the C costs associated with biomass production and maintenance.

Specifically, we assessed power scaling relationships ($Y = a \times X^b$) of xylem, phloem and leaf/needle traits vs. distance from the branch apex. Trait conservativism would occur when both allometric parameters (*a* and *b*) do not differ between treatments, whereas plastic modifications would occur when *a* and/or *b* differ in drought stressed vs. control trees.

2.1.2) Materials And Methods

Study site and plant material

The study site (Kranzberg Forest, Southern Bavaria, Germany; N48°25'12", E11°39'42"; elevation: 490 m a.s.l.) is a mixed stand of mature Norway spruce (*Picea abies* Karst.) and European beech (*Fagus sylvatica* L.) with an average height of ~30 m. Air temperature has an annual mean of 7.8°C and a growing season average of 13.8°C (May–September). The total annual precipitation is 750–800 mm, whereas during the growing seasons is 460–500 mm (Grams*et al*., 2021). In spring 2010, 12

plots of 110–220 m^2 including 3–7

P. abies and 3–7 *F. sylvatica* trees were trenched along the perimeter down to 1 m (reaching a dense clay layer), and ditches were subsequently impermeabilized with plastic tarp impermeable to root growth and refilled with soil (Pretzsch *et al*. 2016).

Since May 2014, rainfall has been excluded from six plots by means of automated roofs at ~3 m aboveground, closing in case of precipitation during the growing season (i.e., approximatively from the mid of April until the mid of November) and reducing the annual throughfall by about 70% on the treatment plots. A detailed description of the experimental site and design can be found in Grams *et al*. (2021). Trees growing under drought experienced severe drought stress for five consecutive growing seasons with pre-dawn water potentials as low as −1.8 MPa and soil water content close to the permanent wilting point (Grams *et al*., 2021). Target trees were identified in three roofed (Throughfall Exclusion, TE: drought stress treatment) and three unroofed (control: CO) plots, and their upper crown was accessible through a canopy crane.

Branch xylem and leaf biomass sampling

For both *P. abies* Karst. and *F. sylvatica* L. trees, a 1.5–2 m long branch was sampled from 5 TE and 5 CO trees in 2018. Sampling was designed to minimize the possible occurrence of anatomical adjustments related to crown position (Bettiati *et al*. 2012) and mechanical support (i.e., reaction wood). Along the main axis of each branch, 5–8 sampling points, numbered progressively starting from the most apical one, were selected at 1 cm above the base of each visible internode. The correct calendar year of formation was assigned to each internode and its length (ΔL) was measured. Instead, since annual increments in *F. sylvatica* were not precisely identifiable by visual inspection of internodes, for this species ΔL was estimated as the distance (l) between two sampling positions along the branch divided by the difference in the number of their year rings in the xylem ($\Delta L = l/\Delta N_{RINGS}$). For each point, the distal distance to the branch apex in previous years was then calculated by subtracting the corresponding ΔLs to DA. A segment of ~1.5 cm was cut at each sampling location and enclosed into a 50 ml container filled with a solution of 50% ethanol in distilled water for the following anatomical analyses. Starting from the first (i.e., most apical) sampling point, all the distal leaves/needles (*LMd*) were removed and placed in a labelled paper bag together with the total distal branch biomass (*BMd*). The sampling of the remaining *LMd* and *BMd*, and their placement into the respectively labelled paper bag proceeded progressively to the next sampling point towards the base. Paper bags containing *LMd* and *BMd* were then oven-dried at 72°C for 24 h. The amount of leaves/needle (*LM*) and branch biomass (*BM*) for each sampling point was calculated as the cumulative sum of *LMd* and *BMd*, respectively, starting from the apical sampling point. Furthermore, for each branch, a subset of ~20 leaves/needles

were placed in a separate paper bag and scanned before drying in the oven. Images were then analyzed with ImageJ (Schindelin *et al*. 2012) and the total leaf area was measured. The ratio of leaf/needle dry mass: area *(LMA*) was then assessed for each subset of leaves/needles. For each sampling point of each branch, the total leaf area cumulated starting from the apex was then calculated as $LA = LM/LMA$.

Xylem core sampling at breast height

From the base of each sampled tree, a wood core to the pith was extracted from the stem at breast height with an increment borer (diameter = 0.5 cm). Together with the branch segments, the cores were sent to the laboratory of the Dept. LEAF of the University of Padua (Italy) for the following anatomical analyses.

Anatomical analyses on stem and branch xylem/phloem

Cores have been first cut into segments of max. 4 cm, which were then rehydrated for 10 min at high vapor pressure into a pressure cooker. Core segments were then mounted on a custom-made clamping support designed for core transversal sectioning. Branch segments were removed from the preserving ethanol solution and directly mounted on the microtome clamping support. Each core and branch segment were cut at 15–20 μm thickness with a rotary microtome (Leica RM2245; Leica Biosystems, Nussloch, Germany), stained with a solution of Safranin Astra Blue (1% and 0.5% in distilled water, respectively) and permanently fixed on glass slides with Eukitt (BiOptica, Italy).

Images of the entire cross-section of each core and branch segment were acquired with a Dsight slide scanner (Menarini Group, Florence, Italy) at 100× magnification. Image analysis was performed with ROXAS (von Arx & Carrer, 2014). The analysis was performed on a known angle α of 20–60°. The software required an outlining of the annual ring borders, used to assign the correct calendar year (n) and then automatically measured several anatomical traits at ring scale: those used in this study were the ring area (RA), the hydraulically weighted mean xylem conduit diameter ($DH = \Sigma d^5/\Sigma d^4$, where d is the diameter of the n-conduit, (Kolb & Sperry, 1999), the mean cell wall thickness of the conduits (CWT, μm) and the ring hydraulic conductivity (i.e., the sum of the conductivity of each conduit, calculated with Hagen–Poiseuille [Tyree & Ewers, 1991]: KHr). Data of RA and KHr were rescaled to the full cross-sectional area by multiplying them by $360/\alpha$. Phloem mean cell area (CA_{PHL}, μm^2) was also obtained through ROXAS by measuring the largest 20–30 sieve elements in the non-collapsed area of the phloem.

Statistical analyses

We tested for the differences between treatments and species in several allometric scaling relationships using linear mixed-effects models fitted with restricted maximum likelihood (REML). Statistical analysis was made by using the lme4 package (Bates *et al.*, 2015)of the software R (R Core Team, 2022). Data were first $\log_{10}$- transformed to accomplish the assumption of normality and homoscedasticity (Zar, 1999). For each target trait, we tested for the fixed effects of the distance from the apex (*DA*) and treatment (TE/CO), and their interaction, using the tree ID as a random factor in all initial models. The best model was chosen based on Akaike Information Criterion (AIC) using the maximum likelihood method (Zuur *et al.*, 2009).

2.1.3) Results

Xylem and phloem anatomy in branches

The five last annual xylem rings (from 2014 to 2018) showed clear axial patterns of ring area (*RA*, Figure 2.1.1) and hydraulically weighted conduit diameter (*Dh*, Figure 2.1.2). *RA* increased with the distance from the branch apex (*DA*) according to a nearly isometric scaling ($b \sim 1$) in both *F. sylvatica* and *P. abies*. The statistical models revealed significant variability for both the *y*-intercept (corresponding to $\log_{10}a$ of power scaling equation, Equation 1: $Y = a \times X^b$) and slope (corresponding to the exponent *b* of Equation 1) only for *F. sylvatica*, while *RA* resulted not significantly affected by precipitation exclusion in *P. abies* (Figure 2.1.1; Table 2.1.1A).

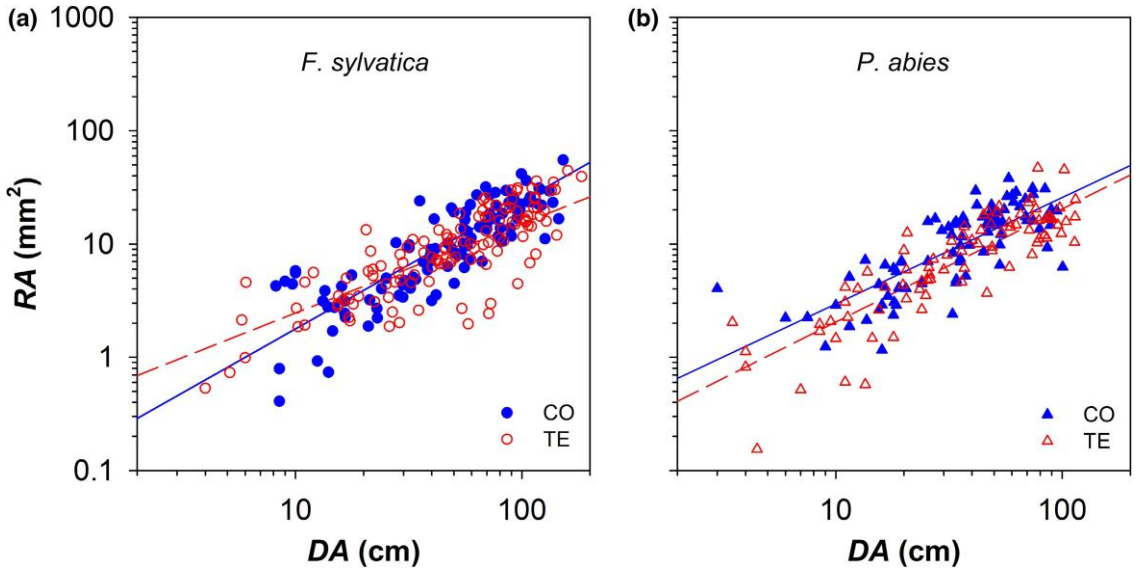

Figure 2.1.1 Variation in the ring area (*RA*) with the distance from the branch apex (*DA*) in control (CO: Filled blue symbols) and droughted (TE: Empty red symbols) for (a) *F. sylvatica* (circles) and (b) *P. abies* (triangles). Fitting lines (solid for CO and dashed for TE) are according to Table 2.1.1A.

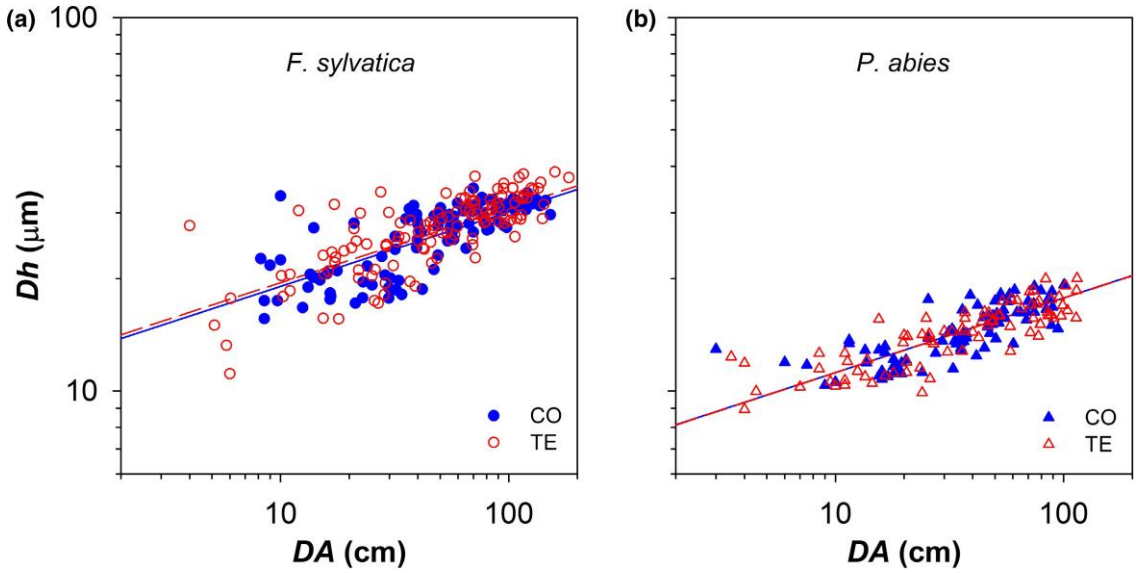

Figure 2.1.2 Variation in the mean hydraulically weighted diameter of xylem conduits (*dh*) with the distance from the branch apex (*DA*) in control (CO: Filled blue symbols) and droughted (TE: Empty red symbols) for (a) *F. sylvatica* (circles) and (b) *P. abies* (triangles). Fitting lines (solid for CO and dashed for TE) are according to Table 2.1.1B.

The relationship of *Dh* with *DA* revealed a rigid axial scaling, significantly invariant across years and between treatments (CO and TE), with *F. sylvatica* having significantly larger conduits (i.e., higher *y*-intercept) than *P. abies* (Figure 2.1.2.; Table 2.1.1B).

The cell wall thickness (*CWT*) of *P. abies* tracheids slightly in- creased with *DA*, but showed no significant differences between CO and TE trees (Figure 2.1.3; Table 2.1.1C).

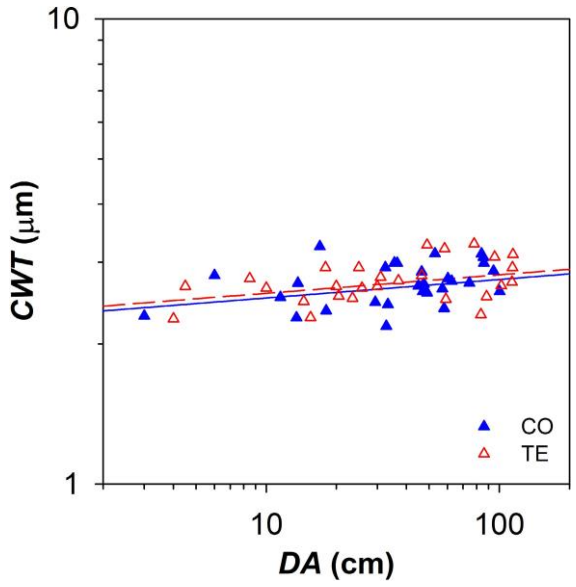

Figure 2.1.3 Variation in the thickness of tracheid cell walls (*CWT*)with the distance from the branch apex (*DA*) in control (CO: Filled blue triangles) and droughted (TE: Empty red triangles) for *P. abies*. Fitting lines (solid for CO and dashed for TE) are according to Table 2.1.1C.

The axial variation of the lumen area of phloem sieve cells (CA_{PHL}) with DA revealed species-specific patterns with y-intercept and slope significantly differing between *F. sylvatica* and *P. abies*, but no significant effects of precipitation exclusion in both scaling parameters (Figure 2.1.4; Table 2.1.1D).

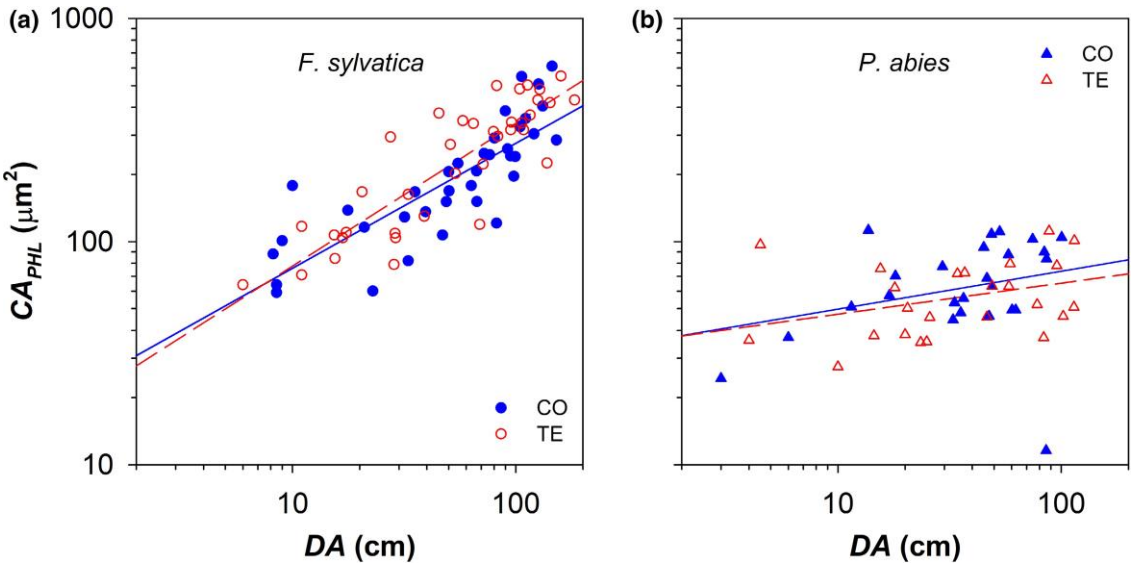

Figure 2.1.4 Variation in the mean lumen area of phloem sieve cells (CA_{PHL}) with the distance from the branch apex (DA) in control (CO: Filled blue symbols) and droughted (TE: Empty red symbols) for (a) *F. sylvatica* (circles) and (b) *P. abies* (triangles). Fitting lines (solid for CO and dashed for TE) are according to Table 2.1.1D.

Branch elongation

Since 2014, the annual branch elongation (ΔL) showed high intraspecific variability. Although an overall difference in ΔL between control and droughted trees for the whole period of precipitation exclusion in both species did not emerge, yet the lowest annual ΔL observed in some TE trees in both species. Furthermore, in *F. sylvatica* ΔL was significantly lower in TE than CO trees in 2016, while in *P. abies* TE trees showed a significant trend of decreasing ΔL withtime, although only in 2017 ΔL resulted significantly lower than control trees (Figure 2.1.7).

TABLE 2.1.1 Results of the optimal linear mixed-effect models predicting the effects of $\log_{10}DA$ and *species* + *treatment* on (A) $\log_{10}RA$, (B) $\log_{10}Dh$ and (C) $\log_{10}CWT$ (assessed for *P. abies only*). Tree ID was used as random factor in models, except (A) where nested random factors were ID/year. Abbreviations for species and treatments: FSCO Fagus Sylvatica COntrol, FSTE Fagus Sylvatica throughfall exclusion, PACO Picea Abies COntrol, PATE Picea Abies throughfall exclusion.

Model	Fixed effects and covariates	Estimate	SE	*df*	*t*-value	*p*-value
(A) $\log_{10}RA \sim \log_{10}DA$ + (species + Treat) random ID/year	Intercept (FSCO)	−0.88	0.10	292	−8.64	<.0001[A]
	$\log_{10}DA$ (slope) (FSCO)	1.13	0.05	292	21.41	<.0001[a]
	FSTE	−0.40	0.14	18	3.46	.0028[B]
	PACO	−0.47	0.15	18	2.73	.0136[B]
	PATE	−0.69	0.14	18	1.36	.1909[AB]
	$\log_{10}DA \times$ FSTE	0.79	0.07	292	−4.81	<.0001[b]
	$\log_{10}DA \times$ PACO	0.94	0.08	292	−2.36	.0189[bc]
	$\log_{10}DA \times$ PATE	1.00	0.08	292	−1.76	.08[ac]
$R^2_m = 0.67$ $R^2_c = 0.83$						
(B) $\log_{10}DH \sim \log_{10}DA$ + (species + Treat) random ID	Intercept (FSCO)	1.08	0.02	375	66.41	<.0001[A]
	$\log_{10}DA$ (slope) (FSCO)	0.20	0.01	375	24.24	<.0001
	FSTE	1.09	0.01	18	0.60	.5542[A]
	PACO	0.85	0.01	18	−17.23	<.0001[B]
	PATE	0.85	0.01	18	−17.18	<.0001[B]
$R^2_m = 0.87$ $R^2_c = 0.88$						
(C) $\log_{10}CWT \sim \log_{10}DA$ + Treat random ID	Intercept (PACO)	0.36	0.02	47	14.94	<.0001
	$\log_{10}DA$ (slope) (PACO)	0.04	0.01	47	3.03	.0039
	PATE	0.37	0.01	6	0.29	.7843
$R^2_m = 0.14$ $R^2_c = 0.24$						
(D) $\log_{10}CA_{PWL} \sim \log_{10}DA$ + (species + Treat) random ID	Intercept (FSCO)	1.32	0.13	99	10.45	<.0001[A]
	$\log_{10}DA$ (slope) (FSCO)	0.56	0.07	99	7.79	<.0001[a]
	FSTE	1.25	0.18	16	−0.37	.7147[A]
	PACO	1.53	0.19	16	1.06	.3034[A]
	PATE	1.53	0.18	16	1.15	.2664[A]
	$\log_{10}DA \times$ FSTE	0.64	0.10	99	0.83	.411[a]
	$\log_{10}DA \times$ PACO	0.17	0.11	99	−3.40	.001[b]
	$\log_{10}DA \times$ PATE	0.14	0.11	99	−3.80	.0002[b]
$R^2_m = 0.79$ $R^2_c = 0.80$						

Allocation to leaf area and branch biomass

The total leaf mass that progressively accumulated starting fromthe branch apex along the main branch axis (*LM*) increased with was *DA* according to a similar axial scaling between the CO trees of the two analyzed species (significantly similar *y*-intercept and slope). While throughfall precipitation exclusion did not affect the *LM* al- location pattern in *P. abies*, the most distal portion of the branchof *F. sylvatica* TE trees loaded more *LM* than CO trees did (corresponding to higher *y*-intercept and lower slope) (Figure 2.1.5a and b; Table 2.1.2A).

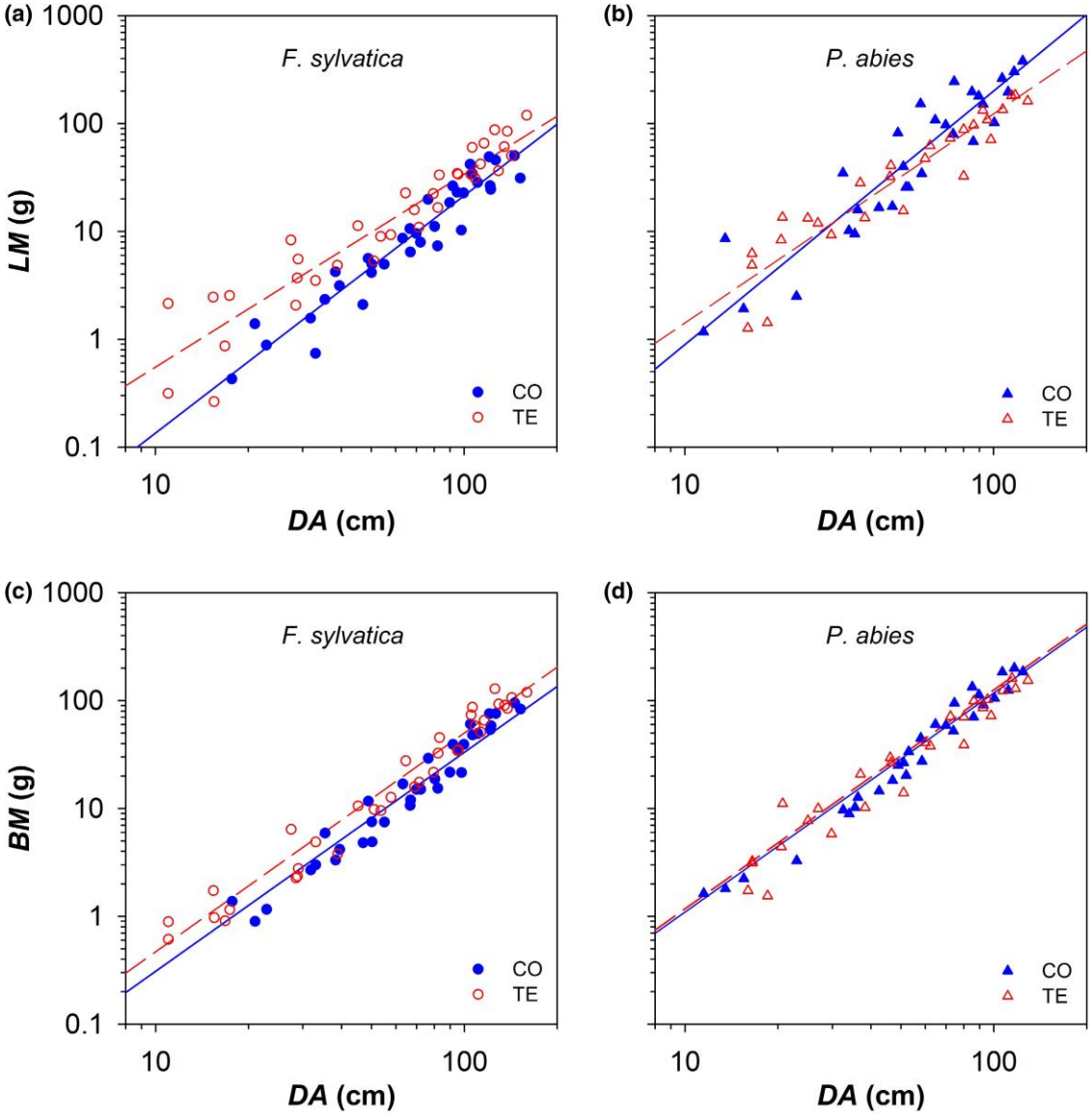

Figure 2.1.5 Basipetal patterns of allocation to leaf biomass (*LM*: a, b) and branch biomass (*BM*: c, d) along the main branch axis. Variation in *LM* cumulated along the branch axis starting from the apex with the distance from the branch apex (*DA*) (CO: Filled blue symbols) and droughted (TE: Empty red symbols) for (a, c) *F. sylvatica* (circles) and (b, d) *P. abies* (triangles). Fitting lines (solid for CO and dashed for TE) are according to Table 2.1.2 A and C.

The total branch biomass that progressively accumulated starting from the branch apex along the main branch axis (*BM*) scaled to the second power ($b = 2$) of *DA* irrespective of species and

treatment (Figure 5b). Species differed for a higher *BM* in *P. abies* (higher *y*-intercept). A treatment effect was observed only in *F. sylvatica*, with TE trees loading more *BM* along the branch axis (i.e., higher *y*-intercept) than CO trees (Figure 5c and d; Table 2C).

The allometric relationship expressing the biomass partitioning between leaf area and branch biomass (i.e., *BM* vs. *LA*) was significantly similar (i.e., same *y*-intercept and slope) between the CO trees of both species. While precipitation exclusion didnot affect the allocation pattern in *P. abies*, *F. sylvatica* TE trees showed a significantly higher *y*-intercept and lower slope, corresponding to distal branches with a lower ratio *BM*:*LA* (Figure 2.1.6; Table 2.1.2D).

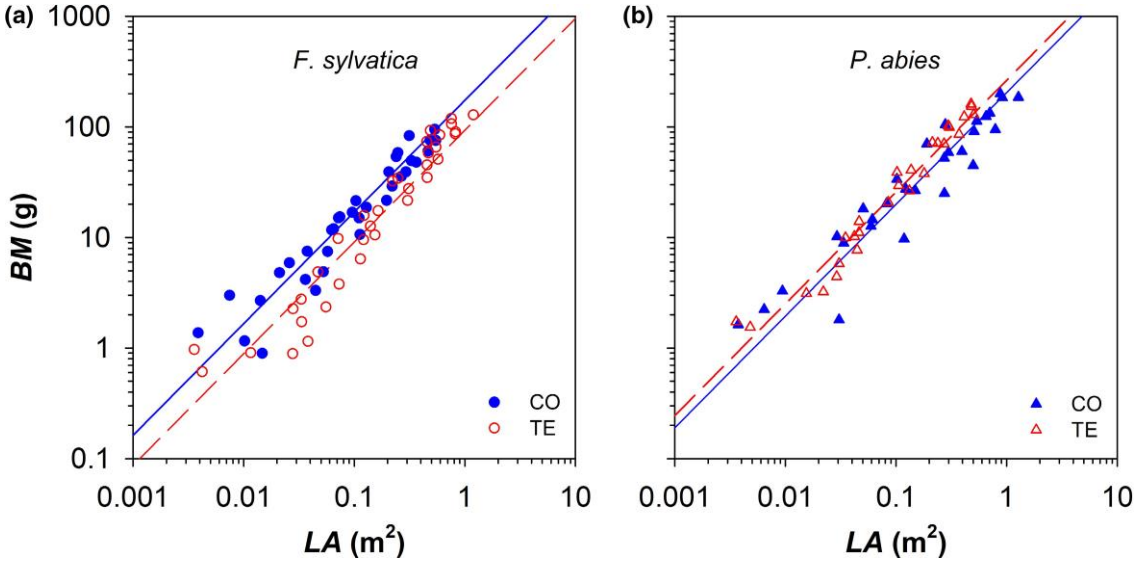

Figure 2.1.6 Relationship between the total branch biomass cumulated starting from the branch apex (*BM*) and the total leaf area cumulated starting from the branch apex (*LA*) in control (CO: Filled blue symbols) and droughted (TE: Empty red symbols) for (a) *F. sylvatica* (circles) and (b) *P. abies* (triangles). Fitting lines (solid for CO and dashed for TE) are according to Table 2D.

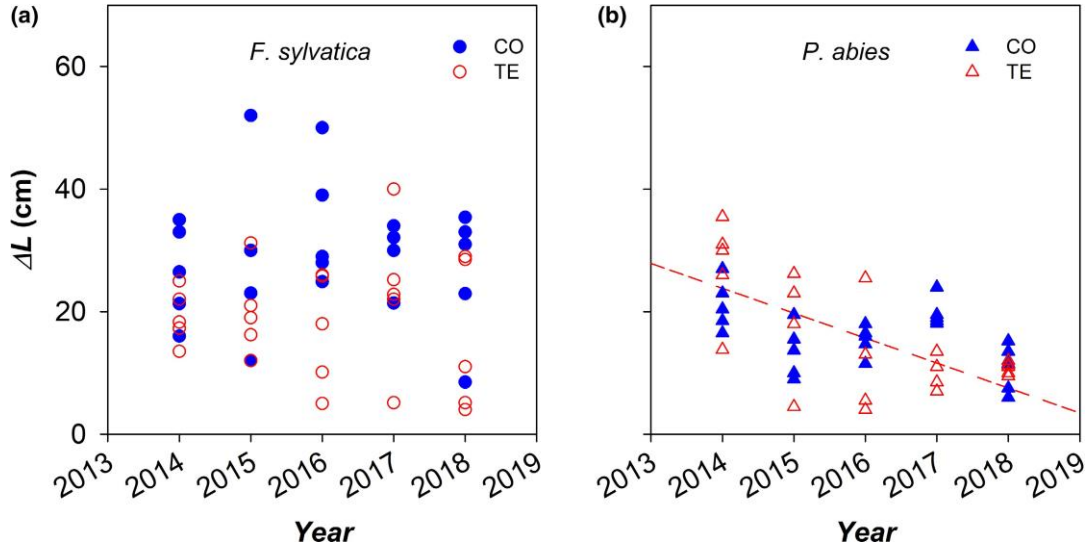

Figure 2.1.7 Annual variation of the axial elongation (*ΔL*) in the analysed top branches of control (CO: Filled blue symbols) and droughted (TE: Empty red symbols) (a) *F. sylvatica* (circles) and (b) *P. abies* (triangles) trees during the whole experimental period (2014–2018) of throughfall precipitation exclusion.

TABLE 2.1.2 Results of the optimal linear mixed-effect models predicting the effects of $\log_{10}DA$ and *species* + *treatment* on (A) $\log_{10}LM$, (B) $\log_{10}LA$ and (C) $\log_{10}BM$. (D) Results of the optimal linear mixed-effect models predicting the effects of $\log_{10}LA$ and *species* + *treatment* on $\log_{10}BM$. Tree ID was used as random factor in all models. Different letters indicate different estimates with significance at $p < .05$, or at $p < .1$ in case of symbol #. Abbreviations for species and treatments: FSCO Fagus Sylvatica COntrol, FSTE Fagus Sylvatica throughfall exclusion, PACO Picea Abies COntrol, PATE Picea Abies throughfall exclusion.

Model	Covariates and fixed effects	Estimate	SE	*df*	*t*-value	*p*-value
(A) $\log_{10}LM \sim \log_{10}DA$ + (species + Treat) random ID	Intercept (FSCO)	−3.07	0.20	102	−15.30	<.0001^{A}
	$\text{Log}_{10}DA$ (slope) (FSCO)	2.20	0.10	102	22.14	<.0001$^{a\#}$
	FSTE	−2.05	0.25	16	4.08	.0009^{B}
	PACO	−2.40	0.28	16	2.41	.0282^{A}
	PATE	−1.79	0.27	16	4.80	.0002^{B}
	$\text{Log}_{10}DA \times$ FSTE	1.79	0.12	102	−3.34	.0012^{b}
	$\text{Log}_{10}DA \times$ PACO	2.35	0.14	102	1.10	.2722^{a}
	$\text{Log}_{10}DA \times$ PATE	1.94	0.13	102	−1.93	.0565$^{b\#}$
$R^2_m = 0.89$ $R^2_c = 0.96$						
(B) $\log_{10}LA \sim \log_{10}DA$ + (species + Treat) random ID	Intercept (FSCO)	−5.06	0.21	102	−24.05	<.0001^{A}
	$\log_{10}DA$ (slope) (FSCO)	2.20	0.10	102	21.07	<.0001^{a}
	FSTE	−3.88	0.26	16	4.49	.0004^{B}
	PACO	−4.76	0.29	16	1.01	.3295^{A}
	PATE	−4.2	0.28	16	3.07	.0074^{B}
	$\log_{10}DA \times$ FSTE	1.75	0.13	102	−3.55	.0006^{b}
	$\log_{10}DA \times$ PACO	2.29	0.15	102	0.59	.5567$^{a\#}$
	$\log_{10}DA \times$ PATE	1.88	0.14	102	−2.26	.0259$^{b\#}$
$R^2_m = 0.85$ $R^2_c = 0.95$						
(C) $\log_{10}BM \sim \log_{10}DA$ + (species + Treat) random ID	Intercept (FSCO)	−2.54	0.08	99	−32.01	<.0001^{A}
	$\log_{10}DA$ (slope) (FSCO)	2.03	0.04	99	54.86	<.0001
	FSTE	−2.36	0.06	18	3.06	.0067^{B}
	PACO	−1.99	0.06	18	8.94	<.0001^{C}
	PATE	−1.96	0.06	18	9.15	<.0001^{C}
$R^2_m = 0.95$ $R^2_c = 0.98$						
(D) $\log_{10}BM \sim \log_{10}LA$ + (species + Treat) random ID	Intercept (FSCO)	2.24	0.07	99	32.13	<.0001$^{A\#}$
	$\log_{10}LA$ (slope) (FSCO)	1.01	0.02	99	45.43	<.0001
	FSTE	1.97	0.09	18	−2.89	.0097^{B}
	PACO	2.31	0.10	18	0.77	.4522^{C}
	PATE	2.42	0.10	18	1.87	.0776$^{C\#}$
$R^2_m = 0.90$ $R^2_c = 0.95$						

Stem diameter growth and xylem anatomy

The 10 outermost annual xylem rings of the stem showed a progressive reduction in mean width (*RW*) with time in both speciesand treatments. However, TE trees appeared to diverge from CO trees starting from the beginning of the throughfall exclusion in 2014, showing a progressive and sharper decline in *RW* (Figure 8a and b). At the anatomy level, the hydraulically weighted diameter of xylem conduits (*Dh*) did not vary significantly across years, although a slight, but not significant,

decline since 2014 was emergent in the TE trees of both species (Figure 2.1.8c and d).

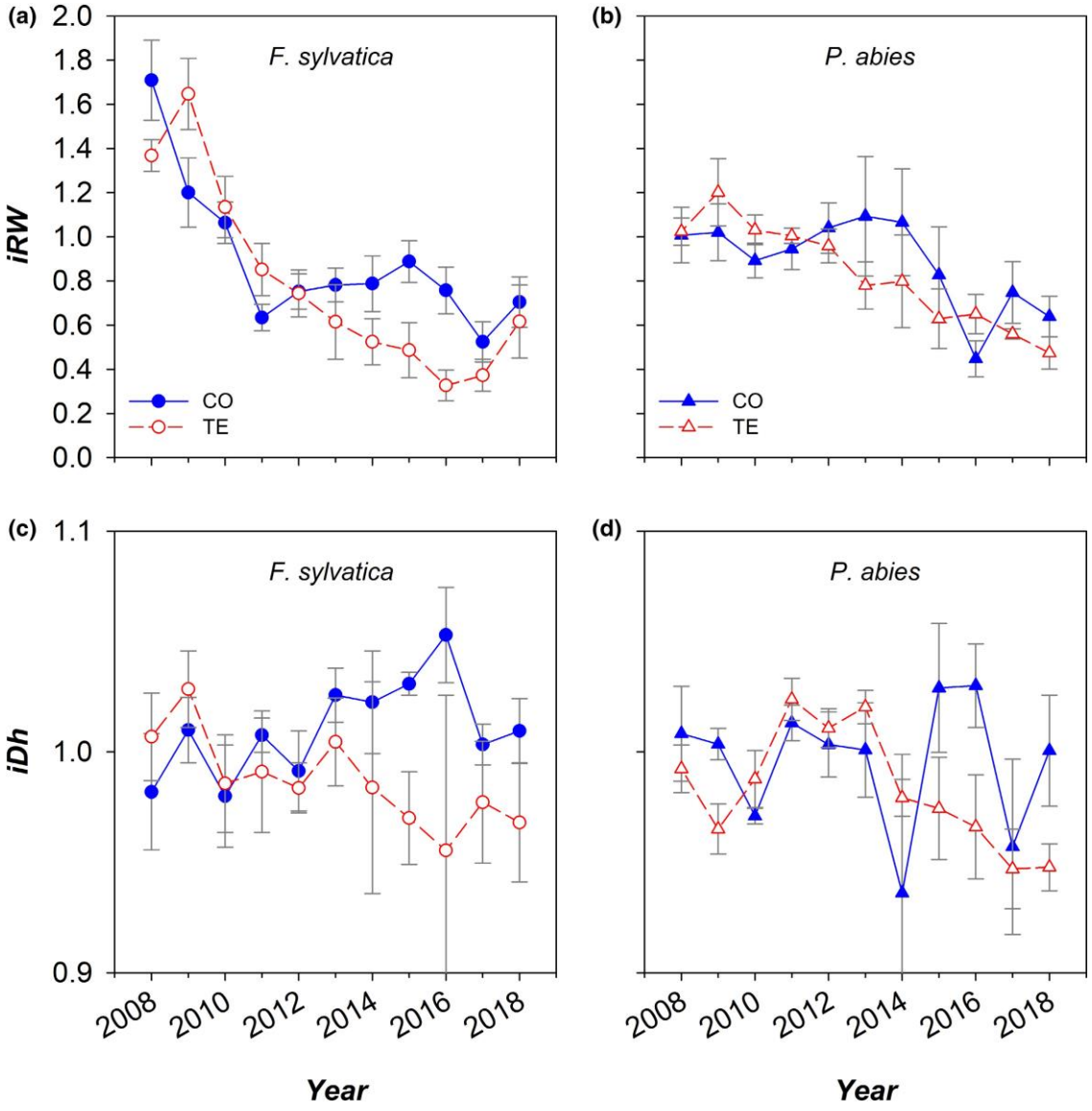

Figure 2.1.8 Mean annual variation of the indexed ring width (*iRW*: a, b) and the indexed hydraulically weighted diameter of xylem conduits (*iDH*) in the analysed stem cores of control (CO: Filled blue symbols) and droughted (TE: Empty red symbols) (a, c) *F. sylvatica* (circles) and (b, d) *P. abies* (triangles) trees. *iRW* and *iDh* are relative values calculated over the reference period 2008–2013 (i.e., the 5 years preceding the drought experiment). Error bars indicate standard errors.

2.1.4) Discussion

In this study, we carried out different analyses aimed at understanding the possible patterns of morphological/anatomical acclimationto decreased water availability in coexisting *F. sylvatica* and *P. abies* mature trees. We investigated whether trees exposed to 5 yearsof throughfall precipitation exclusion during the growing season

(i) modified the conductive architecture of xylem and phloem,

(ii) reduced/increased the C investment into new biomass of leaves and branch/stem tissues, and (iii)

modified the C costs associated to the maintenance respiration of living tissues.

Conservativism of xylem anatomy at the branch level

Dh increased with the distance from the branch apex according to a power scaling with exponent $b = 0.2$ independent of species and treatment. Such a result is consistent with the hypothesis of strong conservativism of the axial xylem design during ontogeny (Prendin, Petit, *et al*. 2018) and across species and environmental conditions (Anfodillo *et al*., 2013; Olson *et al*., 2014). According to Hagen–Poiseuille, the conductance of a given xylem conduit scales with the fourth power of its diameter (Tyree and Ewers 1991b), and the resistance to drought-induced cavitation has been commonly reported to decrease with increasing conduit diameters (Pittermann *et al*. 2006, Hacke *et al*. 2006, Larter *et al*. 2017, Nardini *et al*. 2017). The typical xylem's axial configuration has been proposed to represent the optimal gain-cost solution for maximizing the hydraulic conductance and the resistance to drought-induced embolism formation for a given C investment for the build-up of the long distance transport network (Mencuccini *et al*., 2007). Such a hypothesis would imply that the production of a more embolism resistant xylem while contextually maintaining the total xylem conductance would increase the C costs as- sociated to the tissue production because more conductive cells should be formed to compensate for the lower conductance of their narrower lumen diameter. At the other extreme, larger and more efficient conduits would allow a lower C investment into the xylem tissue to maintain the total xylem conductance, at the cost of likely increasing the vulnerability to air embolism. Net of the axial conduit widening, *Dh* resulted larger in the *Fagus sylvatica* vessels compared with the spruce tracheids (i.e., higher *y*-intercept in the allometric relationship $log_{10}Dh = a + b \times log_{10}DA$), but it was not affected by the artificial drought in the analysed branches of both species. This result is consistent with other anatomical studies reporting the axial variation of xylem conduit diameter along stem or branches. These studies showed that trees growing under low water availability produce either marginally (Guérin *et al*., 2018; Kiorapostolou *et al*., 2018; Kiorapostolou *et al*., 2020, Kiorapostolou & Petit, 2019) or substantially (Petit *et al*., 2016) larger xylem conduits compared with those in moister conditions. In particular, results from a long-term experiment of 50% exclusion of incoming precipitation in a dry mountain piñon-juniper dry forest revealed a marginal increase in the tracheid lumen area in the analysed *Pinus edulis* (Engelm.) in response to the chronic reduction in water availability (Guérin *et al*., 2018). Contextually, it was found that an episodic drought occurring during the experiment at the time of in- tense cambial activity negatively affected the final conduit diameter (Guérin *et al*., 2018). Similar results were obtained by Kiorapostolou *et al*. (2020), reporting slightly larger tracheids in declining mature trees in a Scots pine stand in the Iberian peninsula. On the contrary, a large body of published

studies reported analyses commonly carried out applying a punctual sampling approach, i.e., measurements taken at one single position along the branch/stem axis, selected at the organ (branch/stem) base, or on the basis of the branch age (i.e., number of xylem rings: typically 2–3) or diameter (typically 1–2 cm). This type of sampling procedure is pervasive in ecological studies, but substantially neglects the (possible) existence of axial variations in several xylem anatomical traits. Consequently, the wide body of data obtained with a punctual sampling approach as described above can likely and tragically represent a large source results that could be unsatisfactory interpreted. No longer it should be neglected that trees sampled according to the classical punctual approach most likely would show narrower and more embolism resistant conduits in case of short stature and if the axial stem/branch elongation is slow (like trees under dry conditions): samples would be simply taken at a shorter distance from the stem/branch apex compared with those in taller and/or faster growing trees.

The thickness of the tracheid cell walls (*CWT*) has been proposed to contribute, in tandem with the conduit's lumen diameter (*d*), to the mechanical resistance against cell wall collapse under the effect of xylem tension ($[2 \times CWT/d]^2$: Hacke *et al*., 2001). In the analysed *P. abies* branches, we found no evidence that *CWT* was affected by artificial drought. It was characterized by a significant and rather flat axial trend (b = 0.05), although the statistical model revealed that the distance from the branch apex did not explain the majority of the trait variance (R^2 = 0.24), consistent with a previous report (Prendin, Petit, *et al*. 2018). Since in the analysed branches neither *CWT* (spruce) nor *Dh* (spruce and beech) were significantly affected by the applied precipitation exclusion in both species and that *Dh* varied axially at a faster rate than *CWT*, this would suggest that variations in implosion resistance mostly depends on the *Dh* patterns. Again, all else being equal, analyses based on classical punctual sampling most likely would reveal higher resistance against implosion in short and slow growing trees, as commonly reported for trees growing under water limiting conditions (Barigah *et al*. 2013, Rowland *et al*. 2015).

Conservativism of phloem anatomy at the branch level

Phloem sieve elements increased in lumen area (CA_{PHL}) axially with increasing *DA*. The axial scaling slightly differed between *F. sylvatica* and *P. abies*, but in the range of those reported in literature. Altogether, the available data would suggest a convergent axial scaling of CA_{PHL} across species, characterized by an exponent in the range of that reported for the xylem conduit diameter (b ~ 0.1–0.3) (Petit and Crivellaro 2014, Jyske and Hölttä 2015, Savage *et al*. 2017, Kiorapostolou and Petit 2018, Kiorapostolou *et al*. 2020). In fact, according to the Munch's circulation hypothesis, the transport of phloem sap should be coordinated to that of water along the

xylem (Hölttä *et al*., 2006). In the analysed branches of *F. sylvatica* and *P. abies*, CA_{PHL} was not affected by artificial drought, suggesting no acclimation of phloem anatomy to drought. Phloem sap conductance can be negatively affected by a drought-related increase in sap viscosity due to tissue osmoregulation or/and dehydration (Sevanto, 2014). Consistently, the phloem sap velocity has been reported to decrease by nearly 50% in the droughted compared with control *Fagus sylvatica* trees (Hesse *et al*. 2019), although NSC concentration was reported not to differ between treatments (Hesse *et al*. 2021). However, we did not measure the area of conductive phloem, and therefore no definitive conclusion can be made on whether a larger phloem tissue area was produced under drought to compensate for the potential limitations to phloem transport due to the likely higher sap viscosity. In a few studies accounting for the path length effects on phloem anatomy, the phloem area and the lumen area of sieve elements resulted to be larger at drier sites (Kiorapostolou & Petit, 2019), and in trees showing signs of drought- induced decline of vigor (Kiorapostolou *et al*., 2020). Thus, in a carbon-starvation scenario, where the NSC may decrease drastically (Hesse *et al*., 2021) the ability to transport and mobilize carbon in different tissues, plays a key role for the survival of the trees at the cost of reduced growth. On the contrary, small beech trees exposed to a long-term drought treatment have been reported to produce narrower sieve tubes at the stem base (i.e., by applying the classical punctual sampling approach) (Dannoura *et al*. 2019).

Allocation patterns of leaf and xylem biomass at branch level

Leaf biomass provides with photosynthesis, the necessary resources to maintain a long-term positive C balance, when stored C resources can sustain physiological needs in case of lack of resources. Besides, its production and maintenance represent relevant energetic costs. Therefore, it has been proposed that plants acclimate to conditions of limiting stomatal conductance by increasing the total leaf area while reducing the allocation to current axial and radial growth (Anfodillo *et al*., 2016). Indeed, recent empirical measurements seemed to support this hypothesis (Anfodillo *et al*., 2016; Kiorapostolou *et al*., 2018; Kiorapostolou & Petit, 2019; Petit *et al*., 2016).

The analysed *F. sylvatica* and *P. abies* trees differed in axial and radial growth. The branch elongation rate was higher in beech (~34.5 cm/year) compared with spruce (~23.5 cm/year) with an overall trend of branch elongation reduction, but the high intra-specific variability did not present any statistically significant effect made by prolonged drought. On the contrary, the radial increment of both top branches and stem base was higher in *P. abies* than *F. sylvatica*, and it was differentially affected in the two species.

The total loading of leaf/needle biomass (*LM*) along the analysed top branches was similar in control

beech and spruce trees. *LM* cumulated progressively with increasing *DA* according to the same power scaling (i.e., exponent *b* of ~2.2–2.3). Both species responded to precipitation exclusion by increasing the allocation to *LM* within the first ~1 m from the apex of the main branch axis (Table 2.1.2). Furthermore, leaves from stressed *F. sylvatica* trees were characterized by a significantly lower leaf mass per area (*LMA* = leaf dry weight/area of leaf lamina), which amplified the differences between treatments in the allocation to light interception (i.e., in leaf area, *LA*: Table 2.1.2). Notably, such a plastic response did not characterize the droughted spruce trees, and it is not in agreement with most literature data, reporting increased *LMA* with reducing soil water availability (Poorter *et al*. 2009). However, the *LMA* response in the droughted beech trees was consistent with another study reporting decreased *LMA* of canopy leaves in response to prolonged experimental drought (Kuang *et al*. 2017).

Along the main axis of the analysed top branches, the ring area (*RA*) of the outermost five rings (2014–2018) was significantly higher within the first ~1 m from the apex in the droughted compared with the control beech trees. This resulted in an overall higher branch biomass (*BM*) within the ~1 m from the branch apex. Instead, *RA* and *BM* in spruce top branches were not affected by artificial drought. Since the structural changes in *F. sylvatica* did not result in higher hydraulic conductivity, it could be speculated the larger branch biomass in the distal branch portion of droughted beech trees likely provided the mechanical requirements for sustaining the larger and heavier leaf area. These results would suggest that droughted beech trees in- creased the leaf area per unit of branch axis length to maintain the total leaf area, and contextually reduced the C cost associated to the total biomass production by decreasing *LMA*, and the radial growth towards the stem base. The width of xylem rings at breast height showed an overall progressive decline in both *F. sylvatica* and *P. abies*. However, no significant differences emerged between treatments, except for the narrower vessels of 2015 and the narrower rings of 2016 in *F. sylvatica*.

The progressive decline of xylem ring width and mean conduit lumen area at the stem base have been reported to characterize the growth of trees eventually succumbing even decades after the predisposing drought events (Cailleret *et al*., 2017; Pellizzari *et al*., 2016). Notably, the reduction in the xylem conductivity at the stem base unlikely would cause strong limitations to water trans- port, since the contribution of these tissues to the total hydraulic resistance is negligible compared with those towards the crown periphery (Prendin, Mayr, *et al*. 2018, Lechthaler *et al*. 2020).

Maintenance costs of branch biomass

The relationship of *BM* vs. *LA* can describe the maintenance cost of the branch living biomass for a given leaf area. Indeed, the assessed scaling relationship was isometric (exponent *b* = 1): i.e., *BM*

and *LA* vary with the same proportions.

The branch biomass associated with a given leaf area in the analysed top branches was higher in *P. abies* than *F. sylvatica*. All elsebeing equal, this would suggest that the maintenance respiration cost of the living branch biomass is relatively more expensive in *P. abies* than *F. sylvatica*.

To summarize, while the allocation patterns to *LA* and *BM* were not affected by treatments, droughted beech trees allocated relatively more C to the production of new and more expanded leaves compared with the allocation to the supporting branch biomass. Results would then suggest that beech trees reacted to drought by reducing the C contribution that a unit leaf must provide to sustain the maintenance respiration of the total living body mass. For spruce, allocation patterns of *LA* and *BM* along the analysed branches were not significantly affected by the precipitation exclusion. Furthermore, these branches did not reveal any acclimation strategy in their topmost part, but supported a more expensive maintenance of the living branch biomass.

In conclusion, although drought-induced xylem embolism has been clearly demonstrated to play a key factor in leading a plant to death (Barigah *et al*., 2013; Rowland *et al*., 2015), yet our study contributed to increase the body of empirical evidence not supporting the hypothesis that acclimation to drought can be achieved by means of the production of a more embolism resistant xylem. On the contrary, the outcomes of this experiment of long-term throughfall precipitation exclusion suggested that drought more negatively affected the C balance of *P. abies* than *F. sylvatica* trees. Beech trees compensated for the negative effects of reduced soil water availability on stomatal conductance and gas exchanges by lowering the minimum leaf water potential (Tomasella *et al*., 2018) and decreased the C cost associated to the production and maintenance of the branch biomass. Instead, *P. abies* substantially showed no signs of acclimation to drought, possibly exposing the species to a greater risk of mortality, that actually occurred (Pretzsch *et al*., 2020).

Chapter 2.2

"How intensity and duration of drought influence resources allocation and xylem-phloem anatomy in a long term throughfall exclusion experiment"

Abstract

Xylem and phloem are the two tissues responsible for the transport of water, nutrients, and carbohydrates for every vascular plant. The plasticity of hydraulic architecture plays a fundamental role in a changing climate where hotter droughts may influence vegetation' potential to acclimate, adapt or die. Long-term throughfall exclusion experiment can therefore provide useful information on future effects of climate change and drought on plants. We measured xylem and phloem traits from mature Piñon Pine trees under different experimental drought conditions in duration and intensity. Xylem and phloem anatomy, branch and leaf biomass were assessed along branches of ~2m length in 5 trees for 4 treatments: legacy (-%45 rain, 12 years), new50 (-50%rain, 1 year), new90 (-90%rain, 1 year) and control. Xylem traits were also measured on wood cores extracted from the trunk base at breast height. In the top branches, the biomass allocation patterns remained stable and did not differ between the treatments. Xylem hydraulic diameter was not affected by drought over the 12 years of rain exclusion. Phloem sieve elements had a plastic response to drought, with increased size in New90 treatment and smaller size in New45. We concluded that acclimation to drought was not achieved by the production of a safer or more efficient xylem or by changing carbon allocation patterns.

2.2.1) Introduction

Forest ecosystems are threatened by a changing climate with increasing intensity and frequency of drought events (Allen *et al*. 2010). These changes are transforming how acute and chronic droughts influence temperature, soil water content and atmospheric vapor pressure deficit, with a cascade of complex effects on trees' physiology and their response to the environment (Brodribb *et al*. 2020, McDowell *et al*. 2020). Droughts have been recognized to play a critical role in canopy desiccation and forest dieback in many biomes and ecosystems (Allen *et al*. 2010, 2015, Anderegg *et al*. 2019), but are often perceived as short and sudden events which are the main cause of tree death. Nonetheless, mild drought conditions lasting consecutive years, may strongly influence tree death, with clear signals and symptom such as a reduction in distal and diameter growth and canopy desiccation (Carnicer *et al*. 2011, Cailleret *et al*. 2017). Different species-specific responses, environmental characteristics, drought length and intensity play a key role to the potential of adaptation and acclimation of plants and their water transport systems.

The vascular system allows plant to move water and solutes over long distances, but the driving force that moves the aqueous solution thorough xylem and phloem is a difference of water potential (Dixon and Joly 1895). In full hydration, stomata open for gas exchange, creating more negative water potential in the leaves. This unbalance of water potential creates flow of water that moves from the roots to the leaves, supported by cohesion and adhesion forces of water molecules between them and with the xylem conduits (Dixon and Joly 1895). In acute or chronic drought scenarios, this system can encounter tissue-specific damages due to excessive high tension. Air bubbles can seed inside xylem conduits (embolism/embolization), blocking the movement of water and thus reducing the total hydraulic conductance of the system (Cochard 2006). The complete loss of the water transport is called hydraulic failure and marks the blockage of every xylem conducting element by air bubbles (Tyree and Sperry 1988). The degree of loss is expressed as a percentage (PLC-percentage loss of xylem conductance) and it strongly depends on the combination of traits in anatomical structures related to transport such as vessel/tracheids diameter and length, pit size and density, cell wall thickness, cell density (Hacke, Sperry, *et al*. 2001).

Hydraulic failure is not the only category of physiological responses happening during prolonged drought. Carbon balance and photosynthetic assimilation play a key role under long stress such as a multi-year drought. During stressful condition, with low water availability and high VPD, plants reduce stomatal conductance to regulate transpiration and avoid hydraulic failure. Depending on the relative decrease of C assimilation, thus affecting C balance, with prolonged stomatal closure plant start depleting C reserves (McDowell *et al*. 2008c, 2011, Sala *et al*. 2010). Carbon starvation and

hydraulic failure do not occur independently and they are strictly bonded together in causing trees' death (McDowell *et al*. 2011, Dickman *et al*. 2015). Terrestrial species may differ in their stomatal behaviour under drought, ranging from isohydric to anisohydry (Tardieu and Simonneau 1998). Pinon pine, which exhibit isohydric behaviour, usually close stomata early to prevent the water potential to drop below the xylem cavitation threshold and consecutive loss of hydraulic function (Plaut *et al*. 2012). The clear effects of a reduced photosynthetic activity and thus a negative carbon balance can be seen as a reduction of growth in stem elongation (Borghetti *et al*. 1998, Llorens *et al*. 2004) and/or radial growth at breast height (Cailleret *et al*. 2017, Petit, Zambonini, *et al*. 2022).

Hydraulic transport and carbon balance find a clear bond also in the xylem counterpart phloem, a tissue composed by living cells, made ex-novo every year. Phloem is the sugar transporting system which plays a critical and relevant role in vigour decline and mortality under drought conditions (Sevanto 2014). Phloematic sieve elements are located nearby the newly formed xylem and they operate in a tightly coupled equilibrium (Thompson and Holbrook 2003a, De Schepper *et al*. 2013). Therefore, under drought conditions where xylem water potential becomes more negative, phloem water potential quickly adjust by dehydration or by osmotic adjustment/osmoregulation (increase of solutes/osmolytes in sap). In both scenarios, a decrease in phloem conductance would be seen due to an increase in the viscosity of sap (Savage *et al*. 2017, Gersony and Holbrook 2022). A decrease in phloem transport capacity would have a cascade of effects on translocation of sugars from sources to sinks, thus impacting more the C balance in drought scenarios (Sevanto 2018). Data on phloem physiological and anatomical acclimation under drought conditions are still a limited number, but they play a critical role in evaluating the climate change impacts on carbon acquisition and plant mortality (Sevanto *et al*. 2018).

The two conductive tissues, xylem and phloem, have a new ring formed every year with an investment of carbon resources. It is commonly expected that their phenotypic plasticity is the key for survival in short term acclimation to drought, which overall also determines acclimation potential of a species in a set environment. Xylem and phloem anatomy is the physical link between the belowground and aboveground parts of the plants, but their plasticity under drought is still debated and with mixed results. One common result is found in xylem conduits which are narrower and more resistant to possible embolism formation in dry environments, compared to wet environments where it is possible to find species with larger cells that increase conductivity but lower the overall safety (Pfautsch *et al*. 2016, Schuldt *et al*. 2016, Larter *et al*. 2017). These studies refer to the hypothesis of the so-called "safety vs efficiency trade-off" , in which is though that there is an inverse relationship between

hydraulic safety (conduit size) and hydraulic efficiency (K, Conductivity), leading to more resistance under dry conditions and faster growth with moist conditions (Sperry *et al*. 2008).

Anatomical analysis that are fixed for age or diameter during sampling procedure usually confirm this hypothesis and show a clear trait adaptation for trees living in different environments. However, those punctual anatomical analysis are not taking in consideration the clear axial pattern of the hydraulic structures from apex of the crown to the base of the stem, which is the main driver of anatomical variation (Anfodillo *et al*. 2013, Olson *et al*. 2014, Lazzarin *et al*. 2016, Pfautsch *et al*. 2018, Lechthaler *et al*. 2019). The axial variation is found to follow a power scaling relationship

$Y = a \times X^b$

both for xylem (Anfodillo *et al*. 2013, Lechthaler *et al*. 2019) and phloem (Kiorapostolou and Petit 2018, Kiorapostolou *et al*. 2020, Petit, Zambonini, *et al*. 2022) with b exponent which is usually between 0.1 and 0.3. This axial widening of the conductive tissues is found in branches (Petit *et al*. 2016) and the stem (Anfodillo *et al*. 2013) with a rapid increase in size in the first few meters, and slowly decrease downwards to the base (Mencuccini *et al*. 2007, Petit *et al*. 2010). Normalizing anatomical data by path length/distance from the apex show a completely different scenario, with limited plasticity for xylem conduits at the stem base in different precipitation gradients (Fajardo *et al*. 2020) or in increasing vapor pressure deficit gradients (Olson *et al*. 2020). Other studies following this sampling approach found the opposite of the safety vs efficiency trade-off hypothesis. These analysis on anatomical traits found no variation on b exponent (rate of variation of conduit size), but higher allometric constant a (intercept, higher absolute size of conduits but with same increment rate) under drought conditions (Petit *et al*. 2016, Guérin *et al*. 2018, Kiorapostolou and Petit 2018, Lechthaler *et al*. 2019).

Throughfall exclusion experiments (TEE) and water manipulation experiments have been of great importance in the last decades to provide data on the response of standing vegetation to drought, but many of them reported none or low plasticity. Pits and tracheid for pine displayed low phenotypic plasticity under drought (Held et al. 2021), xylem anatomy and P50 did not show any changes in oak species under TEE (Limousin *et al*. 2010). In the Kranzberg roof project in Bavaria (KROOF) no changes were found for xylem anatomy in spruce (Tomasella *et al*. 2018b) and in spruce and beech both for xylem and phloem (Petit *et al*. 2022). Low plastic response was found also in tropical rainforest for leaf anatomy in the Amazon (Binks *et al*. 2016) and for xylem anatomy and physiology in Australian wet rainforest (Pivovaroff *et al*. 2021).

The aim of this project was to test potential adaptation or acclimation to different degrees of drought in a long term throughfall exclusion experiment by a modification in the hydraulic architecture or in biomass allocation. Power scaling relationships ($Y = a \times X^b$) were used to test traits differences and in case of plasticity we would see a change in one or both of allometric parameters (a,b). Specifically, we assessed these power scaling relationships for potential changes made

- by a modification of xylem structures over time in a long-term drought scenario
- by a modification of xylem and phloem tissues in short term drought with different intensities
- by an adjustment in the biomass allocation patterns for needles and branches with a possible reduction due to an increased depletion of C storage.

2.2.2) Materials and methods

Study site, sampling, experimental design

This experimental study is set in a long-term ecological research experiment of a pinon-juniper forest in Sevilleta, New Mexico (SEV-LTER, Pangle *et al*. 2012, Plaut *et al*. 2012) and branch sampling was carried out in different plots of a throughfall exclusion experiment. The experimental site is located in the Los Pinos mountain range, inside the Sevilleta National Wildlife Refuge (34° 23' 11" N, 106° 31' 46" W). The average annual temperature is 12.7°C with circa 350 mm/yr of precipitation. Rainfall is concentrated in summer during the monsoon season (July, August and September).The experimental plots consist in 4 pinon pine (*Pinus Edulis* Engelm.) stands in which the incoming precipitation was excluded with parallel domes (thermoplastic polymer sheets) running across the plots. The excluded rain was taken outside the plots, granting the impossibility to the plants within to access that water. The four plots are named: control, legacy (-45% precipitation, 12 years), new50 (-50% precipitation, 1 year) and new90 (-90% precipitation, 1 year).

Sampling was carried out in June 2021. One 1.5-2m long branch was sampled from the topmost, sun exposed part of the crown of 5 trees in each study plot (20 trees total). Branches were cut again 6/9 times along the main axis and labeled progressively with letters from the most apical part to the bottom. Each branch segment was placed afterward in a sealed plastic bag with wet paper to avoid excessive transpiration and desiccation. From the stem base at breast height a wood core was extracted for each tree, labelled and placed in paper containers. Sampling was carried out with a tree corer (diameter = 8mm). Wood cores and branches were immediately shipped to the laboratory of TESAF department in Padua (Italy) for the following analyses.

Biomass measurements and anatomical sampling

Before biomass measurements, short segments of 1-2cm were cut at the basal end of each sampling point and placed in 50ml falcon containers with a solution of 50% distilled water and 50% ethanol for further anatomical analysis. For each branch segment, the distal distance to the apex (DFA, cm) was measured along with the length of the segment (ΔL, cm) and the assignment of the correct calendar year of formation at visible internodes. Since many internodes were not visible anymore, the length increment of every year was estimated as the distance between two sampling points and the difference in the number of rings in the xylem. DFA was also calculated for every ring/year of formation by subtracting the corresponding ΔL to DFA.

Needles were afterwards removed from every branch segment, starting from the most apical one, and placed in labelled paper bags (leaf-mass, LM). The total distal branch biomass supporting the needle biomass was also placed in separate bags for each segment (branch-biomass, BM). Paper bags containing fresh material were then oven dried at 72°C for 48h. Samples were then removed from the oven and placed on a laboratory desk to equilibrate with room temperature and weighted. The amount of needle and branch biomass at each sampling point was obtained as the cumulative sum of LM and BM, from the apex of the branch to the base.

Anatomical analysis on wood cores and branches

Wood cores, which had a length between 10 and 15 cm, were cut again into smaller segments of max 3/4cm. The cut was made diagonally to keep the correct year continuity between the segments and not lose any data. The segments were numbered and labelled and rehydrated at high vapor pressure into a pressure cooker for 10-15 mins. After rehydration wood cores were transferred in distilled water for 2/3 minutes and afterwards mounted on a clamping support designed for core sectioning. Branch cross sections were removed from the solution and mounted directly on the microtome clamping support. Each section was cut at 10-15um thickness with a rotary microtome (Leica RM2245; Leica Biosystems, Nussloch, Germany) and stained for 10 minutes with a solution of safranin and Astra Blue (concentration 1% and 0,5% respectively in distilled water) and permanently fixed with Eukitt mounting medium (BiOptica, Italy) on glass slides.

High resolution images were obtained for every section of wood cores and branch segments at 100x magnification with a Dsight slide scanner (Menarini Group, Florence, Italy). Anatomical analysis were performed with ROXAS software (von Arx and Carrer 2014) on a known angle α of 20° for circular samples from branches and on the whole sample length for wood cores. ROXAS requires manual outlining of the annual ring borders and then it automatically assign the correct calendar year

to each ring and measures many anatomical traits within. The traits used for this study are the ring area (RA, mm^2), the mean xylem conduit diameter hydraulically weighted ($Dh = \Sigma d^5/\Sigma d^4$,µm, with d considered as the diameter of the n-conduit) (Kolb and Sperry 1999), ring hydraulic conductivity (Kh, $m^4*s^{-1}*MPa^{-1}$) calculated with the Hagen-Poiseuille law as the sum of each single conduits. Since RA and Kh were measured on a known angle α the data were afterwards rescaled for the full cross-sectional area by multiplying both by 360/ α. For phloem sieve elements we assessed mean cell perimeter (P_{PHL}, µm) by measuring 20-30 cells in the non-collapsed area of the phloem with FIJI-ImageJ software (Schindelin *et al*. 2012).

Statistics

We tasted for statistical significance between treatments for several allometric relationships using R software (R core team, 2022). Linear mixed-effects model were fitted with restricted maximum likelihood (REML) by using lme4 package (Bates *et al*. 2015). Data from anatomical and biomass measurements were log_{10} transformed for the assumption of normality and homoscedasticity (Zar 1999). Distance from the apex (DFA) and treatments (control, legacy, new50, new90) were tested for the fixed effects and their interactions, using Tree ID and Year as random factors in all initial models. We used Akaike Information Criterion (AIC) to choose the best fitting model (Zuur *et al*. 2009).

2.2.3) Results

Growth and biomass allocation

The outmost year of the xylem rings (2020) showed a clear axial pattern from the tip of the branches for ring area (RA, Figure 2.2.1) which increased with DFA but did not show any significant change between the four different water exclusion treatments (Table 2.2.1). The analysis of xylem anatomical trait was carried out also on the years of legacy treatment water exclusion from 2009 to 2019. In all the rings/years it was found the same axial pattern for RA with a clear increase in size from the tip of the branches to the base but no statistically significant differences in slope or intercept were found between control and legacy plants (Figure 2.2.2, Table 2.2.4). Wood cores analysis revealed an overall decrease both for control and legacy treatments in mean ring width (MRW) in the last 20 years from 2000 to 2019. Overall, when legacy treatment started (dashed vertical line), no significant differences in MRW are seen (Figure 2.2.3).

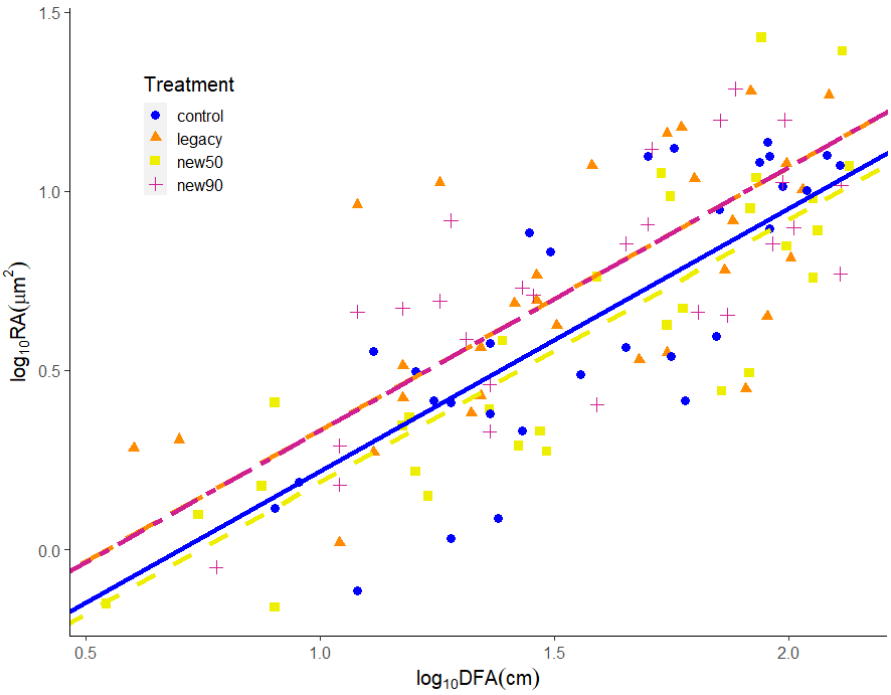

Figure 2.2.1 Variation for year 2020 in ring area (RA) with the distance from the branch apex (DFA) in control (filled blue circles), legacy (filled orange triangles), new50 (filled yellow squares) and new90 (purple crosses). Fitting lines (continuous for con trol, long dash for legacy, single dash for new50 and dashdot for new90) are according to the models in Table 2.2.1.

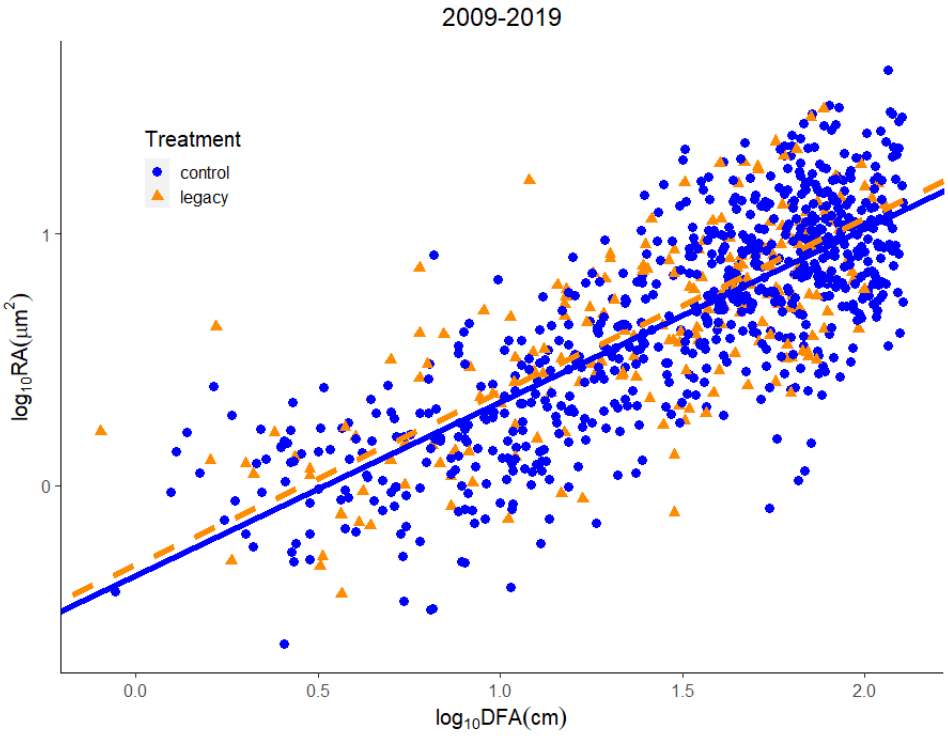

Figure 2.2.2 Variation for legacy treatment duration (2009-2019) in ring area (RA) with the distance from the branch apex (DFA) in control (filled blue circles), legacy (filled orange triangles). Fitting lines (continuous for control, dash for legacy) are according to the models in Table 2.2.1.

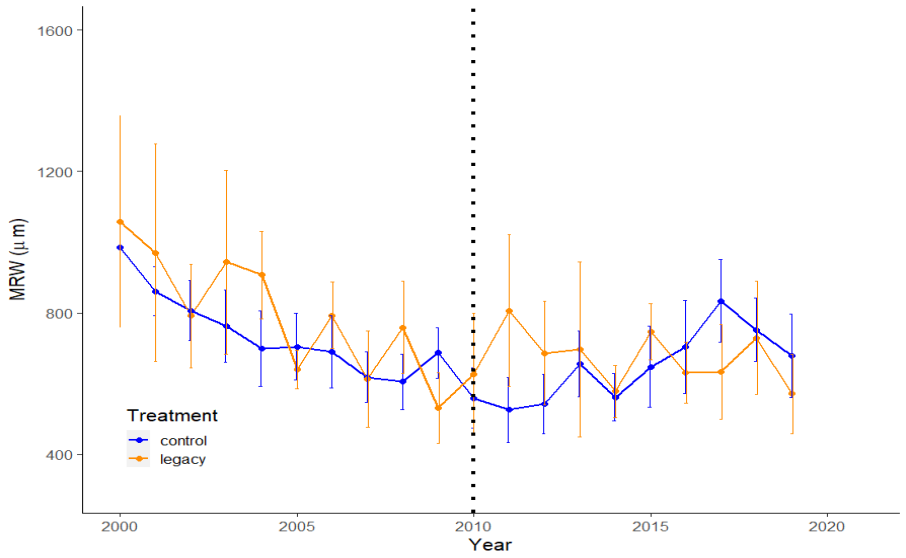

Figure 2.2.3 Variation in mean ring width (MRW) in wood cores between 2000 and 2019. Control (blue line), legacy (orange). Dashed vertical line marks the treatment application year.

TABLE 2.2.1 Results of the optimal linear mixed-effect models predicting the effects of $\log_{10}$*DFA* of year 2020 and *treatment* on (A) $\log_{10}$*Dh*, (B) $\log_{10}$*RA* and (C) $\log_{10}$*PP*. Tree ID was used as random factor in all models. Asterisks indicate different estimates with significance at ** = $p < .05$, or at * = $p < .1$.

	A) log10(Dh)		**B) log10(RA)**		**C) log10(PP)**	
Predictors	*Estimates*	*p*	*Estimates*	*p*	*Estimates*	*p*
(Intercept)	0.80	**<0.001**	-0.51	**<0.001**	2.10	**<0.001**
DFA [log10]	0.11	**<0.001**	0.73	**<0.001**	0.13	**<0.001**
Treatment [legacy50]	0.05	**0.064***	0.11	0.339	-0.00	0.775
Treatment [new50]	0.01	0.839	-0.03	0.797	-0.05	**0.004****
Treatment [new90]	0.05	**0.076***	0.11	0.349	0.03	**0.068***
Random Effects						
σ^2	0.00		0.03		0.00	
τ_{00}	0.00 $_{Tree}$		0.03 $_{Tree}$		0.00 $_{Tree}$	
ICC	0.53		0.51		0.30	
N	20 $_{Tree}$		20 $_{Tree}$		20 $_{Tree}$	
Observations	116		116		111	
Marginal R^2 / Conditional R^2	0.425 / 0.728		0.590 / 0.799		0.697 / 0.788	

The total needle biomass (LM) and branch woody biomass (BM) had similar scaling in relation to DFA with an exponent b ~ 1.3. Throughfall exclusion intensities (new90 and new50) or duration (legacy) did not affect the allocation patterns, and all the treatments had no significant differences in slope or intercept in the models (Figure 2.2.4, 2.2.5; Table 2.2.2). Biomass partitioning expressed by the allometric relationship between wood biomass of the branches (BM) and leaf mass (LM) did not show any significant difference between treatments. The y-intercept and slope of the fitted models followed the same pattern for all 4 treatments (Figure 2.2.6, Table 2.2.3).

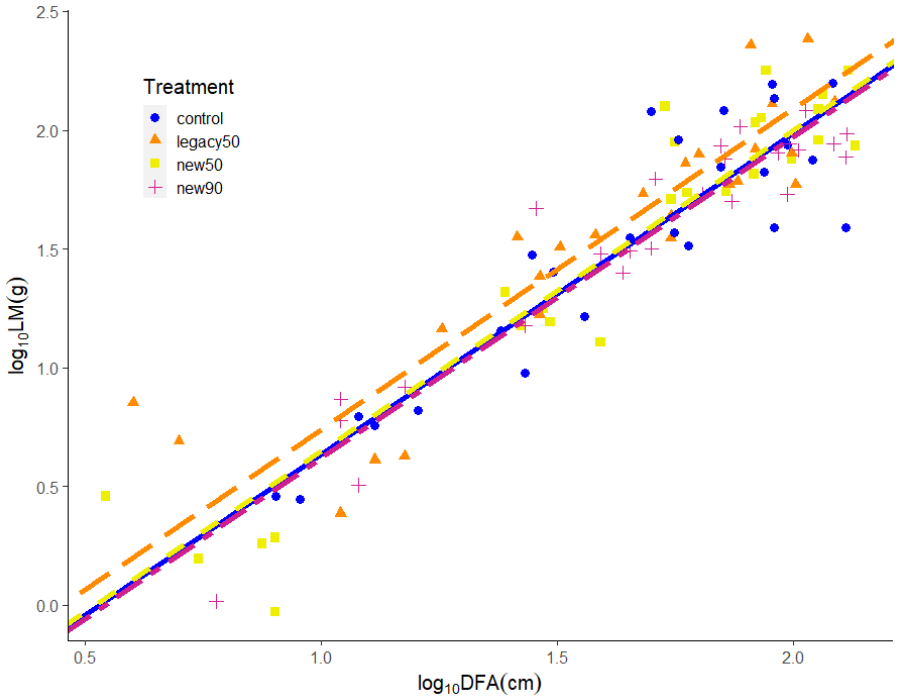

Figure 2.2.4 Variation in cumulated leaf/needle biomass (LM) with the distance from the branch apex (DFA) in control (filled blue circles), legacy (filled orange triangles), new50 (filled yellow squares) and new90 (purple crosses). Fitting lines (continuo us for control, long dash for legacy, single dash for new50 and dashdot for new90) are according to the models in Table 2.2.2.

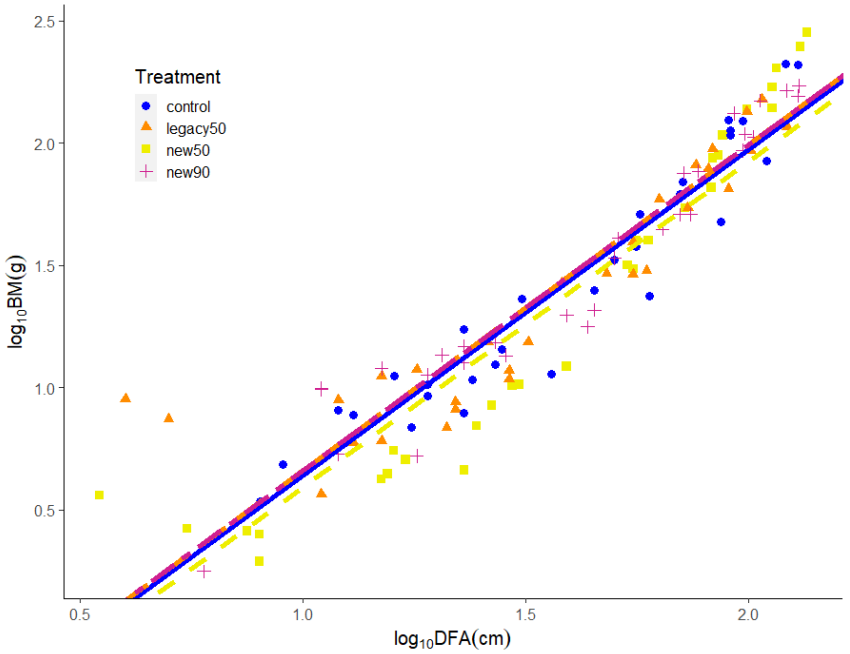

Figure 2.2.5 Variation in cumulated branch biomass (BM) with the distance from the branch apex (DFA) in control (filled blue circles), legacy (filled orange triangles), new50 (filled yellow squares) and new90 (purple crosses). Fitting lines (continuous for control, long dash for legacy, single dash for new50 and dashdot for new90) are according to the models in Table 2.2.2.

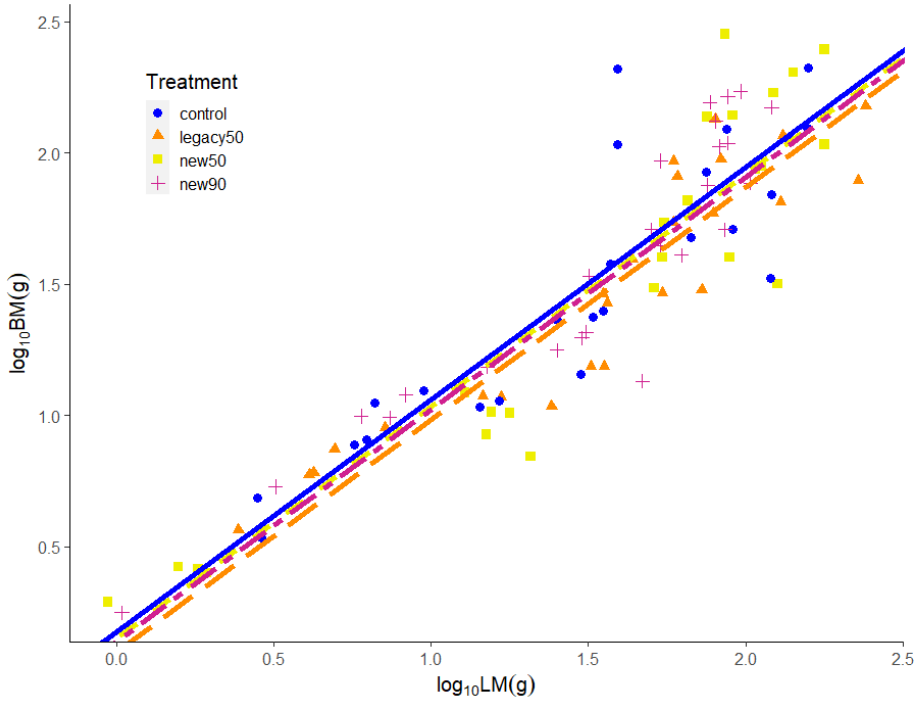

Figure 2.2.6 Variation in branch biomass (BM) with the needle/leaf biomass(LM) in control (filled blue circles), legacy (filled orange triangles), new50 (filled yellow squares) and new90 (purple crosses). Fitting lines (continuous for control, long dash for le gacy, single dash for new50 and dashdot for new90) are according to the models in Table 2.2.3.

TABLE 2.2.2 Results of the optimal linear mixed-effect models predicting the effects of $log_{10}DA$ and *treatment* on (A) $log_{10}BM$, (B) $log_{10}LM$. Tree ID was used as random factor in all models. Asterisks indicate different estimates with significance at $p < .05$, or at $p < .1$.

	A) log10(BM)		**B) log10(LM)**	
Predictors	*Estimates*	*p*	*Estimates*	*p*
(Intercept)	-0.70	**<0.001**	-0.71	**<0.001**
DFA [log10]	1.33	**<0.001**	1.35	**<0.001**
Treatment [legacy50]	0.02	0.749	0.10	0.276
Treatment [new50]	-0.05	0.435	0.01	0.911
Treatment [new90]	0.02	0.745	-0.02	0.852
Random Effects				
σ^2	0.03		0.04	
τ_{00}	0.00 $_{Tree}$		0.01 $_{Tree}$	
ICC	0.10		0.28	
N	20 $_{Tree}$		20 $_{Tree}$	
Observations	120		100	
Marginal R^2 / Conditional R^2	0.879 / 0.891		0.852 / 0.893	

TABLE 2.2.3 Results of the optimal linear mixed-effect models predicting the effects of $log_{10}LM$ and *treatment* on $log_{10}BM$. Tree ID was used as random factor in all models. Asterisks indicate different estimates with significance at $p < .05$, or at $p < .1$.

	log10(BM)	
Predictors	*Estimates*	*p*
(Intercept)	0.17	**0.028**
LEAF BIOMASS CUMULATED [log10]	0.89	**<0.001**
Treatment [legacy50]	-0.08	0.314
Treatment [new50]	-0.03	0.720
Treatment [new90]	0.04	0.620
Random Effects		
σ^2	0.05	
$\tau_{00\ Tree}$	0.01	
ICC	0.11	
$N_{\ Tree}$	20	
Observations	100	
Marginal R^2 / Conditional R^2	0.840 / 0.858	

Anatomy of branches and wood cores

Mean hydraulically weighted conduit diameter (Dh, Figure 2.2.7) and phloem sieve cells perimeter (PP) displayed an axial pattern of increase with DFA in 2020. The relationship between Dh and DFA confirmed a rigid axial scaling of this trait. The statistical models revealed significant difference between treatments for only the y-intercept in new90 and legacy (corresponding in the power scaling Equation 1 $Y = a * X^b$ to the log_{10} transformation of a) but not for slope (Figure2.2.7, Table 2.2.1), meaning an increase in absolute size while maintaining the same pattern along the axis. Phloem perimeter followed the same axial pattern of increase in size along the branches in every treatment (slope b =0.13). Statistical models showed significant effects of the treatment's intensities, with higher y-intercept for new90 and lower for new50 (Figure 2.2.8, Table 2.2.1).

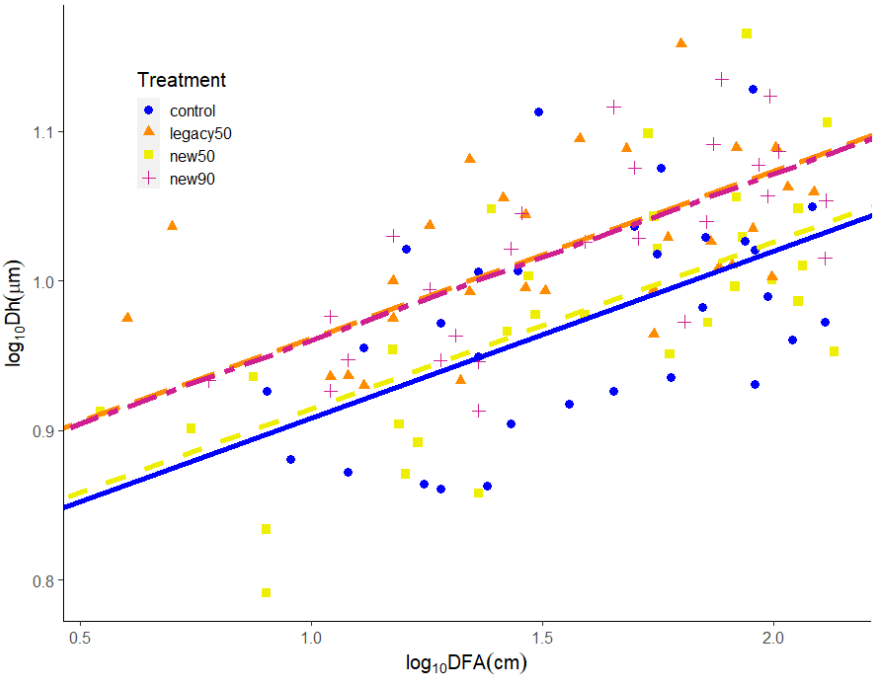

Figure 2.2.7 Variation for year 2020 in xylem tracheids mean hydraulic weighted diameter (Dh) with the distance from the branch apex (DFA) in control (filled blue circles), legacy (filled orange triangles), new50 (filled yellow squares) and new90 (purple crosses). Fitting lines (continuous for control, long dash for legacy, single dash for new50 and dashdot for new90) are according to th e models in Table 2.2.1.

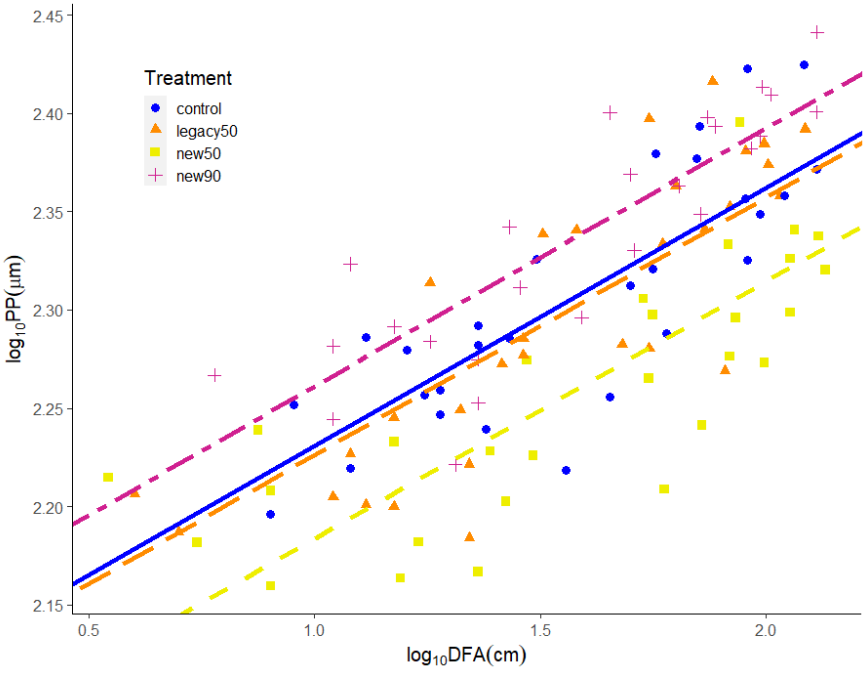

Figure 2.2.8 Variation for year 2020 in phloem perimeter(PP) with the distance from the branch apex (DFA) in control (filled blue circles), legacy (filled orange triangles), new50 (filled yellow squares) and new90 (purple crosses). Fitting lines (continuo us for control, long dash for legacy, single dash for new50 and dashdot for new90) are according to the models in Table 2.2.1.

In the years of legacy treatment water exclusion from 2009 to 2019 all the rings showed the same axial pattern for hydraulically weighted conduit diameter (Dh), with an increase in size from the tip of the branches to the base. Statistical models for Dh display no statistically significant differences in slope or intercept between treatments (Figure 2.2.9, Table 2.2.4). It was also tested the possibility of single-year differences by using the calendar year as a factor in the model. No statistically significant differences were seen between years and treatments.

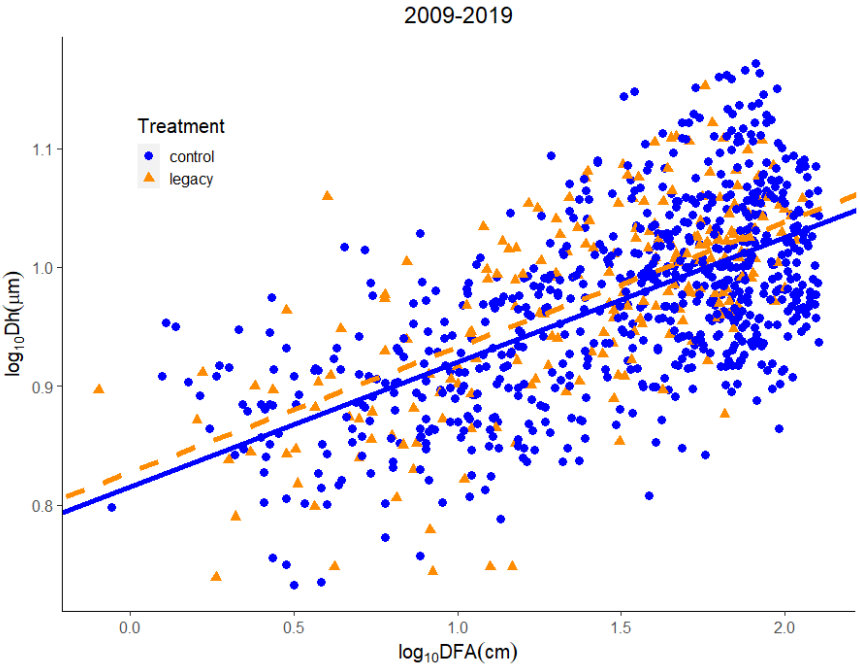

Figure 2.2.9 Variation for legacy treatment duration (2009-2019) in ring area (RA) with the distance from the branch apex (DFA) in control (filled blue circles), legacy (filled orange triangles). Fitting lines (continuous for control, dash for legacy) are according to the models in Table 2.2.4.

TABLE 2.2.4 Results of the optimal linear mixed-effect models predicting the effects of $\log_{10}DFA$ for the period 2009-2019 and *treatment* on (A) $\log_{10}Dh$, (B) $\log_{10}RA$. Results of the optimal linear mixed-effect models predicting the effects of $\log_{10}LA$ and *species* + *treatment* on $\log_{10}BM$. Tree ID was used as random factor in all models. Asterisks indicate different estimates with significance at ** = $p < .05$, or at * = $p < .1$.

	A) log10(Dh)		**B) log10(RA)**	
Predictors	*Estimates*	*p*	*Estimates*	*p*
(Intercept)	0.82	**<0.001**	-0.36	**<0.001**
DFA [log10]	0.11	**<0.001**	0.69	**<0.001**
Treatment [legacy]	0.01	0.530	0.04	0.520
σ^2	0.00		0.06	
τ_{00}	0.00 $_{Tree}$		0.01 $_{Tree}$	
ICC	0.35		0.18	
N	20 $_{Tree}$		20 $_{Tree}$	
Observations	943		939	
Marginal R^2 / Conditional R^2	0.373 / 0.591		0.594 0.666	

2.2.4) Discussion

In this experimental study we performed analysis with the aim to understand how intensity and duration of drought may influence different patterns of morphological and anatomical acclimation in mature trees of *P. edulis.* Specifically, we examined if the intensity and duration of water stress (i) modified xylem structures over time in a long-term drought scenario, (ii) modified xylem and phloem tissues in short term drought with different intensities, (iii) created an adjustment in the biomass allocation patterns for needles and branches with a possible reduction in carbon invested due to an increased depletion of C storage.

Xylem response to drought

Hydraulic diameter of the tracheids increased independently of treatment intensity and duration with a scaling exponent b ~ 0.12 with the increasing distance from the branch apex. This result is in line with others found in anatomical studies and confirms a strong conservativism of the xylem widening design during ontogeny (Prendin, Petit, *et al*. 2018, Petit, Mencuccini, *et al*. 2022) and in different environmental conditions (Anfodillo *et al*. 2013, Olson *et al*. 2014). Efficient water transport is the

key for maximizing transpiration and gas exchange, and since the conductance of xylem tracheids scale with the fourth power of its diameter according to Hagen-Poiseuille law (Tyree and Ewers 1991b), a change in conduits' diameter would greatly influence the overall conductance of the system. At the same time, it was reported in many studies that xylem vulnerability to embolism might become higher with increasing size of conduits (Hacke *et al*. 2006, Larter *et al*. 2017, Nardini *et al*. 2017). The trade-off between conduit size and vulnerability is also influenced by the carbon resources available. The production of a more resistant xylem would mean an increased cost of C invested due to a higher number of smaller cells, otherwise having larger and fewer conductive elements would be translated into a smaller investment of carbon for the same total xylem conductance but with higher risk of embolization and consequently a higher PLC in case of stress. For these reasons, the rigid axial configuration was proposed to be the best possible solution for the 3 factors trade-off (safety, efficiency and C utilization) in which gain-cost is maximized to have enough xylem hydraulic conductance for a given C investment with enough safety from embolism (Mencuccini *et al*. 2007). Our experimental data showed a clear axial widening pattern, with Dh increasing from tip to base, independently of drought stress duration or intensity. For the legacy treatment, which lasted for more than a decade, we did not see any acclimation/plastic effect on conduit size and ring area. This result is supported by other anatomical studies carried out in environmental conditions with low water availability or in water manipulation experiments, in which it was seen none or marginal xylem plasticity (Guérin *et al*. 2018, Kiorapostolou and Petit 2018, Kiorapostolou *et al*. 2018). In 2020 when new treatments were started with different drought intensity, we found a slightly significant increase in mean hydraulically weighted conduit diameter for the high-intensity (new90, 90%of rainfall exclusion) and the legacy treatments. This would suggest a push towards an increased efficiency and a lower carbon cost (Baas 1983, Petit *et al*. 2016, Kiorapostolou *et al*. 2020), but the high variability between trees of the same treatment and the low significance of p-value could lead to the same results of the long term analysis. In the same throughfall exclusion experiment (SEV_LTER), other anatomical studies on pinon pine revealed no long term acclimation of tracheids diameter for the legacy treatment (Plaut *et al*. 2012, Guérin *et al*. 2018, Hudson *et al*. 2018, Sevanto *et al*. 2018). The opposite way, a large amount of published data is reporting a decrease in conduit size and thus, an increased safety under drought conditions. The methods of many of these studies are commonly taking anatomical samples at one single/fixed position along the branches, usually normalizing by diameter or by age. This punctual sampling may lead to erroneous results, with an inverse tendency in respect to the real effects of droughts. In the case of droughted plants which are growing less, this sampling approach would find smaller conduits because the branch elongation would be affected by

smaller growth increments compared to well water trees in which the sampling point would be further down the stem due to larger elongation.

Phloem anatomical plasticity at branch level

Sieve elements of phloem follow the same axial scaling of the xylem conduits, with an increase in phloem perimeter (PP) with an increasing distance from the apex. The exponent of increase with DFA is b=0.13 and it is within the range found in literature (0.1<b<0.3) (Petit and Crivellaro 2014, Jyske and Hölttä 2015, Savage *et al*. 2017, Kiorapostolou and Petit 2018, Kiorapostolou *et al*. 2020, Petit, Zambonini, *et al*. 2022). In this study we found also a tight correlation between the axial widening of xylematic and phloematic elements (exponent b~0.12), which have the same increase with increasing distance from the apex and thus supporting Munch circulation hypothesis for the coordination of transport of sap (Smith *et al*. 1980, Thompson and Holbrook 2003, Hölttä *et al*. 2006). Our experimental data on phloem anatomy show a quick acclimation to drought, with inverse response based on precipitation exclusion intensity but without a legacy effect over multi-year stress. New50 treatment showed smaller sieve elements compared to control and legacy, while new90 treatment have larger elements. Under drought conditions phloem sap movement can be negatively affected and slow down movement due to an increased concentration in osmolytes or by dehydration (i.e. increased viscosity) (Sevanto 2014, 2018, Sevanto *et al*. 2018, Gersony and Holbrook 2022). Sevanto *et al*. (2018) reported similar results for the precipitation exclusion treatment, with an increase in size of the conduit radius under drought. Our results would suggest a decrease in transport rate under mild stress also due to smaller sieve elements, but also a greater reduction under harsh stress that theoretically influenced sap viscosity and was compensated with larger cells. Nonetheless, our measurements did not include the total conductive area of this tissue and thus we cannot infer if the total conductance of the system changed. Phloem, which is made new every year and is a key component for plants sap transport, can be a crucial and decisive determinant of plastic acclimation under drought scenarios.

Branch and needle biomass allocation

Biomass production is an expensive part in the overall carbon budget of a plant. Allocating carbon to needles biomass would provide enough photosynthesis to sustain a positive carbon balance. Branch woody biomass, additionally, provides mechanical support to the photosynthetic biomass, enable newly formed xylem to transport water and the new phloem to mobilize sugars and store them. It is a common expectation that these patterns of biomass allocation to branch and needle biomass would change under limiting environmental conditions, where water availability and temperature could

possibly influence C resources acquisition, transpiration and hydraulic constrains. It was proposed that under limiting conditions that reduce stomatal conductance, plant would increase the total photosynthetic area at the expenses of a reduced radial and axial growth (Poorter *et al*. 2009, Anfodillo *et al*. 2016a). To support this hypothesis, recent findings found increased leaf area under stress (Anfodillo *et al*. 2016, Petit *et al*. 2016, Kiorapostolou *et al*. 2018), but there is not a univocal empirical evidence and other studies reported a decreased LAI, total leaf area or LMA under drought (Lopez et al. 1997, Marron et al. 2003, Kuang et al. 2017). Furthermore, it has been proposed that leaf number, leaf area and leaf biomass might be triggered by different environmental factors, such as temperature, water availability and carbon/nitrogen availability (Meier and Leuschner 2008). Our experimental data did not show any modification or acclimation in the patterns of branch and needle biomass allocation. The total loading of cumulated needle biomass (LM) did not present statistically significant changes between the 4 treatments and they all scaled with the distance from the apex with an exponent b=1.33. Cumulated branch biomass (BM) over DFA showed the exact same pattern of LM, with no statistically significant changes and the same exponent b of increase (b=1.35). These results would suggest no plastic changes in branch and needle biomass allocation, thus providing a hypothesis of a configuration of C allocation that would allow enough gas exchange and hydraulic support to the plants under drought. Furthermore, we also tested the relationship between needle biomass and branch biomass (BM vs LM, Figure 2.2.6) , which can explain the cost of maintenance of the woody living biomass for a given needle mass. The results show a substantial isometric scaling relationship with an exponent b~1 that did not show any statistically significant change between treatment intensity and duration. This result also confirms the hypothesis of a non-plastic response to drought for pinon pine regarding biomass allocation and partitioning.

Wood cores stem diameter growth and xylem anatomy

Many studies have been reporting lower radial grow under drought, with some cases in which it was possible to notice decades-long legacies effects before death (Pellizzari *et al*. 2016, Cailleret *et al*. 2017, 2019). Furthermore, short-term droughts lasting only one growing season, were also reported to show legacy effects on growth for few years after stress (Anderegg *et al*. 2015). Even though the reduction at stem base in mean ring width and conduit diameter, is not as limiting to the water transport compared to the apical branches of the crown (Prendin, Mayr, *et al*. 2018, Lechthaler *et al*. 2020), it is possible to see plastic changes under drought conditions. Data from our wood cores taken at breast height show a progressive decline in mean ring width many years before the treatments started. During the legacy treatment, there are no significant differences between control and stressed trees, but control showed an overall increase in MRW that peaked in 2017. For xylem mean hydraulic

diameter no statistically significant changes were seen between treatments and between the exclusion and pre-exclusion period. In the last years of treatment analyzed (2018, 2019) there was an overall pattern of decrease in conduit size, but not supported by statistical significance.

2.2.5) Conclusions

Duration and intensity of drought, combined with shifts of precipitation patterns and increased temperatures will influence standing vegetation with clear effects on drought induced embolism as a trigger of mortality and hydraulic failure (McDowell *et al*. 2008, Brodribb and Cochard 2009, Choat *et al*. 2012, Barigah *et al*. 2013, Rowland, Da Costa, *et al*. 2015, Adams *et al*. 2017, Brodribb *et al*. 2020). The degree of phenotypic plasticity could allow plants to potentially acclimate to drought, or otherwise die. This study aimed to test potential plastic responses in biomass allocation and xylem and phloem anatomy. Even though pinon pine is reported to suffer both from hydraulic failure and carbon starvation (McDowell *et al*. 2008c, Breshears *et al*. 2009, Sevanto *et al*. 2014) due to an higher vulnerability to drought-induced xylem cavitation and isohydric behaviour (Linton *et al*. 1998), our experimental data are not supporting the hypothesis that acclimation to drought can be achieved by an increased safety in the anatomical structure or via a reduced investment in branch or needle biomass. Prolonged drought also did not affect xylem traits of mean ring width and conduit diameter. The intensity of the drought treatment mostly affected phloem, by pushing a need of a higher efficiency due to a likely increase in sap viscosity. This study further contributes to the overall knowledge of low anatomical plastic responses under drought conditions, highlighting the importance of taking into account xylem and phloem tissues with their axial pattern, and carbon resources allocation. Few or eventually no plastic responses to drought may lead to catastrophic results in a changing climate with stronger and longer droughts.

Chapter 2.3

"Phenotypic adjustments of Scouts pine to different soil and water availability conditions"

Abstract

Xylem vulnerability to embolism and carbon resources availability determine the possibility of a species to survive and adapt to adverse environmental conditions. In general, low water availability can limit growth and may threaten plant survival. Vulnerability to embolism is a complex, species-specific trait within the hydraulic architecture of trees. Furthermore, biomass partitioning, carbon acquisition and carbon resources utilization have great importance in adaptation and acclimation studies. Phenotypic plasticity of xylem or in the photosynthetic apparatus might play a key role for pioneer isohydric species like *Pinus sylvestris* to adapt to new/ harsh environments. In this experimental study we assessed xylem anatomical hydraulic traits and biomass resources in mature Scots pines coming from 2 different environmental conditions which are only few hundred meters apart in the Italian Dolomites. One study area is a mature mixed forest with high water availability and the other one is a pure pine forest growing on a landslide (1814) with low water availability due to the soil conditions. Experimental results display a highly reduced growth for the pines in the landslide area, but with contrasting xylem anatomical results for hydraulic diameter, which shows smaller conduits in the first ~50cm from the branch apex and become larger afterwards. Needle biomass is not statistically different between the two area, with the same pattern of cumulated mass along the branch axis. Low-water availability pines, have the same stomatal density compared to the high-water availability ones, but show increased leaf mass per area (LMA) due to a higher number of smaller, denser, and heavier needles. Scots pine is a pioneer isohydric species that likely close stomata early to avoid excessive transpiration at the cost of reduced growth. This study further pushes the understanding of xylem anatomical patterns and vulnerability being a complex trait where safety, efficiency and carbon resources must be considered in phenotypic plasticity studies.

2.3.1) Introduction

Water in plants is transported through xylem conduits under negative water potential due to forces of adhesion and cohesion (Tyree & Zimmermann, 2002). This negative water potential is created at the canopy level in leaves, where transpired water is needed to maintain gas exchange and photosynthesis. The water lost must be replaced and absorbed from roots to sustain more leaf transpiration. The overall flow is proportional to the total xylem conductance K, multiplied by the difference of water potential Ψ between soil and leaves. The hydraulic conductivity K in Darcy's law ($F = \Delta\Psi \times K$) (Tyree and Ewers 1991a) is dependent on the contribution of every xylem conduit. Wide and large conductive elements have the advantage of having an increased transport capacity and efficiency, because according to Hagen-Poiseuille law, the flow scales at the fourth power of the conduit diameter (Tyree & Zimmermann, 2002, Sperry *et al.*, 2005). Small changes in xylem conduit diameter may result in great increases in the overall conductivity and efficiency of the system. Conditions of good water availability allow plant to sustain elevate leaf transpiration, but when the water potential of the soil decrease, it may come with associated risks at the xylem level. Under high tensions, due to low water availability, cavitation may occur inside the single conductive elements. Air bubbles may seed and spread to adjacent conduits, thus decreasing the total hydraulic conductance and water transport (Cochard 2006). Acclimation to scarce water resources is obtained with the maintenance of a positive carbon balance and a transport system that is not affected by embolism. Plants should benefit from a water transport system that is efficient enough to sustain transpiration and at the same time safe from possible emboli formation, but the so called "safety vs efficiency" trade-off was not found across different species or environments (Gleason *et al*. 2016).Vulnerability to embolism was reported to be strongly related to vessels/ tracheids size (Pittermann *et al*. 2006, Hacke *et al*. 2006) and pits properties (Becker *et al*. 2003, Lens *et al*. 2011, Lazzarin *et al*. 2016).

Phenotypic plasticity and acclimation might be achieved not only by changes in the hydraulic structures. Photosynthetic biomass and carbon allocation are essential in the endurance and survival during stressful conditions, because depending on the balance of carbon acquired and used, plants start to utilize C reserves (McDowell *et al.*, 2008, 2011; Sala *et al.*, 2010). The continuous depletion of stored carbon may lead to carbon starvation, which is strictly bonded with hydraulic failure (inability to deliver water to stomata for transpiration) in causing plant's death (McDowell *et al*. 2011, Dickman *et al*. 2015). One major differentiation between species is given by their stomata regulation. Isohydric species close stomata at a specific leaf water potential while anisohydric species likely operate close to their safety margin and continue gas exchange at lower water potentials. Pine, which is a relatively isohydric species, closes its stomata early in the day and supposedly protect the

hydraulic transport system from embolism, but at the cost of a possible usage of stored carbon, which may lead to carbon starvation in case of prolonged drought (McDowell *et al.*, 2008). Recent studies reported finding of safer and more resistant xylem in drier environments, while the same species from environments with increased water availability exhibit larger conduits but at the cost of an increased vulnerability to embolism (Pfautsch *et al*. 2016, Schuldt *et al*. 2016, Larter *et al*. 2017). Anatomical analysis on tree cores show that the production of xylem cells and their size at the trunk base is strongly reduced in dry environments (Castagneri *et al*. 2020). On the contrary, some studies with different sampling approaches reported an increased efficiency and larger conduits in drier conditions (Petit *et al*. 2016, Guérin *et al*. 2018, Kiorapostolou and Petit 2018, Lechthaler *et al*. 2019). Moreover, other specific studies on conifers and isohydric species displayed no xylem plasticity towards either safety or efficiency under drought (Martínez-Sancho *et al*. 2017, Petit, Zambonini, *et al*. 2022). Commonly, punctual anatomical analysis (fixed for age or internode) does not consider the axial widening pattern of the hydraulic structures. It was reported and confirmed in multiple studies that xylem conduits increase in size from the tip of branches in the crown to the trunk base, and the conduit widening is the main driver of anatomical variation within a single tree (Anfodillo *et al*. 2013, Olson *et al*. 2014, Lazzarin *et al*. 2016, Pfautsch *et al*. 2018, Lechthaler *et al*. 2019).

Functional and structural traits, such as conduit diameter, have been shown to reflect allometric relationships, which are usually following power scaling functions of Equation1 $Y = a * X^b$. In this equation X and Y represent the functional and structural traits, while a and b are the allometric constant and the scaling exponent respectively. It was proposed in theory of optimality principles (West *et al*. 1999) that these trait relationships should converge towards a common scaling exponent, which exhibits the fundamental balance between structure and function in the view of a stable and positive carbon balance (Anfodillo *et al*. 2016). Eventual differences in the allometric constant "a" might be explained by different species strategies or by modification in the absolute proportion of traits within the same species in different environments (Weiner 2004) (e.g. needle biomass over branch biomass).

This study is set in two study areas in the Italian Dolomites. Both study areas are few hundred meters apart and have the same sun exposition, air temperature and rainfall/snowfall patterns. The main difference is due to a landslide dating 1814 on which, after some decades, Scots pine (*Pinus sylvestris* L.) started to colonize. The landslide study area present low organic matter horizon in the soil and scarce water retention and availability for plants. The objective of the study was to test phenotypic plasticity traits that allowed pines to colonize and survive in low water availability conditions. Specifically, we assessed

i) power scaling relationships to test traits plasticity in either absolute proportions of the allometric constant (a) or scaling exponent (b)
ii) adjustment in the biomass allocation patterns for branches and needles
iii) differences or modification in xylem anatomical patterns along the main axis

2.3.2) Materials and methods

Study sites

The two study areas are located close to San Vito di Cadore (Belluno, Italy) in the context of the Italian Dolomites (46.448291, 12.216984), with the same environmental conditions and sun exposition. The control stand is a mature mixed forest and the other one is a pure *Pinus sylvestris* (L.) forest which is growing on a landslide dating back to 1814. The Koppen-Geiger classification is Dfb, with an average yearly temperature of 3°C and 1885mm of precipitation. The landslide soil has reduced water availability and organic matter. Scot pine is a relatively isohydric pioneer species which is the main species in the landslide area.

In the spring of 2022 five trees from the high-water availability area (High) and five trees from low water availability (Low) were selected for the experiment. One 1.5 meters long apical branch was cut from each tree with a tree pruner and brought back to the laboratory. For each branch we selected 5-8 sampling points, measured their distance from the branch apex and progressively labelled with letters from the apical-most point. From each sample we removed and weighted a 2cm disc for anatomical analysis and then we removed needles for biomass measurements. At each internode or sampling position it was assigned its length and calendar year. Since the annual increments of low water availability pines are limited and not easily recognizable by internodes, for these trees the annual elongation increment (ΔL) and corresponding distance from the apex (DFA) at the year of formation was estimated by the difference in the number of rings in the xylem between two sampling points. From some of the analyzed trees, it was also taken a tree core, to have a rough estimation on the tree age and sapwood conductive rings. Trees from the landslide area have 100-120 rings (height 3-4 m) while the trees for the control forest are about 10m of height and have 20-25years.

Needle and branch biomass

From the most apical sampling point of each branch, we removed all the needles of a specific section and placed them in labelled paper bags. The same procedure was followed for branch wood biomass and all the paper bags were afterwards oven-dried for 24h at 72°C. Branch biomass (BM) and

leaf/needle biomass (LM) were measured with an electronic balance and calculated as a cumulative sum, starting from the apical-most point moving downwards. For each tree a subset of 20-30 needles was scanned and dried in separate bags and weighted. The scanned images were analyzed with Fiji-ImageJ (Schindelin *et al*. 2012) to assess leaf area and stomatal density (sd) on a subset of a fixed area. Subsequently, for each tree subset, leaf area was divided by its dry weight to obtain leaf mass per area (LMA, g/m^2).

Xylem anatomy

Branch segments of ~2cm were cut with a rotary microtome (LEICA RM2245, Leica biosystems, Nussloch, Germany) at a known width between 10 and 15 µm. The obtained cuts were firstly stained with a solution of safranine and Astrablue with a concentration of 1% and 0,5% respectively. The staining lasted 5 minutes and the samples were afterwards washed multiple times with solutions of distilled water and ethanol at increasing concentrations (0%, 50%, 100% ethanol on the total). At the end, glass slides were permanently fixed with Eukitt (BiOptica, Italy) mounting medium and scanned at 100x magnification with Axioscan7 (Carl Zeiss Microscopy GmbH, Germany). ROXAS software (von Arx and Carrer 2014) was used for image analysis on a known angle α usually between 20° and 180°. The first part of the analysis consists in the manual assignment and outlining of annual ring borders for the correct calendar year. ROXAS automatically measures different anatomical traits at single cell level, ring level and whole section. The specific traits used in this study are ring area (RA, μm^2) and hydraulically weighted average xylem conduit diameter (Dh, µm; $Dh = \Sigma d5/\Sigma d4$, where d is the diameter of the n- conduit (Kolb and Sperry 1999)). The obtained data of RA were afterwards rescaled to the full cross-section, by a multiplication of RA*360/ α.

Statistics

Statistical tests were carried out for differences between the trees coming from the two different water availability sites for several allometric scaling relationships. We used linear mixed effects models, which were fitted using maximum likelihood (REML). The package lme4 (Bates *et al*. 2015) of the software R (R Core Team, 2022) was used for statical analysis. For the assumption of normality and homoscedasticity, our data were first $\log_{10}$ transformed (Zar 1999). For the selected target traits, we performed the analysis for the fixed effects of the distance from the branch apex (DFA) and site (high/low), the interaction of the two and with tree ID used always as a random factor in all initial models. Significance and best model fitting were decided with the Akaike Information Criterion (AIC). The models were chosen based on the lowest AIC, using the maximum likelihood method

(Zuur *et al*. 2009). Leaf mass per area (LMA), stomatal density (SD) and mean conduit diameter (Dh) at 3 years were also tested with a paired t test for significant differences between the two sites.

2.3.3) Results

Carbon resources

The data on ring area (RA) show a clear pattern of increase with increasing DFA for both study sites (Figure 2.3.1). The computed statistical model displayed statistically significant differences both for slope and y-intercept, corresponding to the two log10 transformation of a and b in the equation $Y = a * X^b$ (Table 2.3.1). The scaling exponent is higher in trees from the low water availability when compared to high water availability trees. The trees from "low" site have smaller rings along the DFA gradient, with increased difference in the most apical point, slowly decreasing towards the branch base.

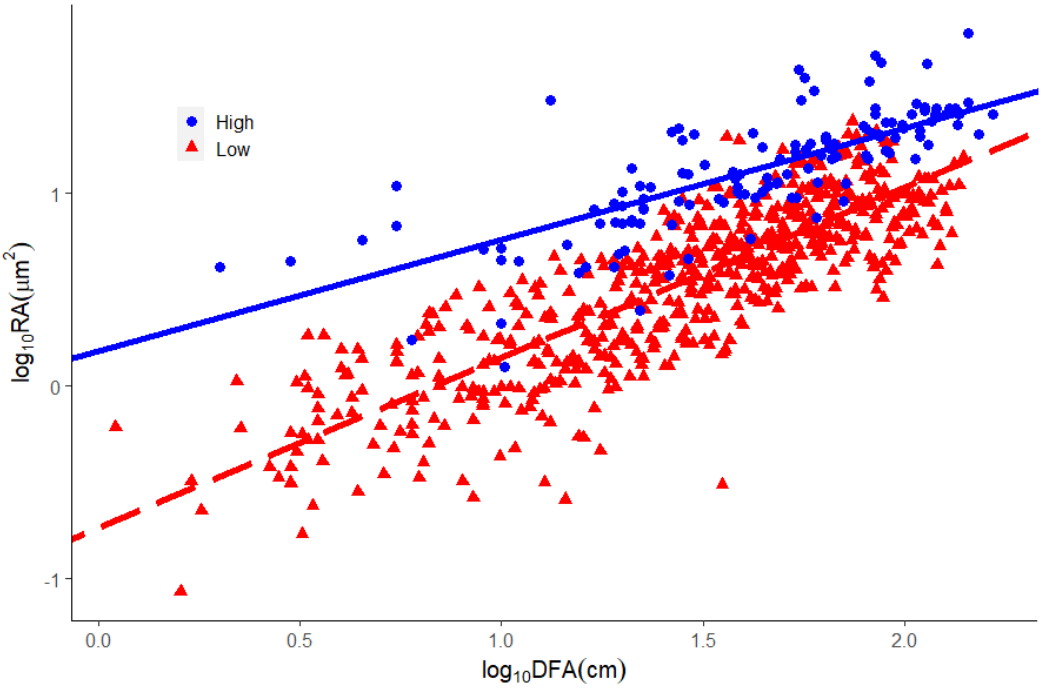

Figure 2.3.1 Variation in ring area (RA) with the distance from the branch apex (DFA) in High water availability (filled blue circles) and Low water availability (filled red triangles). Fitting lines (continuous for High, long dash for Low) are according to the models in Table 2.3.1. The mismatch of data amount in absolute size is given by the fact that Low treatment branches present more rings

The total needle biomass (LM), calculated as a progressive cumulative sum starting from the apex, shows an increment in value moving towards the branch base (Figure 2.3.2). The stable increase in needle biomass is similar and consistent for both study sites, with no statistically significant differences in slope or intercept in the models (Table 2.3.2). For total branch woody biomass (BM) that was progressively calculated as sum starting from the branch apex along the axis (DFA) there is

a significant difference for both y-intercept and slope (Figure 2.3.3, Table 2.3.2). Trees from the two study areas show similar allometric scaling, with an increase of BM over DFA.

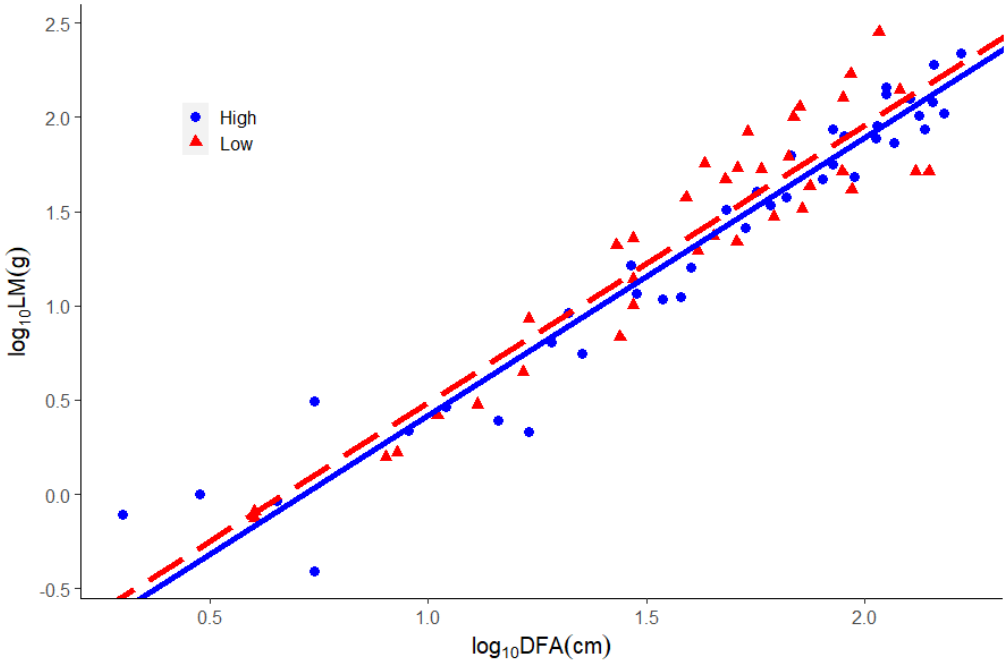

Figure 2.3.2 Variation in needle biomass (LM) with the distance from the branch apex (DFA) in High water availability (filled blue circles) and Low water availability (filled red triangles). Fitting lines (continuous for High, long dash for Low) are according to the models in Table 2.3.2.

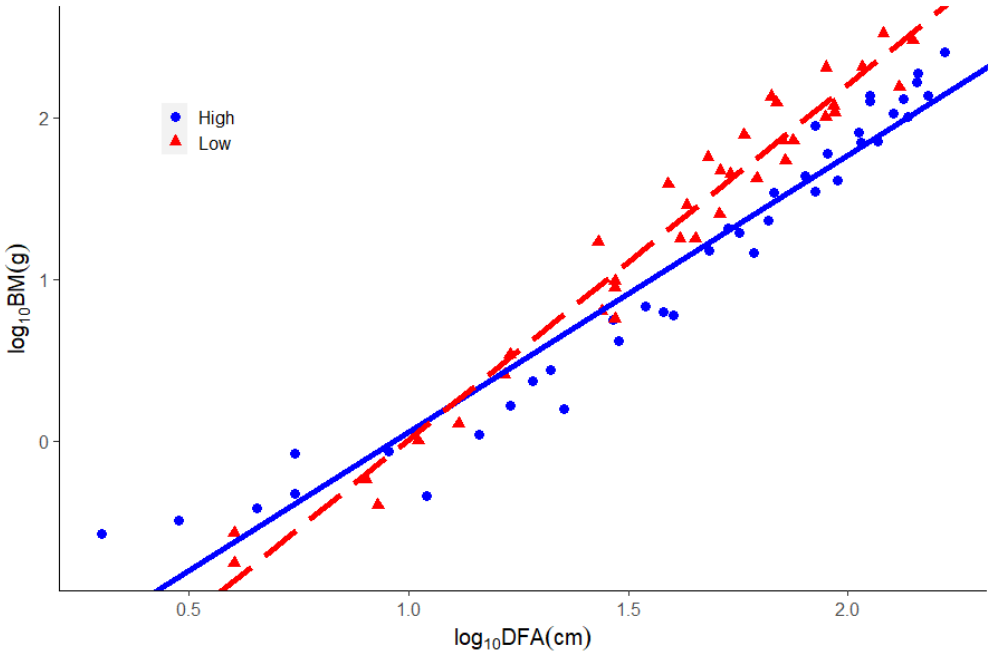

Figure 2.3.3 Variation in branch wood biomass (BM) with the distance from the branch apex (DFA) in High water availability (filled blue circles) and Low water availability (filled red triangles). Fitting lines (continuous for High, long dash for Low) are according to the models in Table 2.3.2.

It was also tested the allometric relationship expressing the biomass partitioning of branch biomass (BM) supported by needle biomass (LM) and the results of the model show statistical differences between the two study areas. The branch biomass accumulated in trees from the low water availability site display higher values in the apical-most points of the branches and lower values, compared to "high" site, at branch base which was showed in the models with higher y-intercept and lower slope (Figure 2.3.4, Table 2.3.2).

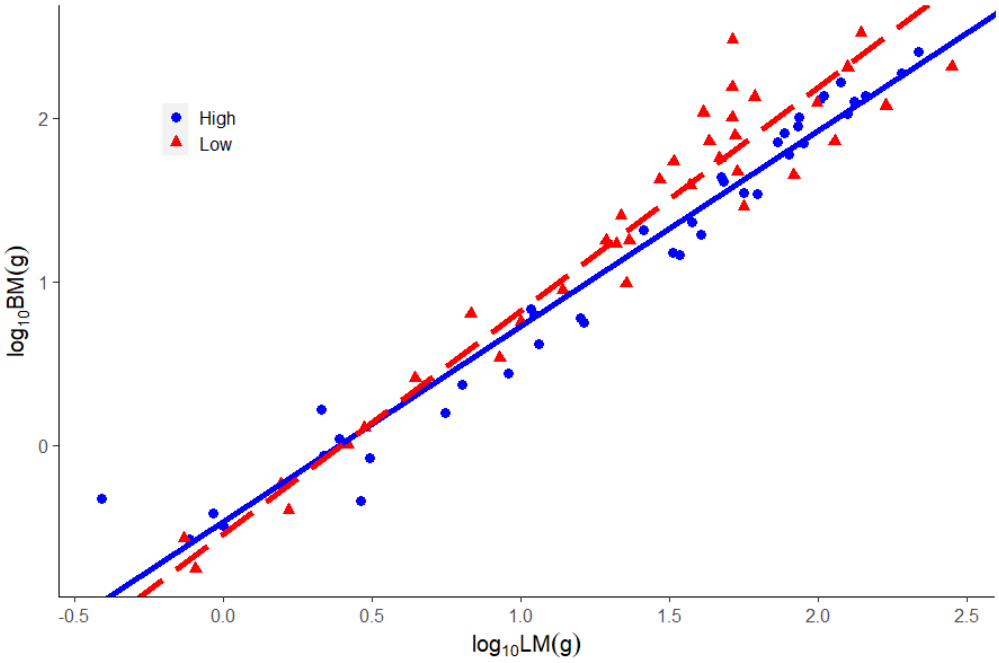

Figure 2.3.4 Variation in cumulated branch wood biomass (BM) with the cumulated leaves biomass (LM) in High water availability (filled blue circles) and Low water availability (filled red triangles). Fitting lines (continuous for High, long dash for Low) are according to the models in Table 2.3.2.

Leaf mass per area (LMA) is significantly different between the trees from "low" site and the trees from "high" site. Low water availability trees display higher LMA (Figure 2.3.5), due to an increased number of smaller, heavier needles. The assessment of stomatal density (SD) did not show any significant statistical difference between the two water availability sites (Figure 2.3.6).

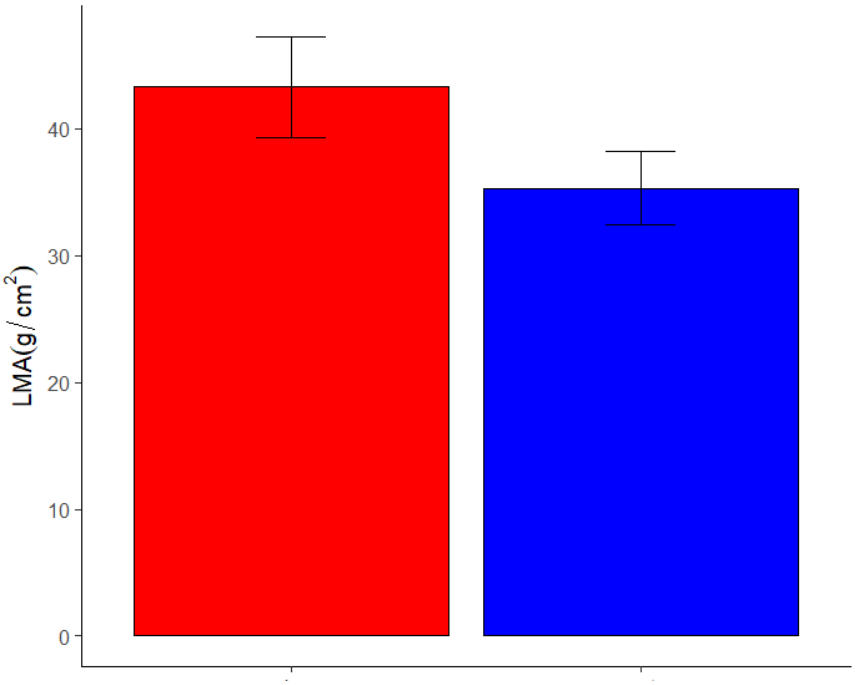

Figure 2.3.5 Differences in leaf mass per area (LMA) in High water availability (blue) and Low water availability (red). The Welch Two Sample t-test t = 3.5913, df = 7.3071, p-value = 0.008226**

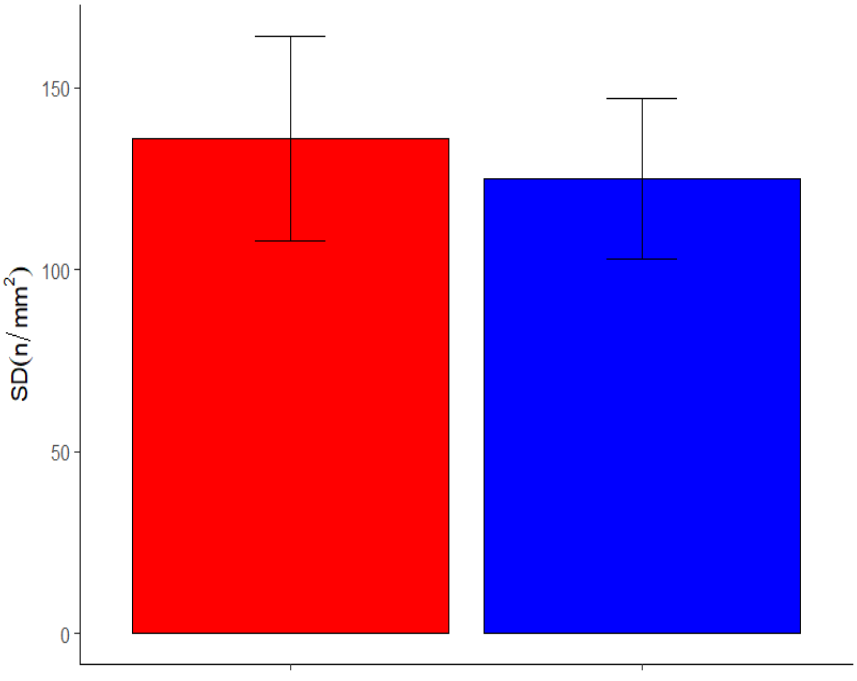

Figure 2.3.6 Differences in stomatal density (SD) in High water availability (blue) and Low water availability (red). The Welch Two Sample t-test t = 3.5913, df = 7.3071, p-value = 0.5091

Xylem anatomy

Ring data for xylem anatomy cover a period of time from 2021 back to 1954 in trees from the landfall site and from 2021 to 2014 in the high-water availability site. The anatomical data from every ring are then assigned to the corresponding DFA at the year of formation. Hydraulically weighted average conduit diameter (Dh) shows a clear pattern of increase along the axial gradient from tip to branch base for both areas (Figure 2.3.7). The statistical models reveal significant differences in both y-intercept and slope (Table 2.3.1), with the pines from the "low" area increasing their conduit diameter with an isometric scaling of the b exponent of ~0.2. The conduit widening along DFA for "high" trees follows a milder increase from apex to branch base with a scaling exponent of ~0.13.

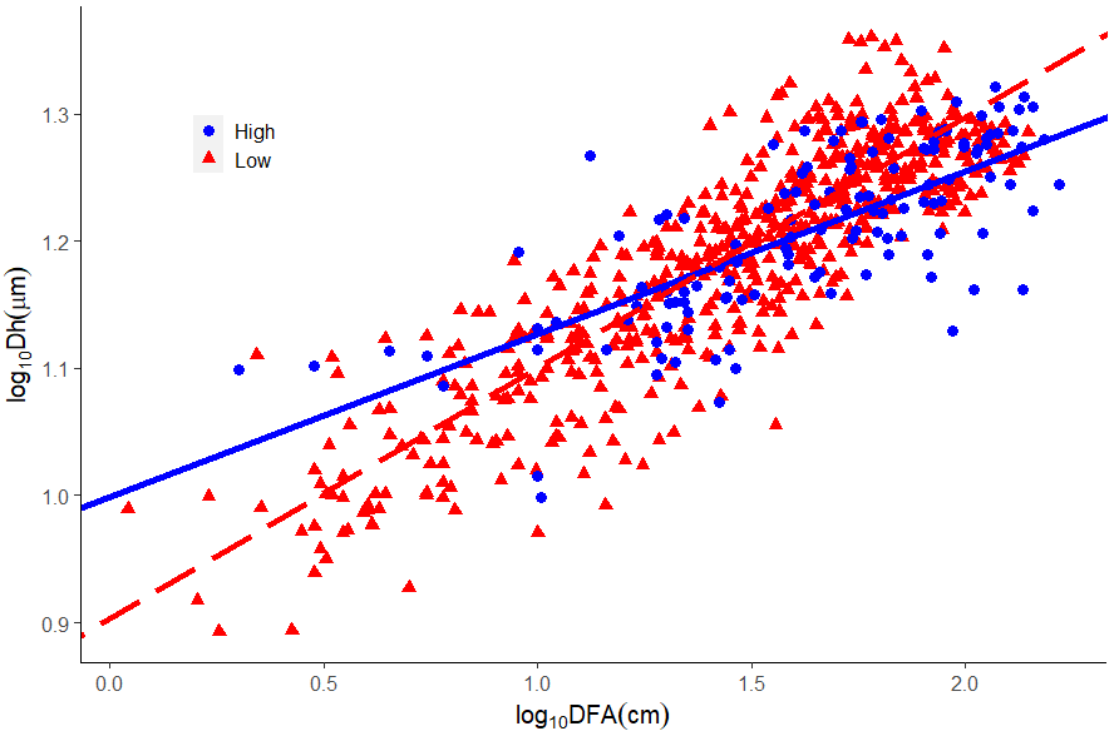

Figure 2.3.7 Variation in conduit hydraulic diameter (Dh) with the distance from the branch apex (DFA) in High water availability (filled blue circles) and Low water availability (filled red triangles). Fitting lines (continuous for High, long dash for Low) are according to the models in Table 2.3.1.

TABLE 2.3.1 Results of the optimal linear mixed-effect models predicting the effects of $\log_{10}DFA$ and *Site* on (A) $\log_{10}Dh$, (B) $\log_{10}RA$ Tree ID was used as random factor in all models. Asterisks indicate different estimates with significance at ** = $p < .05$, or at * = $p < .1$.

	(A) log10(Dh)		**(B) log10(RA)**	
Predictors	*Estimates*	*p*	*Estimates*	*p*
(Intercept)	1.00	**<0.001**	0.18	0.054
DFA [log10]	0.13	**<0.001**	0.58	**<0.001**
Site [Low]	-0.10	**<0.001****	-0.92	**<0.001****
DFA [log10] * Site [Low]	0.07	**<0.001****	0.30	**<0.001****
Random Effects				
σ^2	0.00		0.05	
τ_{00}	0.00 $_{Tree\_ID}$		0.01 $_{Tree\_ID}$	
ICC	0.21		0.17	
N	10 $_{Tree\_ID}$		10 $_{Tree\_ID}$	
Observations	700		731	
Marginal R^2 / Conditional R^2	0.746 / 0.798		0.753 / 0.794	

TABLE 2.3.2 Results of the optimal linear mixed-effect models predicting the effects of $\log_{10}DFA$ and *Site* on (A) $\log_{10}BM$, (B) $\log_{10}LM$.(C) is the model $\log_{10}BMvsLM$. Tree ID was used as random factor in all models Asterisks indicate different estimates with significance at $p < .05$, or at $p < .1$.

	(A) log10(BM)		**(B) log10(LM)**		**(C) log10(BMvsLM)**	
Predictors	*Estimates*	*p*	*Estimates*	*p*	*Estimates*	*p*
(Intercept)	-1.66	**<0.001**	-1.06	**<0.001**	-0.47	**<0.001**
DFA [log10]	1.71	**<0.001**	1.47	**<0.001**		
Site [Low]	-0.53	**0.003****	0.07	0.550	-0.07	0.580
DFA [log10] * Site[Low]	0.49	**<0.001****				
LM[log10]					1.20	**<0.001**
LM [log10] * Site[Low]					0.17	**0.002****
Random Effects						
σ^2	0.04		0.02		0.03	
τ_{00}	0.01 $_{Tree\_ID}$		0.03 $_{Tree\_ID}$		0.03 $_{Tree\_ID}$	
N	10 $_{Tree\_ID}$		10 $_{Tree\_ID}$		10 $_{Tree\_ID}$	
Observations	76		76		76	
Marginal R^2 / Conditional R^2	0.949 / 0.956		0.904 / 0.955		0.940 / 0.970	

2.3.4) Discussion

In this study, we performed xylem anatomical and carbon allocation measurements on branches of Scot pine trees, in two different water availability sites due to a landslide which created different soil conditions. Pinus sylvestris is an isohydric pioneer species which dominated and spread around continental temperate Europe (Irvine *et al*. 1998, Pretzsch *et al*. 2014). The objective of the study was to test if the successful acclimation to low water availability conditions could be achieved by means of phenotypic plasticity traits. The two different populations have been tested for power scaling relationships to see if plasticity was achieved by either a change in absolute proportions of the allometric constant (a) or scaling exponent (b). These relationships were checked for (i) biomass allocation patterns for branches and needles and for (ii) differences or modification in xylem anatomical patterns along the main axis.

Carbon allocation

The Scots pines from the low water availability sites clearly display a reduction of growth, both radial and longitudinal. The photosynthetic leaf biomass such as needles for conifers, are not formed new every year but are essential for carbon fixation, which define the possibility of a plant to avoid carbon starvation if enough sugars are stored (McDowell *et al.*, 2008). Needles production and maintenance is an expensive share in the carbon budget, and needles have to be mechanically and hydraulically supported by branch woody biomass. Under drought conditions it is expected to see a shift in the carbon allocation patterns, to better maximize carbon acquisition and avoid excessive water loss by a reduction of stomatal conductance or an increase in photosynthetic area (Anfodillo *et al.*, 2016). Our results displayed similar stomatal density for both water availability sites and the same cumulated needle biomass pattern along the axis of the branches. The needle biomass loading (Figure 2.3.2) did not show any statistically significant difference either in absolute values or scaling exponent (a and b respectively in Eq. $Y = a * X^b$) and thus, no signs of acclimation to drier conditions for the photosynthetic biomass. On the contrary, branch biomass (BM) did show few statistically significant changes but most likely due to having more rings, and hence denser and heavier latewood. Leaf mass per area (LMA) is reported in literature to have two possible responses under drought. Some studies displayed an increase in LMA under drought (Poorter *et al*. 2009), but some other a decreased under experimental drought conditions (Kuang *et al*. 2017, Petit, Zambonini, *et al*. 2022). In this work we found a statistically significant difference between the two sites, with low water availability pines having smaller needles and higher leaf mass per area. These combined results would suggest a stable pattern of carbon allocation to leaf biomass and stomatal density. Pines in the landslide area are likely fixing carbon in the first hours of the day when the transpirative demand is low and closing stomata

early when the water potential of the soil reaches a certain point (confirming by isohydric behavior of the species), thus resulting in decreased carbon fixation and later, growth.

Xylem anatomy

The hydraulically weighted average conduit diameter (Dh) followed a conduit widening power scaling exponent of b=0.13 for high water availability pine trees and b=0.2 for the low water availability pine trees. These results are coherent with others found in literature which usually show a scaling exponent (b) between 0.1 and 0.3.There is a strong conservativism of the conduit widening trait, and it is found ontogenetically stable (Prendin, Petit, *et al*. 2018) and consistent in different environmental conditions (Anfodillo *et al*. 2013, Olson *et al*. 2014). Our results display not only a different slope in the scaling equation, but also a significantly different intercept (corresponding to "a" in the power scaling equation). The two fitting lines show the xylem conduit diameter being larger in control trees for the first 50cm of the branch, then reaching the same values of the trees from the landslide area, and afterwards being smaller after that point. Since the conductance of a conduits scales with the fourth power of its diameter (Hagen-Poiseuille law (Tyree and Ewers 1991a)) and also the vulnerability to embolism is correlated to the conduit size (Hacke *et al*. 2006), in this experiment the pines in low water availability display two completely different responses within less than two meters from the branch apex. These modifications show a lower vulnerability in the apical-most part of the branch, where the resistances and pressures experienced by the tissues are also higher (lower Ψ (Tyree and Sperry 1989)). The differences along the branch in conduit hydraulic diameter and thus, xylem vulnerability to embolism opens serious problems of interpretation of the data for many studies that fix the sampling for age/internode or collect only one sample per branch. For example, in this study, fixing the sampling at only one given distance from the branch apex would have created biased results towards and increased/decreased vulnerability based on the position of the sampling. In order to understand short- and long-term responses to drought or acclimation strategies to low water availability is therefore essential to design a sampling procedure that consider the rigid axial variation of xylem traits. Our results, in accordance with Lechthaler *et al.* (2019) clearly show that neglecting the distance from the apex of the stem/branch can potentially lead to a not correct interpretation of results. Plants growing in dry environments, which on average have smaller shoot elongation every year, if sampled for one fixed age will wrongly exhibit smaller conduits.

This experimental study further contributes to increase the knowledge on the rigidity of conduit widening pattern along the main axis of the tree. In addition, a stable pattern of biomass allocation and stomal density suggest that many of the traits allometric scalings are constant and rigid even under harsh conditions for growing. Small anatomical changes can greatly influence the ability of a

isohydric species like *Pinus sylvestris* to acclimate and colonize new environments. Scot pines from the landslide area likely operate really close to their survival limit and since pine species were reported to suffer both from hydraulic failure and carbon starvation (McDowell *et al*. 2008c, Breshears *et al*. 2009, Sevanto *et al*. 2014), in a changing climate with more frequent and intense droughts, these pines will likely face increased threats.

Chapter 3

IMPORTANCE OF XYLEM CHARACTERISTICS IN BIOTIC AND ABIOTIC STRESS

Chapter 3.1

"Susceptibility to Xylella fastidiosa and functional xylem anatomy in Olea europaea: revisiting a tale of plant-pathogen interaction"

Giai Petit[1], Gianluca Bleve[2], Antonia Gallo[2], Giovanni Mita[2], Giuseppe Montanaro[3], Vitale Nuzzo[3], Dario Zambonini[1] and Andrea Pitacco[4]

1 Department of Land, Environment, Agriculture and Forestry (LEAF/TESAF), University of Padua, Viale dell'Università 16, 35020 Legnaro (PD), Italy,

2 Institute of Sciences of Food Production, National research Council (ISPA-CNR), via Provinciale Lecce-Monteroni 73100 Lecce, Italy,

3 Department of European and Mediterranean Culture (DiCEM), University of Basilicata, Via Lanera, 20, 75100 Matera, Italy

4 Department of Agronomy, Food, Natural resources, Animals and Environment (DAFNAE), University of Padua, Viale dell'Università 16, 35020 Legnaro (PD), Italy

Annals of Botany PLANTS 2021, Vol. 13, No. 4 doi:10.1093/aobpla/plab027

Abstract

Xylella fastidiosa is a xylem-limited bacterium causing the Olive Quick Decline Syndrome, which is currently devastating the agricultural landscape of Southern Italy. The bacterium is injected into the xylem vessels of leaf petioles after the penetration of the insect vector's stylet. From here, it is supposed to colonize the xylem vasculature moving against water flow inside conductive vessels. Widespread vessel clogging following the bacterial infection and causing the failure of water transport seemed not to be fully supported by the recent empirical xylem anatomical observations in infected olive trees. We tested the hypothesis that the higher susceptibility to the *X. fastidiosa*'s infection in Cellina di Nardò compared with Leccino is associated to the higher vulnerability to air embolism of its larger vessels. Such hypothesis is motivated by the recognized ability of *X. fastidiosa* in degrading pit membranes and also because air embolism would possibly provide microenvironmental conditions more favorable to its more efficient aerobic metabolism. We revised the relevant literature on bacterium growth and xylem physiology, and carried out empirical field, mid-summer measurements of xylem anatomy and native embolism in olive cultivars with high (Cellina di Nardò) and low susceptibility (Leccino) to the infection by *X. fastidiosa*. Both cultivars had similar shoot mass traits and vessel length (~80 cm), but the highly susceptible one had larger vessels and a lower number of vessels supplying a given leaf mass. Native air embolism reduced mean xylem hydraulic conductance by ~58 % (Cellina di Nardò) and ~38 % (Leccino). The higher air-embolism vulnerability of the larger vessels in Cellina di Nardò possibly facilitates the *X. fastidiosa*'s infection compared to Leccino. Some important characteristics of the vector-pathogen-plant interactions still require deep investigations acknowledging both the pathogen metabolic pathways and the biophysical principles of xylem hydraulics.

3.1.1) Introduction

Xylella fastidiosa is a gram-negative, non-flagellated bacterium highly specialized to colonize xylem vessels of several host plant species. Recently, *X. fastidiosa* subsp. *pauca* has been accidentally introduced in Salento (Apulia, Southern Italy) (Saponari *et al*., 2013), where it is causing the olive quick decline syndrome (OQDS), which has already devastated the olive groves of Salento region and is now continuously expanding, threatening all the Mediterranean region (Godefroid *et al*. 2019). The degree of the OQDS symptoms due to the infection of *X. fastidiosa* might greatly differ among olive cultivars to the extent that some of them (including the cv Leccino) appear to tolerate the infection (Martelli 2016). However, the mechanisms behind such a tolerance remain still not fully explored.

Insect vector, pathogen and host plant interactions

There is a general agreement that insect vectors hosting cells of *X. fastidiosa* in their foregut inoculate these bacterial cells into the xylem vasculature while feeding on the leaf petioles of the host plant, from where it spreads into the xylem of branches and stem (Almeida 2016). Since xylem vessels conduct water from roots to leaves, *X. fastidiosa* is supposedly able to spread along the xylem vasculature by efficiently moving against sap flow (Meng *et al*. 2005, Chen and De La Fuente 2020). A common consequence of the plant–pathogen interaction is the clogging xylem vessels by aggregates of tyloses and gels possibly limiting the pathogen spread (Pearce 1996).

Insect vectors and environmental conditions at the sites of inoculation

Xylem-feeding insects, such as sharpshooters leafhoppers (Hemiptera, Cicadellidae) and spittlebugs (Hemiptera, Cercopidae), can spread the pathogen *X. fastidiosa* by inoculating the bacterium into the xylem vessels when feeding from infected to not-infected plants. In the Mediterranean, the spittlebug *Philaenus spumarius* has been recognized as the main vector of *X. fastidiosa* (Cornara *et al*. 2017). This insect can host bacterial cells in its foregut, and may release them into the xylem transport system of the host plants when inserting its stylet into the leaf petiole up to the vessel elements to feed on xylem sap (Backus *et al*. 2015, Cornara *et al*. 2018). *Xylella fastidiosa* will then infect host plants by entering the xylem vasculature while mixed with the insect's salivary egestion (Backus *et al*. 2015). Despite the stylet penetration into the cell wall implies a significant mechanical damage, it has been argued that salivary egestion can prevent vessel

embolization by efficient wound sealing, allowing these specialized insects to feed on xylem sap even under high tension (Malone *et al*. 1999). From one hand, the assumption that such a physical damage to the vessel cell wall does not cause air entry into a vessel with sap pressure being easily at 1 MPa below atmospheric pressure would appear rather unlikely to many plant physiologists. On the other, it is certainly unrealistic that the vessel does not embolize upon stylet retraction, as its lumen would be directly connected with the external atmosphere (see below for details on air-embolism formation). Consequently, it seems arguable that vessels just infected by *X. fastidiosa* cannot remain hydraulically functional.

Bacterial colonization in xylem and spread through pit membranes

According to a functional *in silico* study, *X. fastidiosa* has a very simple and unusual respiratory complex and can use it at high aeration levels, whereas anaerobic respiration is limited to the use of sulfur metabolism (Bhattacharyya *et al*. 2002). Similar results were obtained with analyses of genetic, phenotypic and computational data, suggesting an incomplete anaerobic respiration metabolic network, coupled with a functional and more efficient, although limited, aerobic respiratory system (Gerlin *et al*., 2020). During plant colonization, bacterial cells are in a planktonic plant-competent status and are able to move along the xylem. Concerning the pathogen propagation in planta, open vessels of primary xylem crossing leaf-branch junctions have been hypothesized to facilitate the pathogen spreading (Chatelet *et al*. 2006). However, the colonization of the xylem vasculature requires the movement of bacteria between adjacent vessels across pit membranes (Newman *et al*. 2003, Cardinale *et al*. 2018). Since the pore diameter in pit membranes are in the range of 30–100 nm (Zhang *et al*. 2020), while the body size of *X. fastidiosa*'s cells are in the range of 250–2400 nm (Wells *et al*. 1987), the activation of cell wall-degrading enzymes is of fundamental importance to enlarge the pores allowing the bacteria to move to adjacent vessels and diffusely spread along the xylem vasculature (Pérez-Donoso *et al*. 2010a). Indeed, the presence of high level of diffusible signal factors (DSF) induce the bacteria to synthesize and release cell wall-degrading polygalacturonase and endo-1,4-b-glucanase able to enlarge pores among adjacent xylemic vessels and to allow bacterial cell to pass from one vessel to another (Roper *et al*. 2007, Ionescu *et al*. 2014). Accordingly, the production of surface adhesins and DSF

were suggested to relate to the pathogen virulence (Chatterjee *et al*. 2008, Ionescu *et al*. 2014).

Pit porosity and vulnerability to air embolism

The enlargement of pit pores likely has serious negative consequences on water transport linked to the formation and spread of air emboli. In plants, the water ascending along the xylem conduits is at sub-atmospheric pressure, and therefore in a metastable phase (i.e. at negative pressure, also called tension: Ψ_{XYL}). This means that it remains liquid while it should spontaneously change into its vapor state. According to the Laplace law, the maximum diameter of a dissolved air bubble ($dMAX$) is: $dMAX = -4\gamma/\Psi XYL$ *(1)* where γ is the surface tension at the liquid/air interface at 20 °C: 7.28×10^{-8} MPa m). It follows that pit membranes represents a safe barrier against air embolism, as they filter out air bubbles with diameter larger than pores (30–100 nm, Zhang *et al.* 2020). Therefore, the xylem vulnerability to air embolism is directly proportional to the pore size of pit membranes (Jansen *et al*. 2009).

Xylem anatomy and vulnerability to X. fastidiosa

Although vessel occlusions are widely diffused in the xylem of infected plants, their effect on the plant–pathogen interaction is still debated. According to one hypothesis, more vulnerable plants are less efficient in clogging vessels with tyloses, thus having a limited capacity to compartmentalize the host pathogen (Deyett *et al*. 2019). Instead, an opposite hypothesis would be that the loss of conductance due to vessel occlusions by bacterial aggregates and tyloses produces detrimental consequences on leaf water supply (Hopkins 1989, Sun *et al*. 2013). Consistent with the above hypotheses, a higher vulnerability to *X. fastidiosa*'s infection would be expected either in plants with larger vessel due to the larger volume of vasculature to be filled with tyloses for pathogen compartmentalization, or in plants with narrower vessels because the more efficient clogging of their lumina would more severely limit water transport.
Notably, empirical evidence suggested that the typical desiccation symptoms of *X. fastidiosa*'s infection commonly occur prior to tylose formation (Pérez-Donoso *et al*. 2016), thus implicitly questioning the causal relationship between vessel occlusions and disease symptoms. Furthermore, the appearance of worst disease symptoms is not necessarily associated with widely diffused bacterial aggregates or tyloses occluding vessels. In fact, *X.*

fastidiosa cells can sparsely diffuse on vessel cell walls without producing lumen occlusions (Gambetta *et al*. 2007, De Benedictis *et al*. 2017, Novelli *et al*. 2019).

Consistent with the ability of *X. fastidiosa* to degrade pit membranes, it has been reported that the loss of xylem hydraulic conductance due to drought-induced air embolism is more severe in infected vs. non-infected plants, and typically precedes the appearance of leaf scorch symptoms (McElrone *et al*. 2008). According to established literature on plant hydraulics, the higher vulnerability to air embolism is commonly associated to larger xylem conduits (Hacke *et al*. 2006). Therefore, it could also be hypothesized that the higher vulnerability to *X. fastidiosa*'s infection in some plants is associated with larger and less air- embolism resistant vessels (Sabella *et al*. 2019).

The aim of this work is to clearly characterize the difference in functional xylem anatomy and allocation patterns between two olive cultivars (Cellina di Nardò and Leccino), characterized by very different symptomatology to *X. fastidiosa*'s infection. We test the hypothesis that the more symptomatic Cellina di Nardò, which grows faster and is more productive than Leccino, has larger and fewer vessels sustaining leaf transpiration, thus possibly being more susceptible to drought-induced air embolism and to the pathogen infection.

3.1.2) Material and Methods

The study area was located at Alessano (Lecce, Apulia, Italy) (39°54′55″N, 18°19′16″E), where a 1 ha rainfed plantation of *Olea europaea* grove consisted of two sectors with the presence of the cultivar Cellina di Nardò (planting layout of 7.5 × 7.5 m) and Leccino (planting layout of 4.5 × 4.5 m). Tree age (~20 years) and size (tree height $H \sim 6$–7 m) was similar across individuals. All olive trees showed clear symptoms of infection by *X. fastidiosa*, with desiccated leaf area accounting for >70 % of the total canopy in Cellina di Nardò and <30 % in Leccino (by visual estimate). Due to the widespread diffusion of *X. fastidiosa*'s infection in the area, it was not possible to find a comparative *X. fastidiosa*-free site or with completely asymptomatic plants to be used as control. Sampling took place between the 9th and 14th of July 2019. Details of climate conditions during the season and at the time of field sampling are shown in Supporting Information—Fig. S1.

Measurements of leaf/branch biomass and xylem anatomy

We cut a sun exposed branch sample of ~2 m without visual signs of infection from the apical part of the crown of five tree for both cultivars. In each branch, we identified 4–

5 sampling points distributed at increasing distance from the apex downward along the main branch axis (Fig. 3.1.1), and for each point we measured the distance from the branch apex (*DFA*).

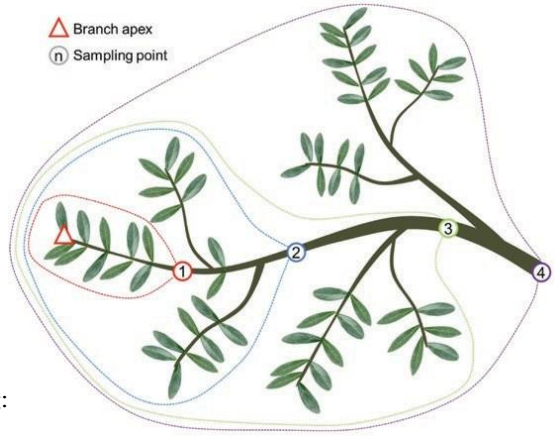

Figure 3.1.1. Branch sampling: d along the main branch axis, and the distance from the branch apex (*DFA*) measured. The dotted lines identify the total leaf biomass (LM_{CUM}) and the total xylem mass, BM_{CUM}) distal to each sampling point (i.e. cumulated from the branch apex).

Starting from the branch apex, we measured the total leaf biomass (LM_{CUM}) and the total branch biomass (BM_{CUM}, including the bark) that cumulated down to each sampling point (i.e. between the branch apex and the given sampling point: see dotted lines in Fig. 3.1.1). Leaf and xylem biomass were measured as dry weight after 48 h at 60 °C in the oven.

Furthermore, at each sampling position we extracted a segment of ~1.5 cm for the anatomical analyses. Segment ends were trimmed with a sharp blade to clearly visualize the cross-sectional surface free of sawdust, and then were observed under a stereomicroscope to check for the presence of vessel occlusions. Afterwards, they were put in a pressure cooker under vapour pressure for 1 h to soften the xylem tissues, and then cut with a rotary microtome (Leica RM2245; Leica Biosystems, Nussloch, Germany) at 15–20 μm. Sections were stained with safranine and AstraBlue (1 and 0.5 % in distilled water, respectively), and slides permanently fixed with Eukitt (BiOptica, Milan, Italy). Section images were acquired at 100× magnification, using a D-sight slide scanner (Menarini Group, Florence, Italy), and analysed with ROXAS (von Arx and Carrer 2014). The analysis was performed on a wedge of known angle (α, between 10 and 40 degrees) centered at the pith. Among many different parameters, the software automatically measured the lumen area of each individual vessel (*VA*) and calculated the total number of vessels (*VN*), the mean vessel lumen diameter (*VLD*, simplifying vessels as cylinders with length of 1 mm) and the total hydraulic conductivity (*Kh*) (based on the Hagen- Poiseuille law: Tyree and Ewers 1991). Data of *VN* and *Kh* were

finally multiplied by 360/α to rescale the ROXAS outputs to the total cross-sectional area of the sample.

Hydraulic measurements

The maximum vessel length (VL_{MAX}) was estimated on one asymptomatic branch from 5–6 trees per cultivar. Sun exposed branches of 1.5–2 m were excised and immediately transported to the lab into a black plastic bag containing a moist paper. In the lab, the branch base was re-cut under water to remove the basal 20 cm, and the cut surface trimmed with a sharp blade. The branch basal end, with bark removed for ~2 cm, was then attached to a source of degassed Levissima® mineral water, naturally containing several elements in ionic form as in xylem sap (Nardini *et al*. 2007) and flushed at a pressure P = 0.2 MPa for 15 min to remove all gas emboli. After flushing, we injected air at low pressure (P = 0.02 MPa). The main branch axis was then cut under water starting from the apex downwards approximately every 2 cm. VL_{MAX} was then estimated as the length of the remaining branch segment once a stream of air bubbles appeared at the apical cut surface.

The assessment of native air embolism was carried out on a sun exposed and asymptomatic branch from 5 to 6 trees per cultivar sampled before 8.00 a.m., i.e. before the development of low leaf water potentials. Immediately after excision, sampled branches were closed into a black plastic bag containing a moist paper to saturate vapour content and to limit leaf gas exchanges, and then transported to the lab. Hydraulic measurements were carried out after a sufficient time (>30 min) to re-equilibrate the water potential gradients inside the branches. Relaxed branches were then progressively cut under water starting from the base for a length of >80 cm (i.e. $>VL_{MAX}$), thus removing long vessels possibly embolized upon branch excision in the field (Torres-Ruiz *et al*. 2015). The apical part of the branch axis was also cut under water in order to obtain a branch segment of length$>VL_{MAX}$. Both the apical and basal cut surfaces were trimmed under water with a sharp razor blade to remove ~1 mm. The branch base, with bark removed for a length of ~2 cm, was then attached to a source of degassed Levissima® mineral water with a pressure head of ~0.02 MPa. The water flow rate (F, g s^{-1}) was then estimated based on the weight of water collected at the apical end of the branch pressurized for a period of 3 min into an Eppendorf vial containing a dry sponge of known weight. We repeated three measurements per sample. The initial branch conductance (Ki) was then

calculated as *F*/*P*. Branch samples were then flushed at $P = 0.2$ MPa for 15 min to remove all gas emboli, and then remeasured three times at $P = 0.02$ MPa (maximum branch conductance, *Kmax*). The percentage loss of hydraulic conductance (*PLC*) was then calculated as: $PLC = 1 - K_i / K_{max} \times 100$ (2)

Estimate of bacterial contamination

We estimated the presence of *X. fastidiosa* cells in a subset of leaves detached from the branches sampled for the measurements of biomass allocation and xylem anatomy, and in the water extracted from the xylem during the hydraulic measurements.

Petioles and leaf basal parts were sampled from 20 leaves of each branch and pulverized in liquid nitrogen. The resulting material was processed for CTAB-based DNA extraction according to the procedure reported in EPPO Bulletin focussed on diagnostics of *X. fastidiosa* (2019). Specifically, 0.5–1 g of fresh material was homogenized with 10 volumes of CTAB buffer (CTAB 2 %, Tris–HCl pH 8 100 mM, EDTA 20 mM, NaCl 1.4 M, PVP-40 1 %). An extract aliquot (1 mL) was incubated at 65 °C for 30 min and after centrifugation to remove plant tissue debris (16 000 g for 10 min), the supernatant was treated with chloroform: isoamyl alcohol (24:1) and total nucleic acids were isolated by precipitation with 2-propanol. After washing with 70 % ethanol, the pelleted DNA was resuspended in 100 µL of TE buffer.

During the hydraulic measurements, the water flowing at $P = 0.02$ MPa was collected from branches before (500 µL) and after (2 mL) flushing at $P = 0.2$ MPa. Samples were centrifuged at 8000gn× 5 min to collect bacterial cells and the pellet was resuspended in 45 µL of NaOH 50 mM. After boiling for 10 min, 5 µL of Tris–HCl 1 M were added. In the case of water collected after flush at $P = 0.2$ MPa, a further phenol: chloroform extraction step was performed, followed by precipitation and washing in ethanol. The pelleted DNA was resuspended in 100 µL of TE buffer.

DNA concentration was evaluated by absorbance at 260 nm and concentration of samples was adjusted to 100 ng μL^{-1}. Absolute quantification of *X. fastidiosa* in plants was performed by qPCR (Harper *et al*. 2010).

The assay was performed on the Applied Biosystem Step One system by adding 2 µL of DNA sample in a reaction volume of 20 µL containing ITaq Probe Master Mix 2X (Biorad). Each sample was run in triplicate. A standard calibration curve was used based on DNA extracted from 10-fold dilutions of health olive extract spiked with a bacterial suspension with an initial OD 600 of 0.5, corresponding to about 10^8 CFU mL^{-1}.

Statistical analyses

Structural and anatomical traits of stem and branches are known to vary longitudinally along the main axis of stem and branches. In order to account for the strict dependence of these traits on the distance from the distal apex (*DFA*) (Anfodillo *et al.* 2013; Petit *et al.* 2016), we tested for the differences between cultivars in several allometric scaling relationships: $Y = a*X^b$ (3). Data were first Log_{10}-transformed to accomplish for the assumption of normality and homoscedasticity (Zar 1999), so that equation (3) becomes: $Log_{10}Y = Log_{10}a + b \times Log_{10}X$ *(4).* We then tested differences between cultivars using linear mixed-effects models fitted with restricted maximum likelihood (REML) using the lme4 package (Bates *et al.* 2015) of the software R (R Development Core Team 2014). We used *DFA*, *Cultivar* and their interaction as fixed effects, and tree ID as random factor in all initial models. The best model was chosen based on Akaike Information Criterion (AIC) using the maximum likelihood method (Zuur *et al*. 2009).

3.1.3) Results

Branch biomass allocation and xylem anatomy

The sampled asymptomatic branches of both Cellina di Nardò and Leccino revealed no presence of vessel clogging upon observations at the stereoscope. We found that Cellina di Nardò allocated more biomass along the branch axis than Leccino. Moving from the branch apex downwards along the main branch axis, Cellina di Nardò cumulated more leaf mass (LM_{CUM}) than Leccino (i.e. higher *y*-intercept in the relationship of LM_{CUM} vs. distance from the apex, *DFA*: Fig. 3.2.2A; Table 3.2.1), but had not significantly higher xylem mass (BM_{CUM}) (i.e. not significantly different *y*-intercept in the relationship of BM_{CUM} vs. *DFA*: Fig. 3.2.2B; Table 3.2.1). Consequently, Cellina di Nardò distributed along the branch less xylem in proportion to leaf biomass compared with Leccino (Fig. 3.2.2C; Table 3.2.1), and consistently produced a lower number of vessels (*VN*) connected to the distal leaf mass (i.e. lower *y*-intercept in the relationship of *VN* vs. LM_{CUM}: Fig. 3.2.3A; Table 3.2.1). However, Cellina di Nardò hydraulically compensated the lower *VN* associated to a given leaf mass by producing vessels with significantly larger lumen diameter (*VLD*) (i.e. higher *y*-intercept in the relationship of *VLD* vs. *DFA*: Fig. 3.2.3B; Table 3.2.1). In fact, although the hydraulic conductivity (*Kh*) was higher in Cellina di Nardò compared with Leccino (i.e. higher *y*-

intercept in the relationship *Kh* vs. *DFA*: Fig. 3.2.4A; Table 3.2.1), the scaling of leaf-mass specific conductivity ($K_{LM} = K_H/LM_{CUM}$) vs. *DFA* was not significantly different between the two cultivars (Fig. 3.2.4B; Table 3.2.1), i.e. the absolute branch conductivity necessary to supply a unit of distal leaf mass does not significantly differ between the two cultivars.

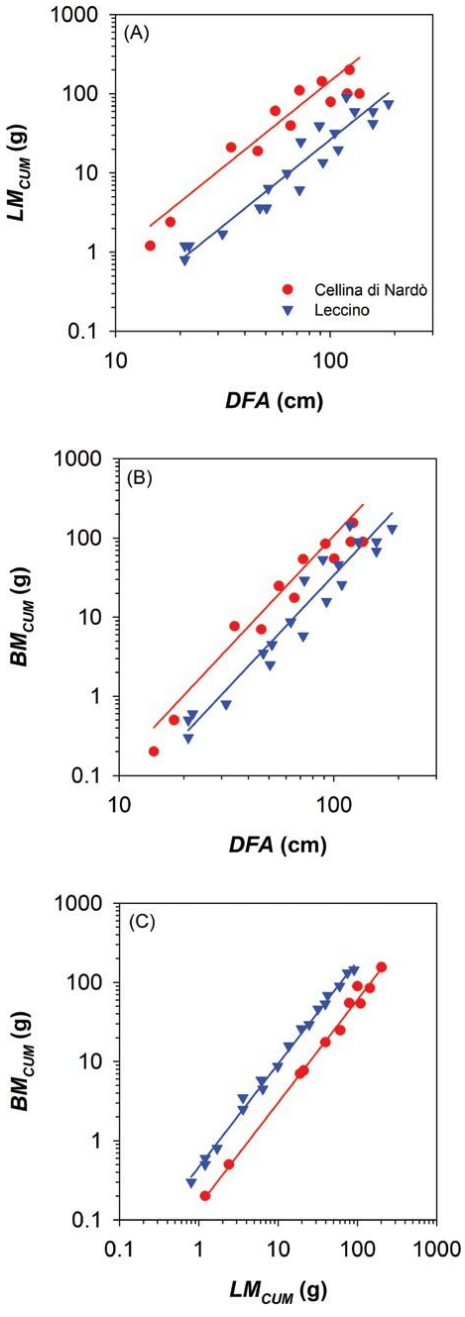

Figure 3.2.2. (A)Relationship between total leaf area (i.e. cumulated starting from the branch apex, LM_{CUM}) and distance from the branch apex (*DFA*).(B Relationship between total branch biomass (i.e. cumulated starting from the branch apex, BM_{cum}) and DFA.(C)relationship between BM and LM, Axes are displayed with logarithmic scale and parameters of fitting lines for Cellina di Nardò (red circles) and Leccino (blue triangles) are according to Table 3.2.1

TABLE 3.2.1. Statistics of the selected linear mixed-effects models predicting the difference between cultivars (Cellina di Nardò and Leccino, with the former taken as reference) on different relationships between traits describing allocational (A), anatomical (B) and functional (C) patterns. Plant ID was used as random factor.

	Model	Covariates and fixed effects	Estimate ± SE	DF	*t*-value	*P*	R^2m	R^2c
(A) ALLOCATION	*A1)* $LOG_{10}LM_{CUM} \sim LOG_{10}DFA + Cultivar (+ID_{PLANT})$	Intercept (y0)	−2.30 ± 0.20	24	−11.75	<0.0001	0.91	0.97
		Slope (β)	2.19 ± 0.08	24	26.22	<0.0001		
		Cultivar (LE)	−2.95 ± 0.17	3	−3.89	0.0301		
	A2) $LOG_{10}BM_{CUM} \sim LOG_{10}DFA + Cultivar (+ID_{PLANT})$	Intercept (y0)	−3.89 ± 0.21	24	−18.65	<0.0001	0.93	0.98
		Slope (β)	2.90 ± 0.08	24	36.01	<0.0001		
		Cultivar (LE)	−4.26 ± 0.20	3	−1.87	0.1589		
	A3) $LOG_{10}BM_{CUM} \sim LOG_{10}LM_{CUM} + Cultivar (+ID_{PLANT})$	Intercept (y0)	−0.82 ± 0.04	24	−20.03	<0.0001	0.99	0.99
		Slope (β)	1.31 ± 0.02	24	76.50	<0.0001		
		Cultivar (LE)	−0.34 ± 0.04	3	11.70	0.013		
(B) ANATOMY	*B1)* $LOG_{10}NV \sim LOG_{10}LM_{CUM} + Cultivar (+ID_{PLANT})$	Intercept (y0)	3.04 ± 0.11	24	26.85	<0.0001	0.90	0.91
		Slope (β)	0.94 ± 0.05	24	17.37	<0.0001		
		Cultivar (LE)	3.48 ± 0.10	3	4.28	0.0234		
	B2) $LOG_{10}VLD \sim LOG_{10}DFA + Cultivar (+ID_{PLANT})$	Intercept (y0)	0.87 ± 0.05	29	15.83	<0.0001	0.67	0.68
		Slope (β)	0.16 ± 0.03	29	5.24	<0.0001		
		Cultivar (LE)	0.75 ± 0.02	4	−6.68	0.0026		
(C) FUNCTION	*C1)* $LOG_{10}Kh \sim LOG_{10}DFA + Cultivar (+ID_{PLANT})$	Intercept (y0)	−12.17 ± 0.30	28	40.38	<0.0001	0.86	0.93
		Slope (β)	2.92 ± 0.19	28	19.93	<0.0001		
		Cultivar (LE)	−12.87 ± 0.20	4	−3.14	0.0347		
	C2) $LOG_{10}K_{LM} \sim LOG_{10}DFA + Cultivar (+ID_{PLANT})$	Intercept (y0)	−10.00 ± 0.26	24	−38.34	<0.0001	0.48	0.58
		Slope (β)	0.79 ± 0.14	24	5.73	<0.0001		
		Cultivar (LE)	−10.02 ± 0.13	3	−0.14	0.9		

Xylem air embolism

The maximum vessel length was similar along the distal 2 m of branches in both cultivars (VL_{MAX} ~ 80 cm; Table 3.2.2). The analyses on the diffusion of gas emboli filling vessels in *in vivo* plants (known as native air embolism) through the assessment of the percentage loss of xylem conductance (*PLC*) in living branches in the field revealed a significantly higher *PLC* (P = 0.04) in Cellina di Nardò (*PLC* = 58.0 %) than Leccino (*PLC* = 37.9 %) (Table 3.2.2).

Bacterial contamination of leaves and branch xylem

The analyses revealed the presence of *X. fastidiosa* subsp. *pauca* cells in leaf samples from

asymptomatic branches of both cultivars, but more abundant in Cellina di Nardò than Leccino (P = 0.008) (Table 3.2.2). Furthermore, the presence of the bacterium in functional vessels of asymptomatic branches was estimated by collecting the outflow during the measurements of Ki at low pressure (P = 0.02 Pa), and from the previously embolized vessels by collecting the water during the flushing at high pressure (P = 0.2 Pa). In both cases, it was not possible to determine the presence of bacteria likely because they were below the minimum detectable value (10^2 CFU mL^{-1}) (Table 3.2.2). However, for one out of four Cellina di Nardò samples, we found *X. fastidiosa* cells (2.8 10^2 CFU mL^{-1}) only after removing the gas emboli by flushing the sample at high pressure.

TABLE 3.2.2. Mean values (standard deviation between parentheses) of measured maximum vessel length (VL_{MAX}), percentage loss of hydraulic conductance (PLC), count of *X. fastidiosa* cells in the leaves (XF_{LEAF}) and in the water flowing through the xylem vessels during the hydraulic measurements (at low pressure: $XF_{FUNCT.\ VESSELS}$; during perfusion at high pressure: $XF_{EMB.\ VESSELS}$) (n.d.: under limit of detection of 10^2 CFU mL^{-1}). *Estimated excluding sample C6 = 2.8 × 10^2 CFU mL^{-1}.

Cultivar	VL_{MAX} (cm)	PLC (%)	XF_{LEAF} (CFU mL^{-1} × 10^3)	$XF_{FUNCT.\ VESSELS}$ (CFU mL^{-1})	$XF_{EMB.\ VESSELS}$ (CFU mL^{-1})
Cellina di Nardò	80.8 (5.5)	58.0 (21.7)	35.9 (31.6)	n.d.	n.d.*
Leccino	75.7 (12.7)	37.9 (5.6)	9.61 (8.2)	n.d.	n.d.

3.1.4) Discussion

Our results revealed clear differences in functional xylem anatomy and allocation patterns between the olive cultivars Cellina di Nardò and Leccino. In natural field conditions, these cultivars showed different susceptibility to the infection by *X. fastidiosa* (Martelli 2016). Since inoculation is dependent on the feeding activity of the insect vector *P. spumarius* (Cornara *et al*. 2017), the different symptomatology between olive cultivars likely depends on intrinsic differences in structure/ function relationships and/or response/defensive mechanisms to the pathogen attack.

Trees used in this experiment showed leaf scorch symptoms in various sectors of the crown denoting the bacteria infection, but also the sampled asymptomatic branches were infected as proved by the significant level of bacterial contamination at the leaf level (Table 3.2.2). We can, therefore, assume that asymptomatic infected branches were

sampled before the appearance of desiccations symptoms and possibly before the formation of vessel occlusions.

Cellina di Nardò (highly susceptible) produced shoots with more leaf and branch biomass compared with Leccino. However, the theoretical efficiency in leaf water supply did not differ between cultivars, because larger vessels would compensate for the reduced number of vessels per leaf mass in Cellina di Nardò compared to Leccino. Consequently, embolization of single vessels would be more limiting to water transport in Cellina di Nardò.

Vessels increased in diameter from the branch apex downwards (Fig. 3.2.3B), according to a pattern that is extremely stable across years (Anfodillo *et al.* 2013; Prendin *et al.* 2018). Because of this pattern, most of the total hydraulic resistance would be concentrated within the very last/apical portion of branches (Yang and Tyree 1993, Lechthaler *et al*. 2020), and the contribution of the narrower vessels of inner rings would be much less important than that of the outermost one.

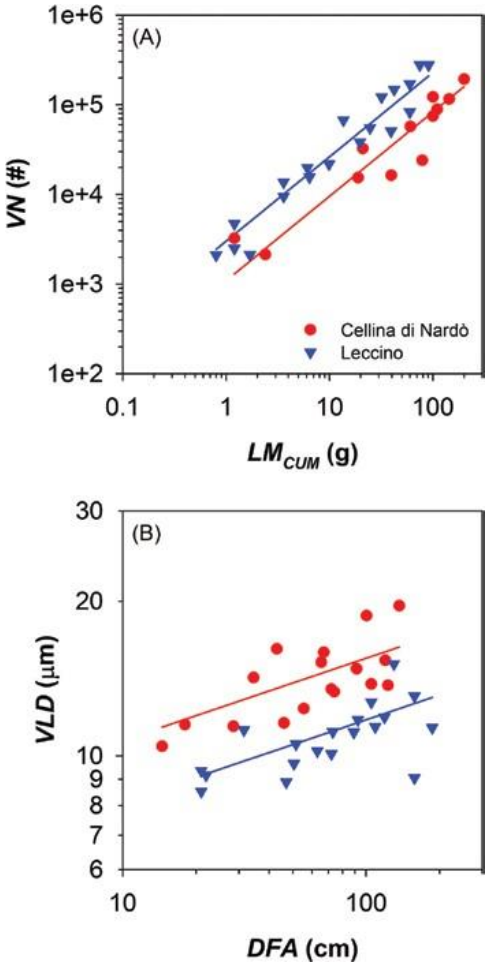

Figure 3.2.3. (A) Relationship between number of vessels (*VN*) and total supplied leaf mass (LM_{CUM}). (B) Variation in vessel lumen diameter (*VLD*) and distance from the branch apex (*DFA*). Axes are displayed with logarithmic scale and parameters of fitting lines for Cellina di Nardò (red circles) and Leccino (blue triangles) are according to Table 3.1.1.

Substantially, we did not observe vessel occlusions in our 1–2-year-old branches. Seemingly, a recent study reported a very low percentage of occluded vessels in the current (<2 %) and previous year (2–5 %) xylem rings of branches of both Cellina di Nardò and Leccino, and only in older rings the percentage increased at 15–20 % and 5–10 %, respectively (Sabella *et al*. 2020).

Notably, such a magnitude of vessel occlusions unlikely would determine a percentage loss of xylem conductance seriously limiting the leaf water supply. Typically, *X. fastidiosa* produces aggregates into xylem vessels of petioles (Sun *et al*. 2013, Sabella *et al*. 2019), but the bacterial colonization further down along the branch vasculature is less intense (Baccari and Lindow 2011). Furthermore, occlusions most often are caused by tyloses and gels produced by the plant rather than the direct proliferation of bacterial cells (De Benedictis *et al.* 2017; Sabella *et al.* 2019), thus questioning the relationship between the degree of leaf scorch symptoms and the abundance of *X. fastidiosa* cells in the xylem vasculature of the host plant (Gambetta *et al.* 2007; De Benedictis *et al.* 2017).

Our limited empirical hydraulic data on native embolism would suggest that Cellina di Nardò is more vulnerable to air embolism than Leccino (Table 3.2.2). Notably, the highest *PLC* of ~84 % was recorded in some branches of Cellina di Nardò. Such degrees of xylem hydraulic dysfunction have been argued to seriously compromise the plant survival, with foliar color changes typically lagging behind hydraulic failure (Urli *et al*. 2013, Hammond *et al*. 2019). However, these data did not prove that the vulnerability to air embolism increased following the progression of the infection.

The higher xylem vulnerability to air embolism in infected Cellina di Nardò compared to Leccino could be related either to simple intrinsic differences in xylem anatomical structures, like the larger vessel diameters (Fig. 3.2.3B), or possibly to an amplification effect by *X. fastidiosa* degrading pit membranes.

In this context, future studies comparing whole vulnerability curves of branches from infected vs. non-infected trees in the more symptomatic vs. the less symptomatic olive cultivars possibly will provide a clarifying information on the potential role of air embolism in the aetiology of the infection by *X. fastidiosa*.

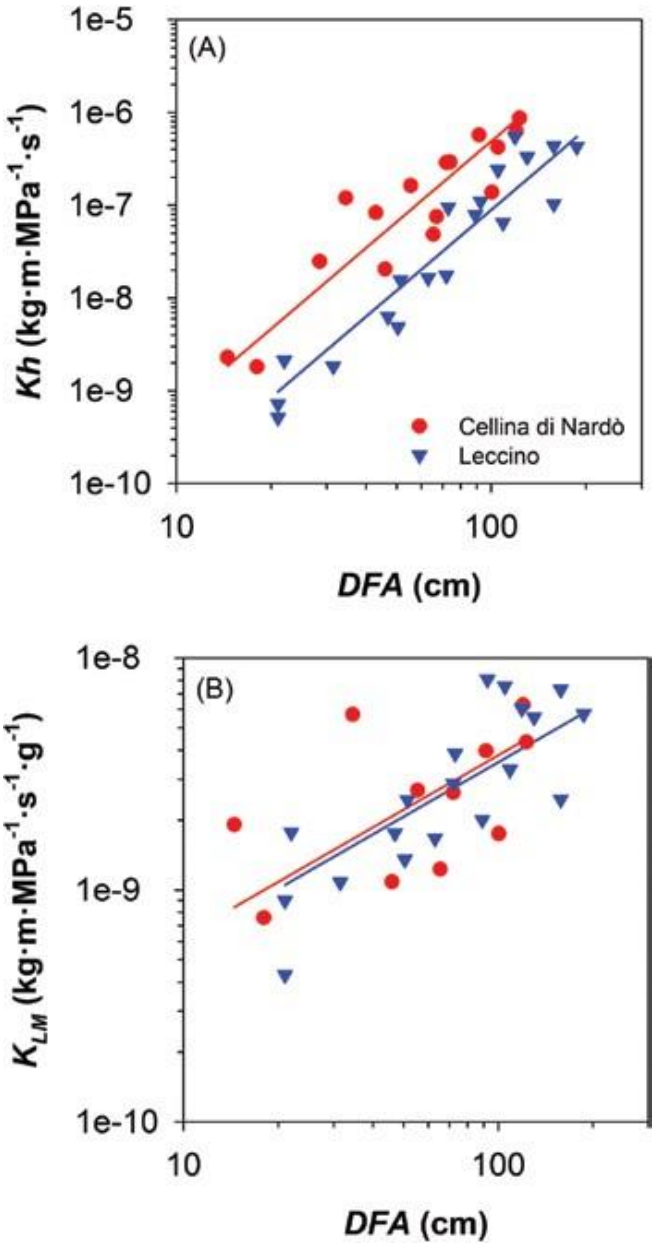

Figure 3.2.4. (A) Relationship between xylem hydraulic conductivity (*Kh*) and distance from the branch apex (*DFA*). (B) Relationship between leaf-mass specific hydraulic conductivity (K_{LM}) and *DFA*. Axes are displayed with logarithmic scale and parameters of fitting lines for Cellina di Nardò (red circles) and Leccino (blue triangles) are according to Table 3.2.1.

In the simplest case that infected olive trees were not more vulnerable to air embolism than non-infected ones, than the higher air-embolism vulnerability in Cellina di Nardò could likely predispose this cultivar to a more virulent infection by *X. fastidiosa* compared to Leccino, especially under drought conditions (McElrone *et al*. 2003), as typically occurs in the study area.

A worse-case scenario would be if infected olive trees were more vulnerable to air embolism than non-infected ones. This situation could be further corroborated by anatomical analyses on pit membrane integrity, as high pit membrane porosity is associated to higher xylem vulnerability to air embolism (Wheeler *et al*. 2005). Indeed, previous observations revealed pit membrane degradation following the digestion of the cellulosic and hemicellulosic components of the plant cell walls (Roper *et al*. 2007). Damages on pit membranes were reported to facilitate the bacterium spread to neighboring vessels (McElrone *et al*. 2008, Pérez-Donoso *et al*. 2010b). Although not tested in our study, and to date never been accounted for in previous studies, we push forward the hypothesis that xylem embolism could play a key role in the aetiology of the infection by *X. fastidiosa*, possibly providing more favorable conditions for its preferred and more efficient aerobic respiration.

Indeed, *X. fastidiosa* can perform both limited anaerobic and aerobic respiration (Bhattacharyya *et al.* 2002). However, in its metabolic network there is a functional and preferred aerobic respiration since no complete anaerobic respiration was found to be functional (Gerlin *et al.* 2020). Furthermore, functional vessels represent a difficult environment for life under water: water is under very negative pressure with low oxygen concentration, as big-sized air bubbles are filtered out by the small pores of pit membranes (Zhang *et al.* 2020).

We tried a novel hydraulic method to test for the presence of *X. fastidiosa* in air-embolized vs. functional vessels. Notably, a relatively small but significant number of *X. fastidiosa* cells was found only in air-embolized vessels form one branch of Cellina di Nardò. However, bacteria cells could possibly strongly adhere the infected xylem walls, thus limiting the removal potential of perfusing wood samples both at high and low pressure. A possible methodological improvement to better quantify the presence of *X. fastidiosa* in functional vs. air-embolized vessels could be the use of biofilm disrupting compounds increasing the *X. fastidiosa* release from vessel cell walls.

We push forward also the hypothesis that air embolism likely occurs at the moment of *X. fastidiosa* inoculation while vector insects feed on leaf petioles. Based on the known laws of physics, a great mechanical damage to the vessel cell wall would be produced as the insect vector inserts the stylet into the petiole tissues. This would cause the water tension to be immediately released, reaching atmospheric pressure by the suction of air into the lumen, thus possibly providing aerobic conditions during the first phases of infection.

In conclusion, we provided evidence for clear differences in the functional xylem anatomy between the two olive cultivars Cellina di Nardò and Leccino. The more *X. fastidiosa* symptomatic Cellina di Nardò appeared to be more vulnerable to drought-induced embolism formation because of its larger and fewer vessels. Since the magnitude of vessel clogging in infected olive trees appeared unlikely to provide hydraulic limitations to water transport (Sabella *et al.* 2020), we encourage the scientific community to further investigate on the potential relationship between xylem air embolism and the metabolic activity of the xylem-limited pathogen *X. fastidiosa*.

Chapter 3.2

"Plant's assimilation of Perfluoroalkyl compounds (PFAS) increases hydraulic vulnerability to embolism and bioaccumulation of the contaminants in tissues"

Poly- and Per-Fluorinated Alkyl Substances (PFAS) are among the most common pollutants derived from industry causing worldwide environmental contamination. PFAS are a class of more than 4700 artificial aliphatic compounds partially or fully fluorinated, which may contain functional groups. This chemical structure makes PFAS extremely persistent and resistant to degradation, and provides both hydrophobic and lipophobic properties, as well as high chemical and thermal stability. PFAS can move across water and are known to translocate and accumulate in living organisms, according to their chain length and functional group. Toxic effects on human health have been widely reported (Fenton *et al*. 2021)

PFAS occurrence in the xylem of the stem was demonstrated by DESI-MS and TEMEDS technologies by Wang *et al*. (2020), but there is still limited knowledge about PFAS effects on the plant vascular system and physiology. The aim of this research was to investigate if accumulation of PFAS may occur in conductive elements of willow plants, thus altering their hydrophilicity and hydraulic properties.

PFAS (Perfluoroalkyl compounds) are known to alter plant physiology by modifying metabolism and biochemical and physiological functions. It was previously observed that willow plants treated with PFAS exhibited increased photosynthesis and increased stomatal conductance (Sharma et al. 2020). A positive effect on some physiological functions was also reported, which somehow contradicts the general view of a negative impact on plant growth, which is also widely reported in literature. This discrepancy may be explained by the difficulty to compare different species under different experimental conditions (e.g., types of molecules, concentration, plant species, plant developmental stage, hydroponics *vs.* soil), which makes any comparison unrealistic and hardly possible. The comparison includes many changing variables, which are difficult to separate in the causal relationship. It is likely that accumulation of PFAS may occur in conductive elements, while altering their hydrophilicity and hydraulic conductivity. This may have paramount effects on xylem elements, represented by a highly hydrophilic lignocellulosic matrix where adhesion forces with the xylem sap enable capillarity and facilitate water transport (Dixon and Joly 1895). We therefore hypothesized that PFAS would be accumulated in the water transporting tissues and could negatively affect xylem conductivity.

Chemicals

PFAS included in the experiment are: perfluorobutanoic acid (PFBA), perfluoropentanoic acid (PFPeA), perfluorohexanoic acid (PFHxA), perfluoroheptanoic acid (PFHpA), perfluorooctanoic acid (PFOA), perfluorononanoic acid (PFNA), perfluorodecanoic acid (PFDA), perfluoroundecanoic acid (PFUnA), perfluorododecanoic acid (PFDoA), perfluorobutane sulfonate (PFBS) and perfluorooctane sulfonate (PFOS) (Sigma Aldrich, St. Louis, MS, USA). Identification and quantification of all PFAS were performed using the isotopically-labelled PFAS standards ($^{13}C_4$-PFBA, $^{13}C_3$-PFBS, $^{13}C_5$-PFPeA, $^{13}C_5$-PFHxA, $^{13}C_4$-PFHpA, $^{13}C_8$-PFOA, $^{13}C_8$-PFOS, $^{13}C_9$-PFNA, $^{13}C_6$-PFDA, $^{13}C_7$-PFUnA, $^{13}C_2$-PFDoA, Wellington laboratories, Guelph, ON, Canada) added at a fixed concentration as internal standards in mass spectrometry analysis.

Plant growth and treatment

Willow cuttings (*Salix triandra*) collected from the Plant Biodiversity and Agroforestry Center of Veneto Agricoltura, (Montecchio Precalcino, Vicenza, Italy), were grown hydroponically in greenhouse conditions, initially in water for 12 days, then in half strength modified Hoagland nutrient solution (Hoagland, 1933) for 3 days and finally in full strength nutrient solution. After rooting and shooting, 66 plants were selected for uniformity and transferred to single plastic pots equipped with an aeration system and covered with aluminum foil, containing 500 mL of nutrient solution. Plants were maintained in a growth chamber (12/12 h light/dark period, 25/20 °C temperature and 300 μmol photons m^{-2} s^{-1} of photosynthetic active radiation, PAR) for a few days to adapt to the new conditions. Once plants adapted to the new conditions, they were equally divided in two groups and the nutrient solution was changed. In one of the groups the new nutrient solution was spiked with PFAS mixture, each one at 100 μg L^{-1}. The experiment lasted 8 days to avoid refilling with the nutrient solution to compensate for nutrient limitation, transpiration and evaporation losses. The possible loss of PFAS and the evaporation of nutrient solution due to the exposure conditions were also determined. The uptake of PFAS was determined in terms of depletion from the nutrient solution and accumulation in the plant tissues at the end of the experiment. PFAS were extracted from root and leaf samples with methanol using an accelerated solvent extraction system. The amount of PFAS in nutrient solution, roots and leaves samples was measured by LC-MS/MS using a triple quadrupole (TSQ Quantiva, Thermo Fisher Scientific) coupled to a ultra-high performance liquid chromatography (Ultimate 3000 UHPLC, Dionex, Thermo Fisher Scientific).

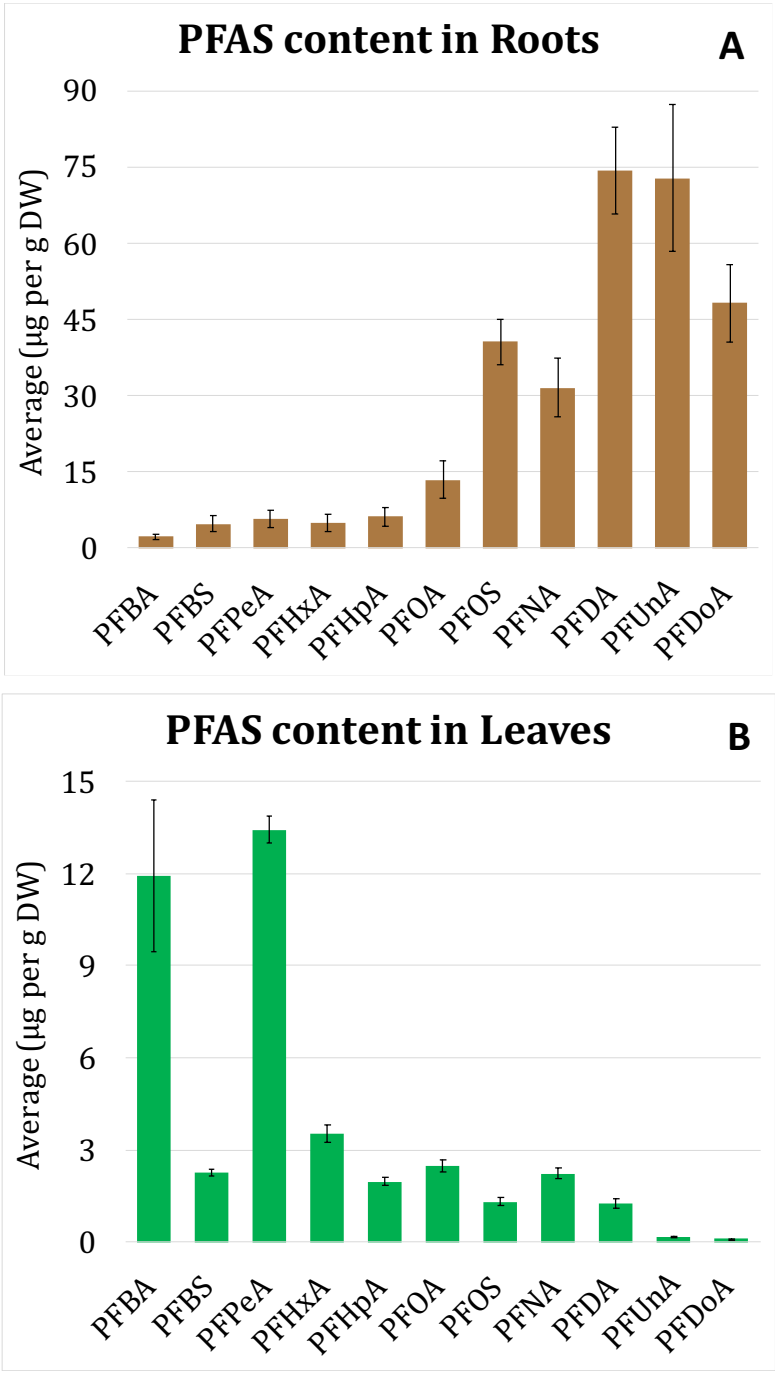

Figure 3.2.1 A) Amount of PFAS molecules quantified in treated roots (brown) samples at the end of the experimental period. Values indicate mean ± standard error (n = 18). B) Amount of PFAS molecules quantified in treated leaves samples (green) at the end of the experimental period. Values indicate mean ± standard error (n = 18).

The bioconcentration factor is defined as the ratio of the concentration of PFAS in plants over the concentration of PFAS available in the medium (Chen et al., 2020). The BCF for both leaves and roots was estimated using Eq. 3.2.1, with the concentration in the biomass referred to the dry weight (DW).

$$Bioconcentration\ factor = \frac{PFAS\ concentration\ in\ plant\ biomass\ (ng/kg\ DW)}{Initial\ PFAS\ concentration\ in\ the\ nutrient\ solution\ (ng/l)} \qquad \text{Eq. 3.2.1}$$

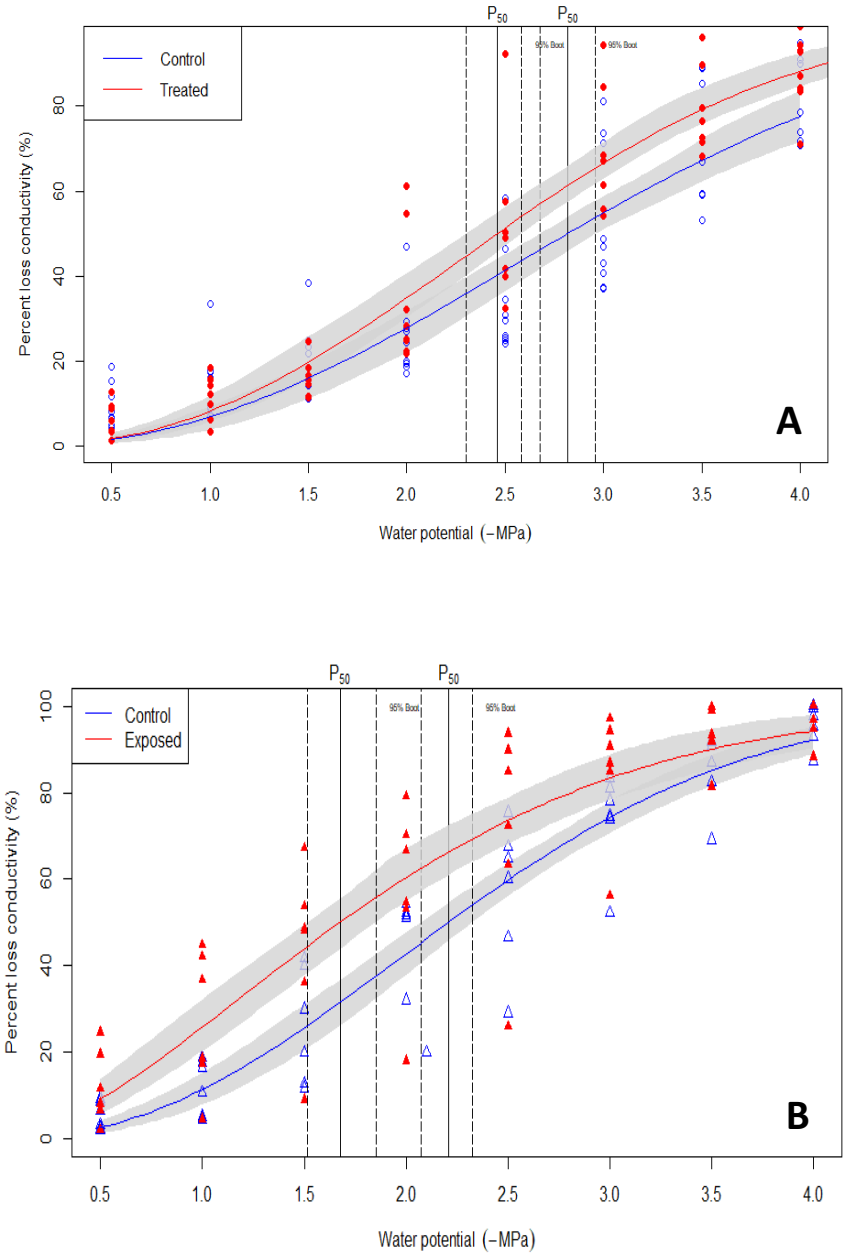

Figure 3.2.2 Vulnerability curves for willow cuttings grown hydroponically in a climatic chamber (A, n= 5 per treatment) and field-sampled branches in contaminated are of Castelgomberto (B, n= 3 trees per site). Measurements are obtained with the air-injection technique and interpolated with the package fitplc in software R.

Whole samplings had leaves and roots removed in the morning and transported in their growing containers to the lab. For field sampling, three 1m long branches were cut with a telescopic tree pruner and transported to the lab in black plastic bags with wet paper inside to minimize transpiration and water loss. After some preparatory trials, a minimum length of 200 mm (higher than maximum vessel length) was chosen and samples were cut and debarked underwater. Prior to hydraulic measurements, specimens were re-cut several times with clean razor blades and

subsequently connected to the measurement system. Samples were connected to a water reservoir installed at known height, a flow meter sensor (SLI-2000, Sensirion) and a pressure collar. Initial hydraulic conductivity was measured under a hydraulic pressure head of 9.5 kPa (950 mm water column) with distilled and degassed water. Samples were afterwards flushed for 15 minutes with water at high pressure (~ 0.2 MPa) to remove possible embolisms. After the flush the pressure was removed and the sample was re-connected for measurement to the water reservoir and flow sensor. The first value obtained is supposed to be the maximum flow at full hydration or P = 0. Air overpressure was then applied from the pressure collar at a known pressure of 0.5 MPa for 1 minute (double-ended pressure chamber, PMS Instruments, Corvallis, OR, USA), thereafter the specimen was re-connected again to water reservoir and flowmeter in order to determine the consecutive loss of conductivities at a given pressure application. The pressure in the chamber was gradually increased with steps of 0.5 MPa to reach a maximum of 4 MPa. The duration of the pressure exposition was always standardized to 1 minute (Rosner *et al*. 2019). Hydraulic vulnerability curves were achieved with the methods described by Duursma & Choat (2017) in the fitplc package for R and subsequently tested for statistical differences and significance.
Figure A shows the vulnerability curves obtained from the willow cuttings from the hydroponics experiment. Figure B shows the vulnerability curves made on fresh material obtained from a PFAS-exposed area after human contamination.

PFAS were detected in all the nutrient solution samples at a lower concentration compared to the beginning of the experiment, indicating that they were partially absorbed by the plants but remained available throughout the experiment. All the PFAS were detected in both leaves and roots: short chain molecules were accumulated at higher concentration in the leaves, whereas long chain PFAS were more abundant in the roots, consistent with the previous literature (Ghisi *et al*. 2019, Sharma *et al*. 2020). Phenotypical differences between control and treated plants were not observed. To evaluate possible effects on the xylem vulnerability to drought-induced embolism formation due to PFAS presence, we compared the values of the water potential at which 50% of hydraulic conductance is lost (P50) between control and treated plants. P50 values were calculated from the vulnerability curves showed in Figure 3.2.2. PFAS-exposed plants are characterized by a higher P50 value (less negative) with respect to untreated plants and this reflects an increased susceptibility to xylem embolism under drought conditions. These results support the hypothesis that PFAS can adhere to inner walls of xylem conduits and to plant tissues, making them more hydrophobic. Although the driving force for water movement in plants is the lower water potential established by stomatal opening, adhesion forces play a major role in preventing cavitation events.

The reduction of adhesion forces provoked by PFAS increases the vulnerability to embo lism and strong adhesion of PFAS to xylem conduits, granting hydrophobicity. To summarize and conclude we assessed:

- Accumulation of PFAS in different organs, based on molecular weight.
- PFAS treated and exposed plants display increased hydraulic vulnerability (less negative P50).
- Under future drought or water shortage conditions, PFAS exposed plant may be more vulnerable.
- PFAS creates two main problems: bioaccumulation in plant tissues (human health) and induce increased vulnerability in plants (resources).

GENERAL DISCUSSION AND CONCLUSIONS

The aim of the doctoral project was to improve the knowledge on the link between the anatomy of hydraulic architecture of trees and their functioning in water transport. The importance of anatomical and carbon allocation axial patterns was always kept in mind for the sampling design, but also for results' understanding and interpretation. Furthermore, it was tested whether environmental stresses could push some plastic responses in mature trees and how xylem anatomy could explain the effect of these stresses.

It was found a strong inverse correlation between conduits and pit size with P50, suggesting that the variation of embolism vulnerability as a function of distance from the apex (DFA) is changing due to anatomical patterns along the main axis. Caution should always be taken during sampling of material for VCs analyses, since our data clearly showed that hydraulic architecture and apex-to-base conduit widening (Anfodillo *et al*. 2013) may significantly affect the VCs shape, as well as the derived parameters (e.g. P50) (Domec and Gartner 2001). The first chapter, with the solidity of anatomical data of the other studies, pushes further the concept of vulnerability being a complex "trait" which can vary within the same plant or tissue. The experimental results give strength to the hypothesis that conduits embolization is tightly related to cell lumen area, conduits distribution and pit membrane size (Wheeler *et al*. 2005, Pittermann *et al*. 2010), all of which show mutual scaling and great differences between the tree apex and the trunk base.

In the context of drought and climate change, the three experimental projects of Chapter2 displayed similar results converging to few or no plastic changes (Petit, Zambonini, *et al*. 2022). These results may be alarming since duration and intensity of drought, combined with shifts of precipitation patterns and increased temperatures will influence standing vegetation with clear effects on drought-induced embolism as a trigger of mortality and hydraulic failure (McDowell *et al*. 2008, Brodribb and Cochard 2009, Choat *et al*. 2012, Barigah *et al*. 2013, Rowland, Da Costa, *et al*. 2015, Adams *et al*. 2017, Brodribb *et al*. 2020). Different degrees of phenotypic plasticity could potentially allow plants to acclimate to a changing climate and possibly leading to adapt to newly transformed environments (Nicotra *et al*. 2010). Considering the importance of carbon fixation via photosynthetic processes and the importance of carbon reserves, we could expect some differences of C allocation in drought conditions (Trugman *et al*. 2018). In the three experiments the carbon allocation patterns to leaf mass, leaf area and branch biomass were not affected by treatment duration or intensity, with only the droughted beech trees of the KROOF project allocating relatively more C to the production of new and more expanded leaves than to the allocation to the supporting branch biomass. The other results would suggest that the analyzed branches were not significantly affected by the precipitation

exclusion and did not reveal any acclimation strategy in their topmost part, but just a reduced growth with a maintenance of the allometric scaling.

Acclimation to drought may be achieved also with changes in the hydraulic architecture of the two transporting tissues, xylem and phloem. Two diverging hypotheses have been proposed and seen in some experimental studies. One suggests that plant could lower the vulnerability to embolism by producing smaller and safer conduits. This hypothesis[c] would imply the production of a xylem more resistant to embolism while contextually maintaining the total xylem conductance (Sperry *et al*. 2008). The trade-off would be an increase in the C costs associated with tissue production because more conductive cells should be formed to compensate for the lower conductance of their narrower lumen diameter. The other hypothesis, in opposition to the first, suggests that larger and more efficient conduits would allow a lower C investment in xylem tissue to maintain the total xylem conductance, at the cost of likely increasing the vulnerability to air embolism (Gleason *et al*. 2016). The anatomical analysis of the three projects of Chapter2 displayed robust and coherent data on the axial widening of xylem and phloem conduits. *Dh* increased with the distance from the branch apex according to a power scaling with exponent $b \sim 0.2$ independent of species and treatment. This result is consistent with the hypothesis of strong conservativism of the axial xylem design during ontogeny (Prendin, Petit, *et al*. 2018) and across species and environmental conditions (Anfodillo *et al*., 2013; Olson *et al*., 2014). In the case of prolonged or intense drought, our experimental data are not supporting the hypothesis that acclimation to drought can be achieved by an increased safety in the anatomical structure or via a reduced investment in branch or needle biomass. Prolonged drought also did not affect xylem traits of mean ring width and conduit diameter both for KROOF and SEV-LTER experimental sites. The intensity of the drought treatment affected phloem sieve elements in the pinon pines (Sevilleta), by pushing a higher efficiency due to a likely increase in sap viscosity (Sevanto 2014, 2018, Savage *et al*. 2017). The only significant changes in xylem anatomy were evident in the Scots pines with reduced water availability. These results for low water availability trees contrastingly display an increased efficiency (larger tracheids) in the first part of the branch and after that point an increased safety (smaller tracheids). This study, combined with the results of the other two, highlight the importance in vulnerability studies of taking into account xylem and phloem tissues with their axial pattern (Lechthaler *et al*. 2019). Neglecting the axial pattern or performing the classical punctual approach most likely would show narrower and more embolism resistant conduits for trees in dry conditions. For shorter trees with a slow axial stem/branch elongation, the sampling would be taken at a shorter distance from the stem/branch apex compared with those in taller and/or faster growing trees. Thus, showing not a real plastic change to drought, but just a different DFA (distance from the apex) in the allometric scaling of the conduits.

In the last chapter, including the two projects regarding biotic (*Xylella f.*) and abiotic (PFAS) stress, we further investigated how anatomical traits could be used to explain the plant response to these stresses (Brodribb and Hill 1999, Venturas *et al*. 2016, Lens *et al*. 2022). Quantitative wood anatomy was successfully used to refuse the old hypothesis according to which olive trees varieties with smaller vessels were more susceptible to the pathogen infection and proliferation (Petit *et al*. 2021). On the contrary, our experimental results clearly showed that Leccino variety, the less susceptible one, has smaller conductive elements compared to the more susceptible one, which displayed fewer and larger vessels. Anatomical characteristics of the hydraulic transport were also considered for the assessment of PFAS effects on plants. The chemical properties of PFAS (hydrophobicity) have a strong impact in the transport of water, which is subjected to adhesion and cohesion forces of water molecules to the xylem cell walls. PFAS-exposed plants displayed higher vulnerability to embolism suggesting that the contaminants can adhere to inner walls of xylem conduits and to plant tissues, granting hydrophobicity also to the surfaces of the vessels. Although the driving force for water movement in plants is the lower water potential established by stomatal opening, adhesion forces play a major role in preventing cavitation events. The reduction of adhesion forces provoked by PFAS increases the vulnerability to embolism and is crucial in drought conditions.

To conclude and summarize, this doctoral project highlighted the importance of stable axial patterns of the hydraulic architecture of trees. Assessing vulnerability to embolism is of great importance in the context of a changing climate, but this vulnerability is changing along the main xylem axis of the tree due to a combination of functional and anatomical traits. Delivering water to leaves is essential to sustain photosynthesis, but transporting water comes with intrinsic hazards. In a drought scenario, xylem, phloem, and biomass have great importance in the response to stresses and eventual modification of these components may successfully allow plants to acclimate to the new conditions. Our experimental studies show that anatomical patterns are quite rigid and did not exhibit high phenotypic plasticity under stress. In addition, this thesis provides relevant information for the understanding of vulnerability to drought. Future studies are highly recommended to consider the axial trends of plant traits and additional research should be carried out on anatomical and physiological responses to stress. In a changing climate with stronger and longer droughts, few or eventually no plastic responses may lead to catastrophic results which in part we can be already seen at present day.

AKNOWLEDGEMENTS

The first person to acknowledge on this list is surely my supervisor, prof. Giai Petit. Thank you for the nice work that we have done together during these last 3 years. I really enjoyed our coffee-talks in which we were discussing work, projects, and science. The second person to thank is my co-supervisor, prof. Michela Schiavon, for helping in the revision processes and always having time for a call and a kind word for me.

I would like to extend my sincere thanks to the two thesis reviewers, Anna Lintunen and Francesca Secchi, for the helpful comments and tips.

The biggest thanks go to my family for the continuous and unconditional support through the years of my studies and research. You have been fundamental for this achievement.

I am extremely grateful to my girlfriend, Aleksandra, who had to deal with the worst, grumpy and stressed PhD student, and yet was able to see the best part of me.

The last “thank you” goes to friends, colleagues, and scouts. You all made this journey enjoyable and worth living.

REFERENCES

Adams HD, Zeppel MJB, Anderegg WRL, Hartmann H, Landhäusser SM, Tissue DT, Huxman TE, Hudson PJ, Franz TE, Allen CD, Anderegg LDL, Barron-Gafford GA, Beerling DJ, Breshears DD, Brodribb TJ, Bugmann H, Cobb RC, Collins AD, Dickman LT, Duan H, Ewers BE, Galiano L, Galvez DA, Garcia-Forner N, Gaylord ML, Germino MJ, Gessler A, Hacke UG, Hakamada R, Hector A, Jenkins MW, Kane JM, Kolb TE, Law DJ, Lewis JD, Limousin JM, Love DM, Macalady AK, Martínez-Vilalta J, Mencuccini M, Mitchell PJ, Muss JD, O'Brien MJ, O'Grady AP, Pangle RE, Pinkard EA, Piper FI, Plaut JA, Pockman WT, Quirk J, Reinhardt K, Ripullone F, Ryan MG, Sala A, Sevanto S, Sperry JS, Vargas R, Vennetier M, Way DA, Xu C, Yepez EA, McDowell NG (2017) A multi-species synthesis of physiological mechanisms in drought-induced tree mortality. Nat Ecol Evol 1:1285–1291. http://dx.doi.org/10.1038/s41559-017-0248-x

Allen CD, Breshears DD, McDowell NG (2015) On underestimation of global vulnerability to tree mortality and forest die-off from hotter drought in the Anthropocene. Ecosphere 6:1–55.

Allen CD, Macalady AK, Chenchouni H, Bachelet D, McDowell N, Vennetier M, Kitzberger T, Rigling A, Breshears DD, Hogg EH (Ted., Gonzalez P, Fensham R, Zhang Z, Castro J, Demidova N, Lim JH, Allard G, Running SW, Semerci A, Cobb N (2010) A global overview of drought and heat-induced tree mortality reveals emerging climate change risks for forests. For Ecol Manage 259:660–684.

Almeida RPP (2016) Can Apulia's olive trees be saved? Science (80-) 353:346–348.

Anderegg WRL, Anderegg LDL, Kerr KL, Trugman AT (2019) Widespread drought-induced tree mortality at dry range edges indicates that climate stress exceeds species' compensating mechanisms. Glob Chang Biol 25:3793–3802.

Anderegg WRL, Schwalm C, Biondi F, Camarero JJ, Koch G, Litvak M, Ogle K, Shaw JD, Shevliakova E, Williams AP, Wolf A, Ziaco E, Pacala S (2015) Pervasive drought legacies in forest ecosystems and their implications for carbon cycle models. Science (80-) 349:528–532.

Anfodillo T, Carraro V, Carrer M, Fior C, Rossi S (2006) Convergent tapering of xylem conduits in different woody species. New Phytol 169:279–290.

Anfodillo T, Deslauriers A, Menardi R, Tedoldi L, Petit G, Rossi S (2012) Widening of xylem conduits in a conifer tree depends on the longer time of cell expansion downwards along the stem. J Exp Bot 63:837–845.

Anfodillo T, Petit G, Crivellaro A (2013) Axial conduit widening in woody species: A still neglected anatomical pattern. IAWA J 34:352–364.

Anfodillo T, Petit G, Sterck F, Lechthaler S, Olson ME (2016) Allometric trajectories and 'stress': A quantitative approach. Front Plant Sci 7:1–6.

von Arx G, Carrer M (2014) Roxas -A new tool to build centuries-long tracheid-lumen chronologies in conifers. Dendrochronologia 32:290–293.

Atala C, Lusk CH (2008) Xylem anatomy of Betula pendula roth saplings: Relationship to physical vascular models. Gayana - Bot 65:18–27.

Baas P (1983) Some ecological trends in vessels charachters. IAWA J 12:321–324.

Baccari C, Lindow SE (2011) Assessment of the process of movement of Xylella fastidiosa within susceptible and resistant grape cultivars. Phytopathology 101:77–84.

Backus EA, Shugart HJ, Rogers EE, Morgan JK, Shatters R (2015) Direct evidence of egestion and salivation of Xylella fastidiosa suggests sharpshooters can be 'flying syringes'. Phytopathology 105:608–620.

Bacterial G, Growth F (2020) crossm. 5:1–15.

Barigah TS, Charrier O, Douris M, Bonhomme M, Herbette S, Améglio T, Fichot R, Brignolas F, Cochard H (2013) Water stress-induced xylem hydraulic failure is a causal factor of tree mortality in beech and poplar. Ann Bot 112:1431–1437.

Barnard DM, Meinzer FC, Lachenbruch B, Mcculloh KA, Johnson DM, Woodruff DR (2011) Climate-related trends in sapwood biophysical properties in two conifers: avoidance of hydraulic dysfunction through coordinated

adjustments in xylem efficiency, safety and capacitance. Plant Cell Environ 34:643–654.

Bates D, Mächler M, Bolker BM, Walker SC (2015) Fitting linear mixed-effects models using lme4. J Stat Softw 67

Becker P, Gribben RJ, Schulte PJ (2003) Incorporation of transfer resistance between tracheary elements into hydraulic resistance models for tapered conduits. Tree Physiol 23:1009–1019.

De Benedictis M, De Caroli M, Baccelli I, Marchi G, Bleve G, Gallo A, Ranaldi F, Falco V, Pasquali V, Piro G, Mita G, Di Sansebastiano G Pietro (2017) Vessel occlusion in three cultivars of Olea europaea naturally exposed to Xylella fastidiosa in open field. J Phytopathol 165:589–594.

Bettiati D, Petit G, Anfodillo T (2012) Testing the equi-resistance principle of the xylem transport system in a small ash tree: Empirical support from anatomical analyses. Tree Physiol 32:171–177.

Bhattacharyya A, Stilwagen S, Reznik G, Feil H, Feil WS, Anderson I, Bernal A, D'Souza M, Ivanova N, Kapatral V, Larsen N, Los T, Lykidis A, Selkov E, Walunas TL, Purcell A, Edwards RA, Hawkins T, Haselkorn R, Overbeek R, Kyrpides NC, Predki PF (2002) Draft sequencing and comparative genomics of Xylella fastidiosa strains reveal novel biological insights. Genome Res 12:1556–1563.

Binks O, Meir P, Rowland L, da Costa ACL, Vasconcelos SS, de Oliveira AAR, Ferreira L, Christoffersen B, Nardini A, Mencuccini M (2016) Plasticity in leaf-level water relations of tropical rainforest trees in response to experimental drought. New Phytol 211:477–488.

Blackman CJ, Brodribb TJ, Jordan GJ (2010) Leaf hydraulic vulnerability is related to conduit dimensions and drought resistance across a diverse range of woody angiosperms. New Phytol 188:1113–1123.

Borghetti M, Cinnirella S, Magnani F, Saracino A (1998) Impact of long-term drought on xylem embolism and growth in Pinus halepensis Mill. Trees - Struct Funct 12:187–195.

Boyer JS, Silk WK (2004) Hydraulics of plant growth. Funct Plant Biol 31:761–773.

Breshears DD, Myers OB, Meyer CW, Barnes FJ, Zou CB, Allen CD, McDowell NG, Pockman WT (2009) Research communications research communications Tree die-off in response to global change-type drought: Mortality insights from a decade of plant water potential measurements. Front Ecol Environ 7:185–189.

Brodribb TJ (2009) Xylem hydraulic physiology: The functional backbone of terrestrial plant productivity. Plant Sci 177:245–251.

Brodribb TJ, Cochard H (2009) Hydraulic failure defines the recovery and point of death in water-stressed conifers. Plant Physiol 149:575–584.

Brodribb T, Hill RS (1999) The importance of xylem constraints in the distribution of conifer species. New Phytol 143:365–372.

Brodribb TJ, Powers J, Cochard H, Choat B (2020) Hanging by a thread? Forests and drought. Science (80-) 368:261–266.

Cailleret M, Dakos V, Jansen S, Robert EMR, Aakala T, Amoroso MM, Antos JA, Bigler C, Bugmann H, Caccianaga M, Camarero JJ, Cherubini P, Coyea MR, Čufar K, Das AJ, Davi H, Gea-Izquierdo G, Gillner S, Haavik LJ, Hartmann H, Hereş AM, Hultine KR, Janda P, Kane JM, Kharuk VI, Kitzberger T, Klein T, Levanic T, Linares JC, Lombardi F, Mäkinen H, Mészáros I, Metsaranta JM, Oberhuber W, Papadopoulos A, Petritan AM, Rohner B, Sangüesa-Barreda G, Smith JM, Stan AB, Stojanovic DB, Suarez ML, Svoboda M, Trotsiuk V, Villalba R, Westwood AR, Wyckoff PH, Martínez-Vilalta J (2019) Early-warning signals of individual tree mortality based on annual radial growth. Front Plant Sci 9:1–14.

Cailleret M, Jansen S, Robert EMR, Desoto L, Aakala T, Antos JA, Beikircher B, Bigler C, Bugmann H, Caccianiga M, Čada V, Camarero JJ, Cherubini P, Cochard H, Coyea MR, Čufar K, Das AJ, Davi H, Delzon S, Dorman M, Gea-Izquierdo G, Gillner S, Haavik LJ, Hartmann H, Hereş AM, Hultine KR, Janda P, Kane JM, Kharuk VI, Kitzberger T, Klein T, Kramer K, Lens F, Levanic T, Linares Calderon JC, Lloret F, Lobo-Do-Vale R, Lombardi F, López Rodríguez R, Mäkinen H, Mayr S, Mészáros I, Metsaranta JM, Minunno F, Oberhuber W, Papadopoulos A, Peltoniemi M, Petritan AM, Rohner B, Sangüesa-Barreda G, Sarris D, Smith JM, Stan AB, Sterck F, Stojanović DB, Suarez ML, Svoboda M, Tognetti R, Torres-Ruiz JM, Trotsiuk V, Villalba R, Vodde F, Westwood AR, Wyckoff PH, Zafirov N, Martínez-Vilalta J (2017) A synthesis of radial growth patterns preceding tree mortality.

Glob Chang Biol 23:1675–1690.

Cardinale M, Luvisi A, Meyer JB, Sabella E, De Bellis L, Cruz AC, Ampatzidis Y, Cherubini P (2018) Specific fluorescence in situ hybridization (Fish) test to highlight colonization of xylem vessels by xylella fastidiosa in naturally infected olive trees (Olea europaea L.). Front Plant Sci 9:1–9.

Carnicer J, Coll M, Ninyerola M, Pons X, Sánchez G, Peñuelas J (2011) Widespread crown condition decline, food web disruption, and amplified tree mortality with increased climate change-type drought. Proc Natl Acad Sci 108:1474 LP – 1478.

Carrer M, Von Arx G, Castagneri D, Petit G (2015) Distilling allometric and environmental information from time series of conduit size: The standardization issue and its relationship to tree hydraulic architecture. Tree Physiol 35:27–33.

Castagneri D, Carrer M, Regev L, Boaretto E (2020) Precipitation variability differently affects radial growth, xylem traits and ring porosity of three Mediterranean oak species at xeric and mesic sites. Sci Total Environ 699:134285.

Castagneri D, Petit G, Carrer M (2015) Divergent climate response on hydraulic-related xylem anatomical traits of Picea abies along a 900-m altitudinal gradient. Tree Physiol 35:1378–1387.

Chatelet DS, Matthews MA, Rost TL (2006) Xylem structure and connectivity in grapevine (Vitis vinifera) shoots provides a passive mechanism for the spread of bacteria in grape plants. Ann Bot 98:483–494.

Chatterjee S, Almeida RPP, Lindow S (2008) Living in two Worlds: The Plant and Insect Lifestyles of Xylella fastidiosa . Annu Rev Phytopathol 46:243–271.

Chen H, De La Fuente L (2020) Calcium transcriptionally regulates movement, recombination and other functions of Xylella fastidiosa under constant flow inside microfluidic chambers. Microb Biotechnol 13:548–561.

Choat B, Jansen S, Brodribb TJ, Cochard H, Delzon S, Bhaskar R, Bucci SJ, Feild TS, Gleason SM, Hacke UG, Jacobsen AL, Lens F, Maherali H, Martínez-Vilalta J, Mayr S, Mencuccini M, Mitchell PJ, Nardini A, Pittermann J, Pratt RB, Sperry JS, Westboy M, Wright IJ, Zanne AE (2012) Global convergence in the vulnerability of forests to drought. Nature 491:752–755.

Christof A, Ræbild A, Thygesen LG (2020) Pit and pit aperture dimensions in plantation-grown Douglas fir as affected by local growth conditions and height in stem. IAWA J 41:131–140.

Cochard H (2006) Cavitation in trees. Comptes Rendus Phys 7:1018–1026.

Copernicus Climate Change Service (2020) European State of the Climate – Summary 2020.

Cornara D, Cavalieri V, Dongiovanni C, Altamura G, Palmisano F, Bosco D, Porcelli F, Almeida RPP, Saponari M (2017) Transmission of Xylella fastidiosa by naturally infected Philaenus spumarius (Hemiptera, Aphrophoridae) to different host plants. J Appl Entomol 141:80–87.

Cornara D, Garzo E, Morente M, Moreno A, Alba-Tercedor J, Fereres A (2018) EPG combined with micro-CT and video recording reveals new insights on the feeding behavior of Philaenus spumarius. PLoS One 13:1–20.

Dannoura M, Epron D, Desalme D, Massonnet C, Tsuji S, Plain C, Priault P, Gérant D (2019) The impact of prolonged drought on phloem anatomy and phloem transport in young beech trees. Tree Physiol 39:201–210.

Deyett E, Pouzoulet J, Yang JI, Ashworth VE, Castro C, Roper MC, Rolshausen PE (2019) Assessment of Pierce's disease susceptibility in Vitis vinifera cultivars with different pedigrees. Plant Pathol 68:1079–1087.

Dickman LT, Mcdowell NG, Sevanto S, Pangle RE, Pockman WT (2015) Carbohydrate dynamics and mortality in a piñon-juniper woodland under three future precipitation scenarios. Plant Cell Environ 38:729–739.

Dixon HH, Joly J (1895) On the Ascent of Sap Henry H. Dixon; J. Joly Philosophical Transactions of the Royal Society of London. B, Vol. 186. (1895), pp. 563-576. Philos Trans R Soc Londo 186:563–576.

Domec JC, Gartner BL (2001) Cavitation and water storage capacity in bole xylem segments of mature and young Douglas-fir trees. Trees - Struct Funct 15:204–214.

Duursma R, Choat B (2017) fitplc - an R package to fit hydraulic vulnerability curves. J Plant Hydraul 4:e002.

Engelbrecht BMJ, Comita LS, Condit R, Kursar TA, Tyree MT, Turner BL, Hubbell SP (2007) Drought sensitivity shapes species distribution patterns in tropical forests. Nature 447:80–82.

Fajardo A, Martínez-Pérez C, Cervantes-Alcayde MA, Olson ME (2020) Stem length, not climate, controls vessel diameter in two trees species across a sharp precipitation gradient. New Phytol 225:2347–2355.

Fenton SE, Ducatman A, Boobis A, DeWitt JC, Lau C, Ng C, Smith JS, Roberts SM (2021) Per- and Polyfluoroalkyl Substance Toxicity and Human Health Review: Current State of Knowledge and Strategies for Informing Future Research. Environ Toxicol Chem 40:606–630.

Gambetta GA, Fei J, Rost TL, Matthews MA (2007) Leaf scorch symptoms are not correlated with bacterial populations during Pierce's disease. J Exp Bot 58:4037–4046.

Gersony JT, Holbrook NM (2022) Phloem turgor is maintained during severe drought in Ricinus communis. Plant, Cell \& Environ 45:2898–2905.

Ghisi R, Vamerali T, Manzetti S (2019) Accumulation of perfluorinated alkyl substances (PFAS) in agricultural plants: A review. Environ Res 169:326–341.

Gleason SM, Westoby M, Jansen S, Choat B, Hacke UG, Pratt RB, Bhaskar R, Brodribb TJ, Bucci SJ, Cao KF, Cochard H, Delzon S, Domec JC, Fan ZX, Feild TS, Jacobsen AL, Johnson DM, Lens F, Maherali H, Martínez-Vilalta J, Mayr S, Mcculloh KA, Mencuccini M, Mitchell PJ, Morris H, Nardini A, Pittermann J, Plavcová L, Schreiber SG, Sperry JS, Wright IJ, Zanne AE (2016) Weak tradeoff between xylem safety and xylem-specific hydraulic efficiency across the world's woody plant species. New Phytol 209:123–136.

Godefroid M, Cruaud A, Streito JC, Rasplus JY, Rossi JP (2019) Xylella fastidiosa: climate suitability of European continent. Sci Rep 9:1–10.

Grams TEE, Hesse BD, Gebhardt T, Weikl F, Rötzer T, Kovacs B, Hikino K, Hafner BD, Brunn M, Bauerle T, Häberle KH, Pretzsch H, Pritsch K (2021) The Kroof experiment: realization and efficacy of a recurrent drought experiment plus recovery in a beech/spruce forest. Ecosphere 12

Guérin M, Martin-Benito D, von Arx G, Andreu-Hayles L, Griffin KL, Hamdan R, McDowell NG, Muscarella R, Pockman W, Gentine P (2018) Interannual variations in needle and sapwood traits of Pinus edulis branches under an experimental drought. Ecol Evol 8:1655–1672.

Hacke U (2015) Functional and ecological Xylem anatomy. Springer International Publishing.

Hacke UG, Sperry JS (2001) Functional and ecological xylem anatomy. Perspect Plant Ecol Evol Syst 4:97–115.

Hacke UG, Sperry JS, Pockman WT, Davis SD, McCulloh KA (2001) Trends in wood density and structure are linked to prevention of xylem implosion by negative pressure. Oecologia 126:457–461. http://link.springer.com/10.1007/s004420100628 (10 February 2020, date last accessed).

Hacke UG, Sperry JS, Wheeler JK, Castro L (2006) Scaling of angiosperm xylem structure with safety and efficiency. Tree Physiol 26:689–701.

Hacke UG, Stiller V, Sperry JS, Pittermann J, McCulloh KA (2001) Cavitation Fatigue. Embolism and Refilling Cycles Can Weaken the Cavitation Resistance of Xylem. Plant Physiol 125:779–786. http://www.plantphysiol.org/lookup/doi/10.1104/pp.125.2.779 (10 February 2020, date last accessed).

Hammond WM, Yu K, Wilson LA, Will RE, Anderegg WRL, Adams HD (2019) Dead or dying? Quantifying the point of no return from hydraulic failure in drought-induced tree mortality. New Phytol 223:1834–1843.

Harper SJ, Ward LI, Clover GRG (2010) Development of LAMP and real-time PCR methods for the rapid detection of Xylella fastidiosa for quarantine and field applications. Phytopathology 100:1282–1288.

Held M, Ganthaler A, Lintunen A, Oberhuber W, Mayr S (2021) Tracheid and Pit Dimensions Hardly Vary in the Xylem of Pinus sylvestris Under Contrasting Growing Conditions. Front Plant Sci 12:1–11.

Hellkvist J, Richards GP, Jarvis PG (1974) Vertical Gradients of Water Potential and Tissue Water Relations in Sitka Spruce Trees Measured with the Pressure Chamber. J Appl Ecol 11:637.

Hesse BD, Goisser M, Hartmann H, Grams TEE (2019) Repeated summer drought delays sugar export from the leaf and

impairs phloem transport in mature beech. Tree Physiol 39:192–200.

Hesse BD, Hartmann H, Rötzer T, Landhäusser SM, Goisser M, Weikl F, Pritsch K, Grams TEE (2021) Mature beech and spruce trees under drought – Higher C investment in reproduction at the expense of whole-tree NSC stores. Environ Exp Bot 191

Hietz P, Rosner S, Sorz J, Mayr S (2008) Comparison of methods to quantify loss of hydraulic conductivity in Norway spruce. Ann For Sci 65:502–502.

Hölttä T, Vesala T, Sevanto S, Perämäki M, Nikinmaa E (2006) Modeling xylem and phloem water flows in trees according to cohesion theory and Münch hypothesis. Trees - Struct Funct 20:67–78.

Hopkins DL (1989) Xylella fastidiosa: xylem-limited bacterial pathogen of plants. Annu Rev Phytopathol Vol 27:271–290.

Hudson PJ, Limousin JM, Krofcheck DJ, Boutz AL, Pangle RE, Gehres N, McDowell NG, Pockman WT (2018) Impacts of long-term precipitation manipulation on hydraulic architecture and xylem anatomy of piñon and juniper in Southwest USA. Plant Cell Environ 41:421–435.

Ionescu M, Zaini PA, Baccari C, Tran S, Da Silva AM, Lindow SE (2014) Xylella fastidiosa outer membrane vesicles modulate plant colonization by blocking attachment to surfaces. Proc Natl Acad Sci U S A 111:E3910–E3918.

IPCC (2014) Summary for policymakers.

IPCC (2018) Global warming of 1.5°C.

IPCC (2022) IPCC 2022.

Irvine J, Perks MP, Magnani F, Grace J (1998) The response of Pinus sylvestris to drought: Stomatal control of transpiration and hydraulic conductance. Tree Physiol 18:393–402.

Jansen S, Choat B, Pletsers A (2009) Morphological variation of intervessel pit membranes and implications to xylem function in angiosperms. Am J Bot 96:409–419.

Jyske T, Hölttä T (2015) Comparison of phloem and xylem hydraulic architecture in Picea abies stems. New Phytol 205:102–115.

Kiorapostolou N, Camarero JJ, Carrer M, Sterck F, Brigita B, Sangüesa-Barreda G, Petit G (2020) Scots pine trees react to drought by increasing xylem and phloem conductivities. Tree Physiol 40:774–781.

Kiorapostolou N, Galiano-Pérez L, von Arx G, Gessler A, Petit G (2018) Structural and anatomical responses of Pinus sylvestris and Tilia platyphyllos seedlings exposed to water shortage. Trees - Struct Funct

Kiorapostolou N, Petit G (2018) Similarities and differences in the balances between leaf, xylem and phloem structures in Fraxinus ornus along an environmental gradient. Tree Physiol 39:234–242.

Kolb KJ, Sperry JS (1999) Differences in drought adaptation between subspecies of sagebrush (Artemisia tridentata). Ecology 80:2373–2384.

Kuang Y, Xu Y, Zhang L, Hou E, Shen W (2017) Dominant Trees in a Subtropical Forest Respond to Drought Mainly via Adjusting Tissue Soluble Sugar and Proline Content . Front Plant Sci 8:802.

Larter M, Pfautsch S, Domec J-C, Trueba S, Nagalingum N, Delzon S (2017) Aridity drove the evolution of extreme embolism resistance and the radiation of conifer genus Callitris. New Phytol 215:97–112.

Lazzarin M, Crivellaro A, Williams CB, Dawson TE, Mozzi G, Anfodillo T (2016) TRACHEID AND PIT ANATOMY VARY IN TANDEM IN A TALL SEQUOIADENDRON GIGANTEUM TREE. IAWA J 37:172–185.

Lechthaler S, Kiorapostolou N, Pitacco A, Anfodillo T, Petit G (2020) The total path length hydraulic resistance according to known anatomical patterns: What is the shape of the root-to-leaf tension gradient along the plant longitudinal axis? J Theor Biol 502:110369.

Lechthaler S, Turnbull TL, Gelmini Y, Pirotti F, Anfodillo T, Adams MA, Petit G (2019) A standardization method to disentangle environmental information from axial trends of xylem anatomical traits. Tree Physiol 39:495–502.

Lens F, Gleason SM, Bortolami G, Brodersen C, Delzon S, Jansen S (2022) Functional xylem characteristics associated with drought-induced embolism in angiosperms. New Phytol:2019–2036.

Lens F, Sperry JS, Christman MA, Choat B, Rabaey D, Jansen S (2011) Testing hypotheses that link wood anatomy to cavitation resistance and hydraulic conductivity in the genus Acer. New Phytol 190:709–723.

Lens F, Tixier A, Cochard H, Sperry JS, Jansen S, Herbette S (2013) Embolism resistance as a key mechanism to understand adaptive plant strategies. Curr Opin Plant Biol 16:287–292.

Limousin JM, Longepierre D, Huc R, Rambal S (2010) Change in hydraulic traits of Mediterranean Quercus ilex subjected to long-term throughfall exclusion. Tree Physiol 30:1026–1036.

Linton MJ, Sperry JS, Williams DG (1998) Limits to water transport in Juniperus osteosperma and Pinus edulis: Implications for drought tolerance and regulation of transpiration. Funct Ecol 12:906–911.

Lintunen A, Kalliokoski T (2010) The effect of tree architecture on conduit diameter and frequency from small distal roots to branch tips in Betula pendula, Picea abies and Pinus sylvestris. Tree Physiol 30:1433–1447.

Llorens L, Peñuelas J, Estiarte M, Bruna P (2004) Contrasting growth changes in two dominant species of a mediterranean shrubland submitted to experimental drought and warming. Ann Bot 94:843–853.

Loepfe L, Martinez-Vilalta J, Piñol J, Mencuccini M (2007) The relevance of xylem network structure for plant hydraulic efficiency and safety. J Theor Biol 247:788–803.

Lopez FB, Chauhan YS, Johansen C (1997) Effects of timing of drought stress on leaf area development and canopy light interception of short-duration pigeonpea. J Agron Crop Sci 178:1–7.

Losso A, Bär A, Dämon B, Dullin C, Ganthaler A, Petruzzellis F, Savi T, Tromba G, Nardini A, Mayr S, Beikircher B (2019) Insights from in vivo micro-CT analysis: testing the hydraulic vulnerability segmentation in Acer pseudoplatanus and Fagus sylvatica seedlings. New Phytol 221:1831–1842.

Maherali H, Pockman WT, Jackson RB (2004) Adaptive variation in the vulnerability of woody plants to xylem cavitation. Ecology 85:2184–2199.

Malone M, Watson R, Pritchard J (1999) The spittlebug Philaenus spumarius feeds from mature xylem at the full hydraulic tension of the transpiration stream. New Phytol 143:261–271.

Markesteijn L, Poorter L, Paz H, Sack L, Bongers F (2011) Ecological differentiation in xylem cavitation resistance is associated with stem and leaf structural traits. Plant, Cell Environ 34:137–148.

Marron N, Dreyer E, Boudouresque E, Delay D, Petit JM, Delmotte FM, Brignolas F (2003) Impact of successive drought and re-watering cycles on growth and specific leaf area of two Populus x canadensis (Moench) clones, 'Dorskamp' and 'Luisa_Avanzo'. Tree Physiol 23:1225–1235.

Martelli GP (2016) The current status of the quick decline syndrome of olive in southern Italy. Phytoparasitica 44:1–10.

Martínez-Sancho E, Dorado-Liñán I, Hacke UG, Seidel H, Menzel A (2017) Contrasting hydraulic architectures of scots pine and sessile oak at their southernmost distribution limits. Front Plant Sci 8:1–12.

McDowell NG, Allen CD, Anderson-Teixeira K, Aukema BH, Bond-Lamberty B, Chini L, Clark JS, Dietze M, Grossiord C, Hanbury-Brown A, Hurtt GC, Jackson RB, Johnson DJ, Kueppers L, Lichstein JW, Ogle K, Poulter B, Pugh TAM, Seidl R, Turner MG, Uriarte M, Walker AP, Xu C (2020) Pervasive shifts in forest dynamics in a changing world. Science (80-) 368:eaaz9463.

McDowell NG, Beerling DJ, Breshears DD, Fisher RA, Raffa KF, Stitt M (2011) The interdependence of mechanisms underlying climate-driven vegetation mortality. Trends Ecol Evol 26:523–532.

McDowell N, Pockman WT, Allen CD, Breshears DD, Cobb N, Kolb T, Plaut J, Sperry J, West A, Williams DG, Yepez EA (2008) Mechanisms of plant survival and mortality during drought: why do some plants survive while others succumb to drought? New Phytol 178:719–739.

McElrone AJ, Jackson S, Habdas P (2008) Hydraulic disruption and passive migration by a bacterial pathogen in oak tree xylem. J Exp Bot 59:2649–2657.

McElrone AJ, Pockman WT, Martínez-Vilalta J, Jackson RB (2004) Variation in xylem structure and function in stems and roots of trees to 20 m depth. New Phytol 163:507–517.

McElrone AJ, Sherald JL, Forseth IN (2003) Interactive effects of water stress and xylem-limited bacterial infection on the water relations of a host vine. J Exp Bot 54:419–430.

Meier IC, Leuschner C (2008) Belowground drought response of European beech: Fine root biomass and carbon partitioning in 14 mature stands across a precipitation gradient. Glob Chang Biol 14:2081–2095.

Meinzer FC, Johnson DM, Lachenbruch B, McCulloh KA, Woodruff DR (2009) Xylem hydraulic safety margins in woody plants: coordination of stomatal control of xylem tension with hydraulic capacitance. Funct Ecol 23:922–930.

Melvin T. Tyree MHZ (2002) Xylem Structure and the Ascent of Sap.

Mencuccini M, Hölttä T, Petit G, Magnani F (2007) Sanio's laws revisited. Size-dependent changes in the xylem architecture of trees. Ecol Lett 10:1084–1093.

Meng Y, Li Y, Galvani CD, Hao G, Turner JN, Burr TJ, Hoch HC (2005) Upstream migration of Xylella fastidiosa via pilus-driven twitching motility. J Bacteriol 187:5560–5567.

Nardini A, Gascò A, Trifilò P, Lo Gullo MA, Salleo S (2007) Ion-mediated enhancement of xylem hydraulic conductivity is not always suppressed by the presence of Ca2+ in the sap. J Exp Bot 58:2609–2615.

Nardini A, Savi T, Losso A, Petit G, Pacilè S, Tromba G, Mayr S, Trifilò P, Lo Gullo MA, Salleo S (2017) X-ray microtomography observations of xylem embolism in stems of Laurus nobilis are consistent with hydraulic measurements of percentage loss of conductance. New Phytol 213:1068–1075.

Newman KL, Almeida RPP, Purcell AH, Lindow SE (2003) Use of a Green Fluorescent Strain for Analysis of Xylella fastidiosa Colonization of Vitis vinifera. Appl Environ Microbiol 69:7319–7327.

Nicotra AB, Atkin OK, Bonser SP, Davidson AM, Finnegan EJ, Mathesius U, Poot P, Purugganan MD, Richards CL, Valladares F, van Kleunen M (2010) Plant phenotypic plasticity in a changing climate. Trends Plant Sci 15:684–692

Novelli S, Gismondi A, Di Marco G, Canuti L, Nanni V, Canini A (2019) Plant defense factors involved in Olea europaea resistance against Xylella fastidiosa infection. J Plant Res 132:439–455.

Nygren P, Pallardy SG (2008) Applying a universal scaling model to vascular allometry in a single-stemmed, monopodially branching deciduous tree (Attim's model). Tree Physiol 28:1–10.

Oepp B, Bulletin E (2019) PM 7/24 (4) Xylella fastidiosa. EPPO Bull 49:175–227.

Olson ME, Anfodillo T, Rosell JA, Martínez-Méndez N (2020) Across climates and species, higher vapour pressure deficit is associated with wider vessels for plants of the same height. Plant Cell Environ 43:3068–3080.

Olson ME, Anfodillo T, Rosell JA, Petit G, Crivellaro A, Isnard S, León-Gómez C, Alvarado-Cárdenas LO, Castorena M (2014) Universal hydraulics of the flowering plants: Vessel diameter scales with stem length across angiosperm lineages, habits and climates. Ecol Lett 17:988–997.

Pangle RE, Hill JP, Plaut JA, Yepez EA, Elliot JR, Gehres N, McDowell NG, Pockman WT (2012) Methodology and performance of a rainfall manipulation experiment in a piñon–juniper woodland. Ecosphere 3:art28.

Pellizzari E, Camarero JJ, Gazol A, Sangüesa-Barreda G, Carrer M (2016) Wood anatomy and carbon-isotope discrimination support long-term hydraulic deterioration as a major cause of drought-induced dieback. Glob Chang Biol 22:2125–2137.

Pérez-Donoso AG, Lenhof JJ, Pinney K, Labavitch JM (2016) Vessel embolism and tyloses in early stages of Pierce's disease. Aust J Grape Wine Res 22:81–86.

Pérez-Donoso AG, Sun Q, Caroline Roper M, Carl Greve L, Kirkpatrick B, Labavitch JM (2010) Cell wall-degrading enzymes enlarge the pore size of intervessel pit membranes in healthy and Xylella fastidiosa-infected grapevines. Plant Physiol 152:1748–1759.

Petit G, Bleve G, Gallo A, Mita G, Montanaro G, Nuzzo V, Zambonini D, Pitacco A (2021) Susceptibility to Xylella fastidiosa and functional xylem anatomy in Olea europaea: Revisiting a tale of plant-pathogen interaction. AoB Plants 13:1–9.

Petit G, Crivellaro A (2014) Comparative axial widening of phloem and xylem conduits in small woody plants. Trees - Struct Funct 28:915–921.

Petit G, Mencuccini M, Carrer M, Prendin AL, Holtta T (2022) Two path length effects emerging from ontogenetically stable axial xylem design affect the conductance of inner sapwood rings.

Petit G, Pfautsch S, Anfodillo T, Adams MA (2010) The challenge of tree height in Eucalyptus regnans: When xylem tapering overcomes hydraulic resistance. New Phytol 187:1146–1153.

Petit G, Savi T, Consolini M, Anfodillo T, Nardini A (2016) Interplay of growth rate and xylem plasticity for optimal coordination of carbon and hydraulic economies in Fraxinus ornus trees. Tree Physiol 36:1310–1319.

Petit G, Zambonini D, Hesse BD, Häberle KH (2022) No xylem phenotypic plasticity in mature Picea abies and Fagus sylvatica trees after 5 years of throughfall precipitation exclusion. Glob Chang Biol 28:4668–4683.

Pfautsch S, Aspinwall MJ, Drake JE, Chacon-Doria L, Langelaan RJA, Tissue DT, Tjoelker MG, Lens F (2018) Traits and trade-offs in whole-tree hydraulic architecture along the vertical axis of Eucalyptus grandis. Ann Bot 121:129–141.

Pfautsch S, Harbusch M, Wesolowski A, Smith R, Macfarlane C, Tjoelker MG, Reich PB, Adams MA (2016) Climate determines vascular traits in the ecologically diverse genus Eucalyptus. Ecol Lett 19:240–248.

Pittermann J (2010) The evolution of water transport in plants: An integrated approach. Geobiology 8:112–139.

Pittermann J, Choat B, Jansen S, Stuart SA, Lynn L, Dawson TE (2010) The relationships between xylem safety and hydraulic efficiency in the cupressaceae: The evolution of pit membrane form and function. Plant Physiol 153:1919–1931.

Pittermann J, Sperry JS, Hacke UG, Wheeler JK, Sikkema EH (2006) Inter-tracheid pitting and the hydraulic efficiency of conifer wood: The role of tracheid allometry and cavitation protection. Am J Bot 93:1265–1273.

Pivovaroff AL, McDowell NG, Rodrigues TB, Brodribb T, Cernusak LA, Choat B, Grossiord C, Ishida Y, Jardine KJ, Laurance S, Leff R, Li W, Liddell M, Mackay DS, Pacheco H, Peters J, de J. Sampaio Filho I, Souza DC, Wang W, Zhang P, Chambers J (2021) Stability of tropical forest tree carbon-water relations in a rainfall exclusion treatment through shifts in effective water uptake depth. Glob Chang Biol 27:6454–6466.

Plaut JA, Yepez EA, Hill J, Pangle R, Sperry JS, Pockman WT, Mcdowell NG (2012) Hydraulic limits preceding mortality in a piñon-juniper woodland under experimental drought. Plant, Cell Environ 35:1601–1617.

Poorter H, Niinemets Ü, Poorter L, Wright IJ, Villar R (2009) Causes and consequences of variation in leaf mass per area (LMA): a meta-analysis. New Phytol 182:565–588.

Prendin AL, Mayr S, Beikircher B, Von Arx G, Petit G (2018) Xylem anatomical adjustments prioritize hydraulic efficiency over safety as Norway spruce trees grow taller. Tree Physiol 38:1088–1097.

Prendin AL, Petit G, Fonti P, Rixen C, Dawes MA, von Arx G (2018) Axial xylem architecture of Larix decidua exposed to CO2 enrichment and soil warming at the tree line. Funct Ecol 32:273–287.

Pretzsch H, Bauerle T, Häberle KH, Matyssek R, Schütze G, Rötzer T (2016) Tree diameter growth after root trenching in a mature mixed stand of Norway spruce (Picea abies [L.] Karst) and European beech (Fagus sylvatica [L.]). Trees 30:1761–1773.

Pretzsch H, Grams T, Häberle KH, Pritsch K, Bauerle T, Rötzer T (2020) Growth and mortality of Norway spruce and European beech in monospecific and mixed-species stands under natural episodic and experimentally extended drought. Results of the KROOF throughfall exclusion experiment. Trees - Struct Funct 34:957–970.

Pretzsch H, Rötzer T, Matyssek R, Grams TEE, Häberle KH, Pritsch K, Kerner R, Munch JC (2014) Mixed Norway spruce (Picea abies [L.] Karst) and European beech (Fagus sylvatica [L.]) stands under drought: from reaction pattern to mechanism. Trees - Struct Funct 28:1305–1321.

Roper MC, Greve LC, Warren JG, Labavitch JM, Kirkpatrick BC (2007) Xylella fastidiosa requires polygalacturonase for colonization and pathogenicity in Vitis vinifera grapevines. Mol Plant-Microbe Interact 20:411–419.

Rosell JA, Olson ME, Anfodillo T (2017) Scaling of Xylem Vessel Diameter with Plant Size: Causes, Predictions, and Outstanding Questions. Curr For Reports 3:46–59.

Rosner S, Gierlinger N, Klepsch M, Karlsson B, Evans R, Lundqvist SO, Světlík J, Børja I, Dalsgaard L, Andreassen K, Solberg S, Jansen S (2018) Hydraulic and mechanical dysfunction of Norway spruce sapwood due to extreme summer drought in Scandinavia. For Ecol Manage 409:527–540.

Rosner S, Heinze B, Savi T, Dalla-Salda G (2019) Prediction of hydraulic conductivity loss from relative water loss: new insights into water storage of tree stems and branches. Physiol Plant 165:843–854.

Rowland L, Da Costa ACL, Galbraith DR, Oliveira RS, Binks OJ, Oliveira AAR, Pullen AM, Doughty CE, Metcalfe DB, Vasconcelos SS, Ferreira L V., Malhi Y, Grace J, Mencuccini M, Meir P (2015) Death from drought in tropical forests is triggered by hydraulics not carbon starvation. Nature 528:119–122.

Rowland L, Lobo-do-Vale RL, Christoffersen BO, Melém EA, Kruijt B, Vasconcelos SS, Domingues T, Binks OJ, Oliveira AAR, Metcalfe D, da Costa ACL, Mencuccini M, Meir P (2015) After more than a decade of soil moisture deficit, tropical rainforest trees maintain photosynthetic capacity, despite increased leaf respiration. Glob Chang Biol 21:4662–4672.

Sabella E, Aprile A, Genga A, Siciliano T, Nutricati E, Nicolì F, Vergine M, Negro C, De Bellis L, Luvisi A (2019) Xylem cavitation susceptibility and refilling mechanisms in olive trees infected by Xylella fastidiosa. Sci Rep 9:1–11.

Sabella E, Moretti S, Gärtner H, Luvisi A, de Bellis L, Vergine M, Saurer M, Cherubini P (2020) Increase in ring width, vessel number and δ18O in olive trees infected with Xylella fastidiosa. Tree Physiol 40:1583–1594.

Sala A, Piper F, Hoch G (2010) Physiological mechanisms of drought-induced tree mortality are far from being resolved. New Phytol 186:274–281.

Saponari, M. ; Boscia, D. ; Nigro, F. ; Martelli GP (2013) IDENTIFICATION OF DNA SEQUENCES RELATED TO XYLELLA FASTIDIOSA IN OLEANDER , ALMOND AND OLIVE TREES EXHIBITING LEAF SCORCH SYMPTOMS IN APULIA (SOUTHERN Author (s): M . Saponari , D . Boscia , F . Nigro and G . P . Martelli Published by : Springer Stable. 95

Savage JA, Beecher SD, Clerx L, Gersony JT, Knoblauch J, Losada JM, Jensen KH, Knoblauch M, Holbrook NM (2017) Maintenance of carbohydrate transport in tall trees. Nat Plants 3:965–972.

Savi T, Marin M, Luglio J, Petruzzellis F, Mayr S, Nardini A (2016) Leaf hydraulic vulnerability protects stem functionality under drought stress in Salvia officinalis. Funct Plant Biol 43:370–379.

Savi T, Tintner J, Sois L Da, Grabner M, Petit G, Rosner S (2019) The potential of Mid-Infrared spectroscopy for prediction of wood density and vulnerability to embolism in woody angiosperms. Tree Physiol 39:503–510.

De Schepper V, De Swaef T, Bauweraerts I, Steppe K (2013) Phloem transport: a review of mechanisms and controls. J Exp Bot 64:4839–4850.

Schindelin J, Arganda-Carreras I, Frise E, Kaynig V, Longair M, Pietzsch T, Preibisch S, Rueden C, Saalfeld S, Schmid B, Tinevez JY, White DJ, Hartenstein V, Eliceiri K, Tomancak P, Cardona A (2012) Fiji: An open-source platform for biological-image analysis. Nat Methods 9:676–682.

Schuldt B, Buras A, Arend M, Vitasse Y, Beierkuhnlein C, Damm A, Gharun M, Grams TEE, Hauck M, Hajek P, Hartmann H, Hiltbrunner E, Hoch G, Holloway-Phillips M, Körner C, Larysch E, Lübbe T, Nelson DB, Rammig A, Rigling A, Rose L, Ruehr NK, Schumann K, Weiser F, Werner C, Wohlgemuth T, Zang CS, Kahmen A (2020) A first assessment of the impact of the extreme 2018 summer drought on Central European forests. Basic Appl Ecol 45:86–103.

Schuldt B, Knutzen F, Delzon S, Jansen S, Müller-Haubold H, Burlett R, Clough Y, Leuschner C (2016) How adaptable is the hydraulic system of European beech in the face of climate change-related precipitation reduction? New Phytol 210:443–458.

Sevanto S (2014) Phloem transport and drought. J Exp Bot 65:1751–1759.

Sevanto S (2018) Drought impacts on phloem transport. Curr Opin Plant Biol 43:76–81.

Sevanto S, Mcdowell NG, Dickman LT, Pangle R, Pockman WT (2014) How do trees die? A test of the hydraulic failure and carbon starvation hypotheses. Plant, Cell Environ 37:153–161.

Sevanto S, Ryan M, Dickman LT, Derome D, Patera A, Defraeye T, Pangle RE, Hudson PJ, Pockman WT (2018) Is desiccation tolerance and avoidance reflected in xylem and phloem anatomy of two coexisting arid-zone coniferous trees? Plant Cell Environ 41:1551–1564.

Sharma N, Barion G, Shrestha I, Ebinezer LB, Trentin AR, Vamerali T, Mezzalira G, Masi A, Ghisi R (2020) Accumulation and effects of perfluoroalkyl substances in three hydroponically grown Salix L. species. Ecotoxicol Environ Saf 191

Skelton RP, Anderegg LDL, Diaz J, Kling MM, Papper P, Lamarque LJ, Delzon S, Dawson TE, Ackerly DD (2021) Evolutionary relationships between drought-related traits and climate shape large hydraulic safety margins in western North American oaks. Proc Natl Acad Sci 118:e2008987118.

Smith KC, Magnuson CE, Goeschl JD, DeMichele DW (1980) A time-dependent mathematical expression of the münch hypothesis of phloem transport. J Theor Biol 86:493–505.

Sperry JS (2000) Hydraulic constraints on plant gas exchange. In: Agricultural and Forest Meteorology.pp 13–23.

Sperry JS, Hacke UG, Pittermann J (2006) Size and function in conifer tracheids and angiosperm vessels. Am J Bot 93:1490–1500.

Sperry JS, Meinzer FC, McCulloh KA (2008) Safety and efficiency conflicts in hydraulic architecture: scaling from tissues to trees. Plant Cell Environ 31:632–645.

Sun Q, Sun Y, Andrew Walker M, Labavitch JM (2013) Vascular occlusions in grapevines with Pierce's disease make disease symptom development worse. Plant Physiol 161:1529–1541.

Tardieu F, Simonneau T (1998) Variability among species of stomatal control under fluctuating soil water status and evaporative demand: Modelling isohydric and anisohydric behaviours. J Exp Bot 49:419–432.

Thompson M V., Holbrook NM (2003a) Scaling phloem transport: Water potential equilibrium and osmoregulatory flow. Plant, Cell Environ 26:1561–1577.

Thompson M V., Holbrook NM (2003b) Application of a single-solute non-steady-state phloem model to the study of long-distance assimilate transport. J Theor Biol 220:419–455.

Tomasella M, Beikircher B, Häberle KH, Hesse B, Kallenbach C, Matyssek R, Mayr S (2018) Acclimation of branch and leaf hydraulics in adult Fagus sylvatica and Picea abies in a forest through-fall exclusion experiment. Tree Physiol 38:198–211.

Torres-Ruiz JM, Cochard H, Mencuccini M, Delzon S, Badel E (2016) Direct observation and modelling of embolism spread between xylem conduits: a case study in Scots pine. Plant Cell Environ 39:2774–2785.

Torres-Ruiz JM, Jansen S, Choat B, McElrone AJ, Cochard H, Brodribb TJ, Badel E, Burlett R, Bouche PS, Brodersen CR, Li S, Morris H, Delzon S (2015) Direct X-ray microtomography observation confirms the induction of embolism upon xylem cutting under tension. Plant Physiol 167:40–43.

Trugman AT, Detto M, Bartlett MK, Medvigy D, Anderegg WRL, Schwalm C, Schaffer B, Pacala SW (2018) Tree carbon allocation explains forest drought-kill and recovery patterns. Ecol Lett 21:1552–1560.

Tyree MT, Ewers FW (1991) The hydraulic architecture of trees and other woody plants. New Phytol 119:345–360.

Tyree MT, Sperry JS (1988) Do Woody Plants Operate Near the Point of Catastrophic Xylem Dysfunction Caused by Dynamic Water Stress? Plant Physiol 88:574–580.

Tyree MT, Sperry JS (1989) Vulnerability of Xylem to Cavitation and Embolism. :19–38.

Urli M, Porté AJ, Cochard H, Guengant Y, Burlett R, Delzon S (2013) Xylem embolism threshold for catastrophic

hydraulic failure in angiosperm trees. Tree Physiol 33:672–683.

Venturas MD, Rodriguez-Zaccaro FD, Percolla MI, Crous CJ, Jacobsen AL, Pratt RB (2016) Single vessel air injection estimates of xylem resistance to cavitation are affected by vessel network characteristics and sample length. Tree Physiol 36:1247–1259.

Wang T-T, Ying G-G, Shi W-J, Zhao J-L, Liu Y-S, Chen J, Ma D-D, Xiong Q (2020) Uptake and Translocation of Perfluorooctanoic Acid (PFOA) and Perfluorooctanesulfonic Acid (PFOS) by Wetland Plants: Tissue- and Cell-Level Distribution Visualization with Desorption Electrospray Ionization Mass Spectrometry (DESI-MS) and Transmission El. Environ Sci Technol 54:6009–6020.

Wason J, Bouda M, Lee EF, McElrone AJ, Phillips RJ, Shackel KA, Matthews MA, Brodersen C (2021) Xylem network connectivity and embolism spread in grapevine(Vitis vinifera L.). Plant Physiol 186:373–387.

Weiner J (2004) Allocation, plasticity and allometry in plants. Perspect Plant Ecol Evol Syst 6:207–215.

Wells JM, Raju BC, Hung H, Weisburg WG, Mandelco-paul L, Brenner DONJ (1987) Limited , Fastidious Plant Bacteria Related to Xanthomonas spp . Int J Syst Bacteriol 37:136–143.

West GB, Brown JH, Enquist BJ (1999) A general model for the structure and allometry of plant vascular systems . Nature 400:664–667.

Wheeler JK, Sperry JS, Hacke UG, Hoang N (2005) Inter-vessel pitting and cavitation in woody Rosaceae and other vessel led plants: A basis for a safety versus efficiency trade-off in xylem transport. Plant, Cell Environ 28:800–812.

Yang S, Tyree MT (1993) Hydraulic resistance in Acer saccharum shoots and its influence on leaf water potential and transpiration. Tree Physiol 12:231–242.

Zar J (1999) Biostatistical analysis

Zhang Y, Carmesin C, Kaack L, Klepsch MM, Kotowska M, Matei T, Schenk HJ, Weber M, Walther P, Schmidt V, Jansen S (2020) High porosity with tiny pore constrictions and unbending pathways characterize the 3D structure of intervessel pit membranes in angiosperm xylem. Plant Cell Environ 43:116–130.

Zuur AF, Ieno EN, Walker NJ, Saveliev AA, Smith GM (2009) Reviewer: Aaron Christ Alaska Department of Fish and Game Mixed Effects Models and Extensions in Ecology with R. JSS J Stat Softw 32:2–4.